Master Thesis

im Rahmen des
Universitaetslehrganges "Geographical Information Sciences & Systems"
(UNIGIS Msc) am Zentrum für Geoinformatik (Z_GIS)
der Paris-Lodron Universitaet Salzburg

zum Thema

Color Characterization for Digital Aerial Cameras - a new Approach for Radiometric Sensor Fusion

vorgelegt von

DI(FH) Susanne Scholz
U1424, UNIGIS Msc Jahrgang 2008

Zur Erlangung des Grades
"Master of Sciences (Geographical Information Science & Systems) - MSc(GIS)"
Gutachter:
Ao. Univ Prof. Dr. Josef Strobl
Dr. Michael Gruber

STATUTORY DECLARATION

I declare that I have authored this thesis independently, that I have not used other than the declared sources / resources, and that I have explicitly marked all material which has been quoted either literally or by content from the used sources.

....

Abstract

Color characterization is a well known topic in the graphical industry. All devices used throughout the whole process, from photographing down to printing, are calibrated and characterized. The International Color Consortium (ICC) is a consortium of companies that support the characterization of devices with standardized color profiles, which contain information about the colors a device can represent, and device independent color spaces, for a well defined transformation between the color spaces of different devices.

The idea of this thesis is to use this knowledge from the graphical industry developed in color theory and apply it to digital aerial cameras. Furthermore, it is being investigated if the characterization of digital cameras can support the fusion of data from different digital aerial sensors.

In this thesis three different camera characterization methods are compared, the complete calibration workflow introduced and the accuracy evaluated, with a focus on the color quality compared to a reference. The result of a characterization process is a transformation matrix or a Look Up Table (LUT) containing information to convert the colors of a device into another color space (depending which reference values have been used for computation) and includes a color correction. To be able to find out whether the camera characterization (including color correction) brings a benefit for sensor fusion two different camera models with different color recording methods have been used for the investigation.

The evaluation was performed on quality measurement figures suggested in color theory and the visual impression on real aerial images. Outdoor color targets are used for verification.

The results have shown that the quality and accuracy of color representation can be improved with all three methods. There is one method, based on a polynomic adjustment, which produced in nearly all evaluations the best results. The application on real aerial images produced more colorful and bright images.

This thesis is a first approach to use methods developed in color theory to improve colors in digital aerial photography. The results in this thesis show that the color reproduction quality rises. When characterizing two different sensors in the same manner, the colors are reproduced more accurately and with this are more similar to each other. For this reason, this approach brings also advantages when fusing images from different sensors.

Kurzfassung

Farbcharakterisierung ist ein bekanntes Thema in der Grafikindustrie. Es werden alle Geräte, die in dem Prozess vom Photographieren bis zum Druck verwendet werden kalibriert und charakterisiert um Farben korrekt wieder zu geben. Das International Color Consortium (ICC) ist ein Konsortium von Firmen, welche diese Charakterisierung von Geräten unterstützt, indem es Standards entwickelt um Farben von Ein- und Ausgabegeräte, mit so genannten ICC-Farbprofilen, zu beschreiben. Diese Farbprofile beinhalten Informationen zur Transformation von einem geräteabhängigen in einen geräteunabhängigen Farbraum. Diese Arbeit wendet das Wissen aus der Grafikindustrie, welches in der Farbtheorie entwickelt worden ist, auf digitale Luftbildkameras an. Des weiteren, soll die Charakterisierung von digitalen Kameras die Fusion von Daten von verschiedenen digitalen Luftbildsensoren unterstützen.

In dieser Arbeit werden drei verschiedene Kameracharakterisierungsmethoden verglichen, der gesamte Kalibrierablauf vorgestellt und die resultierende Genauigkeit, in Vergleich zu Referenzdaten, evaluiert. Das Resultat einer Charakterisierung ist eine Transformationsmatrix oder Look Up Table (LUT), welche die Information für die Umrechnung in einen anderen Farbraum (je nachdem in welchem Farbraum die Referenzdaten vorhanden sind) und eine Farbkorrektur beinhaltet. Um herauszufinden, ob die Kameracharakterisierung einen Vorteil für die Fusion von verschiedenen Sensordaten bringt, werden zwei verschiedene Luftbildsensoren evaluiert, welche auf unterschiedliche Art und Weise Farben aufnehmen.

Die Genauigkeitsanalyse wird anhand von in der Farbtheorie anerkannten Messgrössen bestimmt und an realen Luftbildern getestet. Die Ergebnisse der Evaluierung zeigen das die Genauigkeit der Farbrepräsentation mit allen drei Methoden verbessert werden kann. Eine Methode, basierend auf einer polynomischen Anpassung, produzierte die besten und genauesten Ergebnisse. Die Anwendung der Farbtransformationsmatrizen produziert im generellen farbenfrohere und hellere Bilder.

Diese Arbeit stellt einen ersten Versuch vor, Methoden aus der Farbtheorie in der digitalen Luftbildphotographie anzuwenden, um die Farbqualität zu verbessern. Die Ergebnisse aus den Evaluierungen zeigen, dass durch die Charakterisierung einer Luftbildkamera die Qualität der Farbrepräsentation steigt. Zusätzlich wird gezeigt, dass wenn zwei verschiedene Sensoren mit der gleichen Methode charakterisiert werden, die Fusionierung dieser besser funktioniert, da bei beiden die Farbausgabe kalibriert ist.

Acknowledgements

My thanks go to my supervisors Dr. Josef Strobl and Dr. Michael Gruber. Both I would like to thank for the prosperous discussions and valuable feedback. My working colleagues at Microsoft Photogrammetry in Graz supported me a lot with the tests in the lab, performing the testflights and many discussions about the topic of this thesis.

Furthermore I would like to thank the supporters from the UNIGIS network in Salzburg, for there engagement and help during the period of my studies.

Last but not least, I would like to thank my family for the support they gave me throughout the time of studying and writing this thesis. Special thanks go to my husband Johannes, who endlessly supported me in personal as well as professional manner.

Contents

List of Figures

List of Abbreviations

CAT	Chromatic Adaption Transform
CCD	Charge-Coupled Device
CCM	Color Correction Matrix
CFA	Color Filter Array
CIE	Commission Internationale de l'Eclairage
CMF	Color Matching Function
CMM	Color Matching Module
CMOS	Complementary Metal Oxide Semiconductor
DN	Digital Number
DR	Dynamic Range
FFT	Fast Fourier Transform
FMC	Forward Motion Compensation
FWC	Full Well Capacity
GIS	Geographic Information System
GPS/INS	Global Positioning System / Inertial Navigation System
ICC	International Color Consortium
IHS	Intensity - Hue - Saturation
LCD	Liquid Crystal Display
IMU	Inertial Measurement Unit
LLS	Linear Least Squares
LTM	Linear Least Squares Transformation Matrix
LUT	Look Up Table
NIR	Near Infrared

PCA Principal Component Analysis

PCS Profile Connection Space

PTM Polynomic Transformation Matrix

RLS Robust Least Squares

RTM Robust Least Squares Transformation Matrix

SNR Signal to Noise Ratio

TDI Time Delay Interval

TRC Tone Reproduction Curve

UC UltraCam

UCL UltraCam L

UV/IR Ultraviolett/Infrared

UCXp UltraCam Xp

Chapter 1

Introduction

In the graphical industry professional color management is well developed, widely spread and used. Pictures are taken with different digital cameras, color device profiles are stored and used for a correct reproduction of the colors on different output medias as screens or printers. The complete industry uses know-how from color theory and the ICC.

An ICC profile is a standard to describe the color space transformation from a device into a device independent color space as XYZ or LAB or vice versa from a color independent color space into an output device color space, as CMYK for printers or sRGB for LCD screens. Figure 1.1 shows a typical color workflow based on ICC profiles and the standardized color transformation space, called PCS within ICC.

Today, it is inevitable to use images from different sensors, no matter if aerial or satellite, in a Geographic Information System (GIS) for analysis or only for visualization image mosaics. The topic multisensory image fusion becomes more eminent as examination areas get bigger and computer technologies faster and cheaper. The color and radiometry of images is one essential topic in the matter of image fusion technologies. The main interest is to get well balanced image mosaics out of different kind of images without seeing any color shifts or problems.

The master thesis bridges technologies developed in color theory and applied in the graphical industry and use it in the field of remote sensing and photogrammetry. It describew how to color characterize a digital aerial camera and with this be able to use all the advantages of standardized color spaces. The topic camera color characterization describes a methodology to find appropriate parameters to change the device dependent RGB color space of a digital camera, also known as color gamut, into a device independent color space and synchronously apply a color correction according to a reference target. The resulting parameters (depending on the method this can be a LUT or a matrix with the transformation parameters) can then be used to define an ICC profile.

The thesis presents possibilities for transforming the color space of an input device such as a digital camera into a device independent, standardized

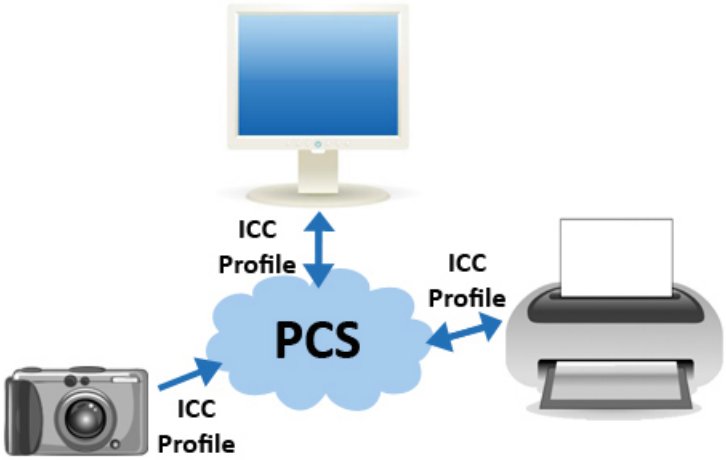

Figure 1.1: Typical color management workflow in the graphical industry, based on ICC profiles and PCS

color space. Methods for this transformation are evaluated and analyzed when applying on images. The main focus of this thesis is to present methods and concepts in color theory which shall be applied in the field of remote sensing, more precisely in radiometric sensor fusion, to improve color quality of aerial images in general, the workflow of color adjustment and finally enhance the quality of radiometric image fusion from different sensors.

1.1 Problem description

The master thesis covers two main topics; in a first step, three different methods for camera color characterization are evaluated and in a further step, the fusion of images from characterized aerial cameras with different sensor techniques are analyzed. The evaluation of the camera characterization method is the basis for the second topic - the evaluation if a camera characterization brings advantages in the fusion of images of different sensors. For this reason the following two assumptions are formed to be verified or falsified within this thesis:

- A camera characterization for digital aerial mapping cameras results in a more accurate color representation of post processed aerial images.
- Camera characterization is a method for improving the quality for radiometric fusion of images of different aerial sensors.

Different kind of analysis known in color theory as well as in GIS and Remote Sensing are used to evaluate and verify the hypothesis. Evaluation methods out of all three sciences are used to find out, if the results make sense in all three and not only in one of the fields mentioned above. This can guarantee that there is no disadvantage for further analysis and work with the given and color corrected image data.

1.2 Literature Overview

This thesis covers topics in remote sensing, more precisely photogrammetry and GIS, digital image processing and color theory. Basic literature and actual conference and journal proceedings of all three disciplines were used for the description of the theoretical background in chapter 2 and 3. In remote sensing one important book about all basic theory comes from Lillesand *et al.* (2004). This book contains comprehensive information about working with images for remote sensing purposes. In the field of photogrammetry basic literature from Kraus (2002), Sandau (2005) and Albertz and Wiggenhagen (2009) have been used. Albertz and Wiggenhagen (2009) is an actual and comprehensive book containing all relevant information about photogrammetry. It is written in German and English and has short and concise definitions. Sandau (2005) is a comprehensice book about all relevant information for digital airborne cameras. It contains information about the actual cameras on the market. Kraus (2002) is standard literature in the field of photogrammetry in German speaking areas as Austria, Germany and Switzerland. All important workflows and formulas necessary for photogrammetric issues can be found in this book. Also detailed descriptions and definitions about further image analysis basics can be found in this book.

A general introduction about the basic techniques in digital image processing and a first rough introduction in color theory is given by Gonzalez and Woods (2002). This book is again standard literature in computer vision because all main techniques about image processing can be found in this literature.

In color theory two basic books have been used for this thesis, which have been written by Reinhard *et al.* (2008) and Sharma (2003). Both books provide very comprehensive information about color in general, device characterization and methods for the adjustment of colors. Reinhard *et al.* (2008) is a comprehensive book which treats all issues in color theory. Basic information about how humans perceive color and what influences the human color perception are described in detail as well as detailed information about color spaces, common techniques and algorithms in color theory

are discussed in detail. Sharma (2003) contains a selection of articles of several well known authors in color theory. The articles describe important topics in color theory, as for example color device characterisation or gamut mapping techniques as well as basic definitions of color specific terms.

Further techniques which have been used for investigations have been taken out of conference proceedings and journals. Important work on this topic comes from researchers like Michael Vrehl, Mark D. Fairchild, Kobus Barnard, H. Joel Trussel, R.W.G. Hunt and Gernot Hoffmann. The paper from Vrhel and Trussel (1999) is basic literature for device characterization. In this paper the mathematical background is explained in detail. Yoon and Cho (1999) and Wolf (2003) discuss two different approaches for the derivation of a CCM which are the basis for the camera characterization.

Information about the ICC was taken from their website http://www.color.org. The specifications and further white paper material can be downloaded from the website. The information about the camera system are all provided by Microsoft Photogrammetry, the company which is producing the UltraCam camera series and the post processing software. The basic information can be downloaded from the website http://www.microsoft.com/ultracam.

1.3 Structure of this Thesis

This thesis gives an insight how to color characterize an aerial camera and with this be able to use all the advantages of standardized color spaces. The transformation into another color space implies a color correction method because the sensor image data is referenced to a known data set, also known as color target. The necessary theoretical background information about aerial sensor fusion, digital aerial cameras is given in chapter 2 and for color theory is given in chapter 3. The aerial sensor fusion section gives an overview about all kind of sensors which are available in remote sensing and actual image fusion methods. The design of a digital camera, background information about radiometric camera calibration and camera specific color characteristics are discussed. Chapter 3 explains topics in color theory with detailed information about the most important color spaces, color transformation methods and basic techniques for color adjustments. Finally, the work of the ICC is being introduced and color device profiles are described.

Chapter 4 comprises the connection between aerial fusion and color theory. The calibration test setup is described and different color transformation with the given test data discussed and evaluated. Furthermore the software used is introduced. Chapter 5 gives a detailed discussion about the

results on the one side focused on the different methods for color transformation and on the other side focused on the accuracy of different sensors.

On the contrary to chapter 4 and 5, which describe the methods and their accuracy with a focus on the camera technology and color theory, chapter 6 bridges the application of methods of color theory for sensor fusion and actual GIS issues. Finally, chapter 7 summarizes the results of the complete investigation and gives an outlook on future work. The resulting workflow is shown in Figure 1.2. The colors red, green and blue represent the content of the corresponding chapters.

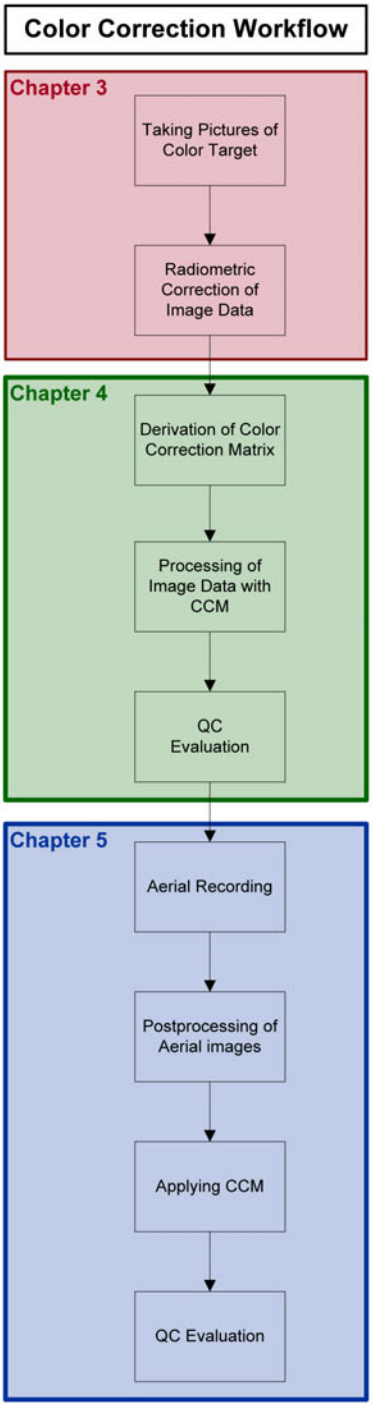

Figure 1.2: Color correction workflow, and color indexed structure of the master thesis

Chapter 2

Radiometric Sensor Fusion and Digital Aerial Cameras

The topic of this thesis covers fields of research in remote sensing and color theory. Remote sensing is a broad topic, for this reason this thesis focuses on images produced with optical systems; no radar systems or laser systems are used for investigations.

This chapter gives the basic theoretical background out of both fields of research that are necessary to perform analyis and evaluations described in the following chapters. This chapter starts with a general introduction in the field of remote sensing and describes basic principles of digital aerial cameras. In the first section the subject of radiometric sensor fusion with an introduction to image fusion methods is being presented. Sensor basics, design of a digital aerial camera and basic radiometric and colorimetric properties of digital aerial cameras follow.

The graphical industry is already a good example how color management can be introduced to photography in general. The remote sensing community needs to adopt workflows and method coming from the graphical industry, as color is an important issue in the further analysis and derivation of cartographic products. This is important when working with images from one sensor, and becomes more important when working with images from different kind of sensors. The radiometric and geometric adjustment when fusing image data from different sensors is more challenging. In literature this is called *data fusion* and is defined in several different ways. Albertz and Wiggenhagen (2009) defines the term *data fusion* as follows

> *... methods that are applied to merge data from different sources and containing disparate information to produce a consistent data set [...] In photogrammetry and remote sensing data fusion is a multi-purpose approach. It is often understood as the integration of image data originating from different sources in order to generate a new image of higher quality.*

This thesis focuses on the adjustment of colors during image fusion. The

geometric fusion is mentioned for completeness but not discussed in detail.

Flight missions produce several hundreds or thousands of images. There are many factors that influence the radiometric response, as for example the

- sun angle, and the changing of this angle during a flight mission
- atmosphere
- weather conditions in general (sunny or cloudy day)
- season
- flying altitude
- recording device (camera)

which finally result in differences in colors. These varieties occur inside one project and even more challenging when fusing images from more missions (recorded on different days) or even different sensors. For this reason, it is inevitable to adjust colors even of a single flight mission. Chandelier and Martinoty (2009) lists the influencing factors mentioned and suggests a comprehensive model for the radiometric correction of aerial images.

Figure 2.1: Sample for radiometric sensor fusion problem in Graz, Austria. The color shift is visible in the center of this screenshot in the field.

To fuse images from different sensors, with varying radiometric response and behavior, different sunlight and illumination situations make it even more difficult to adjust blocks of images. Figure 2.1 shows an example for this kind of sensor fusion problem. In this case images from the same sensor but from different flight lines have been fused without special radiometric

adjustment. The approach introduced in this thesis should not correct all the effects listed above, as there are many scientists working on modelling these effect, but focuses on the last item, the recording device. It should present a new approach to calibrate a sensor to a reference and which results in a more accurate color representation. The possibility to transform the color information of the sensors into another color space opens up more possibilites out of color theory to improve already known models for the correction of the above mentioned influencing factors. This topic is only touched on here but would go beyond the scope of this master thesis.

2.1 Radiometric Image Fusion Techniques

Many different techniques for radiometric image fusion can be found in literature. Pohl (1999) lists the following, mostly used techniques for radiometric image fusion:

- RGB color composites

  This method implies the investigation of the variation in color values in single channels (red, green and blue).

- Intensity - Hue - Saturation (IHS) transformation:

  The image is transformed into the IHS color space (see section 3.2.6). The Intensity image is being replaced by another image and in a further step the image is transformed back to RGB color space (Albertz and Wiggenhagen, 2009).

- Arithmetic combinations

  The arithmetic combination comprise the possibilties of combining data by summation, subtraction, multiplication or ratios.

- Principal Component Analysis (PCA)

  The PCA fusion is similar to the IHS transformation. A PCA transforms correlated datasets into uncorrelated linear datasets. In the case of RGB images these datasets are the color channels. A PCA transformation is computed, the first prinicpal component is replaced by another image and then the image is transformed back to RGB.

- Wavelets

  The computed wavelets (summation of elementary functions from arbitrary functions) are weighted according to their structure characteristics for the images which are being adjusted. In the next step, a transformation which contains the spectral information of the low

resolution image and the resolution of the high resolution image can be computed.

- Regression Variable Substitution

  This method tries to find a linear combination of image channels (regression procedure), that one channel can be replaced.

- combinations of the above mentioned techniques

All methods listed above, excluding the IHS transformation, work in the RGB color space. The color space transformation from IHS to RGB is well defined and described in section 3.2 in detail. Typical software packages for orthophoto generation and general image processing in remote sensing that use the above mentioned algorithms for color adjustment are:

- Inpho OrthoVista - http://www.inpho.de
- ITT ENVI - http://www.ittvis.com
- ERDAS Imagine - http://www.erdas.com/
- Clark Labs IDRISI - http://www.clarklabs.org
- PCI Geomatics - http://www.pcigeomatics.com

Besides the radiometric adjustment in sensor fusion it is often necessary to fuse images of different resolutions. Usually, a more detailed panchromatic channel is available and multispectral channels with lower resolutions. Therefore the color information can be mapped to the high-resolution panchromatic image information, this processing step is called *pansharpening*. It is also possible to merge resolutions of other single sensors (Pohl, 1999). Typical resolution merge algorithms are for example the IHS transform, Fast Fourier Transform (FFT) and Brovey transform (Ehlers, 2005). A more detailed evaluation about state of the art pansharpening algorithms can be found in (Weidner and Centeno, 2009). Parallel to the radiometric image fusion, when merging images with different resolutions or images which have been produced by different sensors this becomes more challenging (Pohl, 1999).

2.2 Types of Sensors

High resolution sensors, depending on the mounted platform, can be either airborne or spaceborne. Nowadays, commericial satellite images can achieve

a resolution of up to 60cm (Ehlers, 2005). Well known high resolution satellites are Ikonos (Space Imaging), Quickbird 2 (Digital Globe), OrbView 3 (Orbimage) and EROS A1 (Imagesat). On the contrary, aerial sensors can achieve a resolution of up to 2.5cm depending on the flying height, pixel size and focal length of the objectives. As this thesis is focusing on aerial sensors, the design and availability on the market is described in a separate section (chapter 2.3).

2.3 Design of Digital Aerial Cameras

This thesis is focusing on the radiometry of images recorded with digital cameras mounted on aerial platforms. In this sector two different techniques can be found, which are the pushbroom cameras and the area based cameras. The major players on this market are Vexcel Imaging GmbH, Intergraph and Leica. Typically, all of the available sensors can achieve a radiometric resolution of up to 12 bit (per color channel). A detailed description to the products of the above mentioned companies can be found in Sandau (2005). Available products on the market can be found in Figure 2.2.

Digital aerial cameras can be divided into two different groups, depending on the design of the camera, the following techniques have arised for recording:

- *pushbroom based or linear array digital aerial camera systems*

  Those kind of systems scan the terrain as the aircraft moves forward. Usually more than one Charge-Coupled Device (CCD) is used for forward, backward and nadir scanning. The image recording is, in this technology, not frame based but continuous. The post processing of these kinds of data is very time consuming and complex. Even color information can be scanned parallel, but in lower resolution. The techniques have originally been developed for satellite remote sensing. Satellites like, Landsat, SPOT or IRS work with this technology (Perko, 2004) as well as the digital aerial camera from Leica (ADS 40 and ADS 80).

- *area based digital aerial camera systems*

  These systems are based on frames. They have typically one or more sensor arrays that record image data. The sensor images are stitched together and geometrically corrected in a further post processing step.

The basic components of a digital aerial camera consist of the sensor unit with CCD(s) and lens system, storage unit(s), which store(s) the collected

Figure 2.2: Overview of the digital aerial cameras available

data and a computing unit, which communicates between all units (Scholz and Gruber, 2009). During a flight, further equipment, as *Global Positioning System / Inertial Navigation System (GPS/INS)* for correct positioning, *Inertial Measurement Unit (IMU)*, for measuring camera movements, and a *mount*, for correcting turbulences during flight, is needed (Kraus, 2002).

Digital aerial cameras have a method implemented to compensate motion blur in flight direction, which is called *Forward Motion Compensation (FMC)*. To avoid this kind of blur, the electronic charge on the CCD is already shifted in flight direction during exposure depending on the aircraft speed and altitude. This method is called Time Delay Interval (TDI) (Perko, 2004). To avoid motion blur across flight direction cameras are fixed in a mount, which equalizes the movements of the aircraft across flight direction. The IMU is recording the movements of the camera, which are later used in post processing for a correct positioning of the recorded frames in the aerotriangulation step.

After the production flight the image data is being downloaded from the data unit to another storage media and further post processing in the office can be done. This postprocessing is usually performed with a software developed by the camera manufacturer. Geometric and radiometric corrections, defined in a calibration, are added to the images which are registered to each other, and in case of a multi-sensor approach stitched together. Further pansharpening steps and color adjustments can also be performed during post processing. More technical details about the cameras used in this thesis can be found in (Gruber, 2005).

2.4 Color Characteristics of Digital Aerial Cameras

The main advantage of digital aerial cameras comparing to analog aerial cameras are the parallel recording of panchromatic and multispectral information. Today most digital systems record more than 12 bit of color information. Three or even four channels (including infrared data) are recorded in parallel to panchromatic data (Scholz and Gruber, 2009).

There are different concepts how multispectral information can be recorded with digital aerial cameras. The color can be collected with three separate, monochrome CCDs having color filters in the front of the objectives (for red, green and blue) in a lower or equal resolution as the panchromatic channel. There is another possibility with a single CCD with a Color Filter Array (CFA), where the color filters are directly installed on the CCD. The missing color information is reproduced by demosaicking algorithms. Again, the size of the resulting color image is equal to or smaller than the

final panchromatic image. The last and latest developed method is the Direct Image Sensor technology where, similar to the analog film, red, green and blue are collected with one CCD and in the complete resolution of the sensor realising this with a special layer technique.

The investigation in this thesis is based on digital aerial cameras with Bayerpattern technique and with separate monochrome Red, Green and Blue color channels. Both have lower resolution than the final, stitched panchromatic image.

2.4.1 Band separated sensor color collection

Color images that are generated out of three monochrome image sensors with color filters in the front of the objective are easier and faster to process as no reconstruction needs to be computed. The only step necessary in post processing is the registration of the three channels to each other and a correct and accurate calibration so that no color bloomings are visible in the final image. The disadvantage of collecting color with three separate sensors is the space for the installation that is necessary in a camera and the distance required to photograph the same objects, as three separate "cameras" are used. Figure 2.3 shows the basic principle for a band separated sensor color collection.

Figure 2.3: Sensor Unit of UltraCam Xp (UCXp) - a sensor that is collecting the color separately with three CCDs with R, G, B and IR color filter

2.4.2 Color Filter Arrays

The Bayerpattern is a well known CFA with a defined ordering of Red, Green and Blue color filters on a CCD-array as it can be seen in Figure 2.4. There are other sensors available with different RGB patterns but the Bayerpattern is the most widely spread CFA pattern on the market.

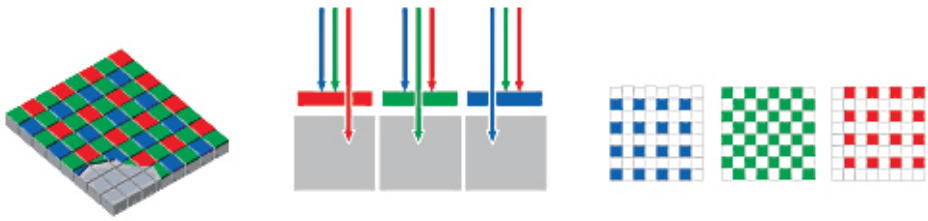

Figure 2.4: Overview how information on a Bayerpattern sensor is collected (source: Foveon (2009))

The raw image coming from the sensor is still grayscale (see figure 2.5). Different techniques for extracting the correct color information over the complete sensor size are available, those methods are named demosaicking algortihms. The reconstruction of the RGB values is depending on the neighbouring pixels and on the algorithm, which information is used. Typically, information about edges or color shifts are incorporated for a better reconstruction performance. Two examples for demosaicking algorithms of CFA with Bayerpattern are Hirakawa and Parks (2005) and Malvar *et al.* (2004)). The main advantage for the CFA is the space needed inside a camera for collecting the information on the contrary to the band separated color collection. The con is that the color is not recorded purely, as the missing pixels are reconstructed from the other two colors.

2.4.3 Direct Image Sensors

Direct image sensors are a new technology developed by the company Foveon (Foveon, 2009). This technology combines the main advantage of the analog film, to record red, green and blue color in parallel, and digital film in recording the information digitally. Three layers record the colors, as the light with different wavelengths go through the silicon wafer. Blue is collected in the first layer, green in the second and in the third layer the red portion of light is collected. Figure 2.6 gives an overview about how this technology collects color information.

As this technology is new, it is slowly entering the market. A few camera models have already installed this sensor technique and communities as for

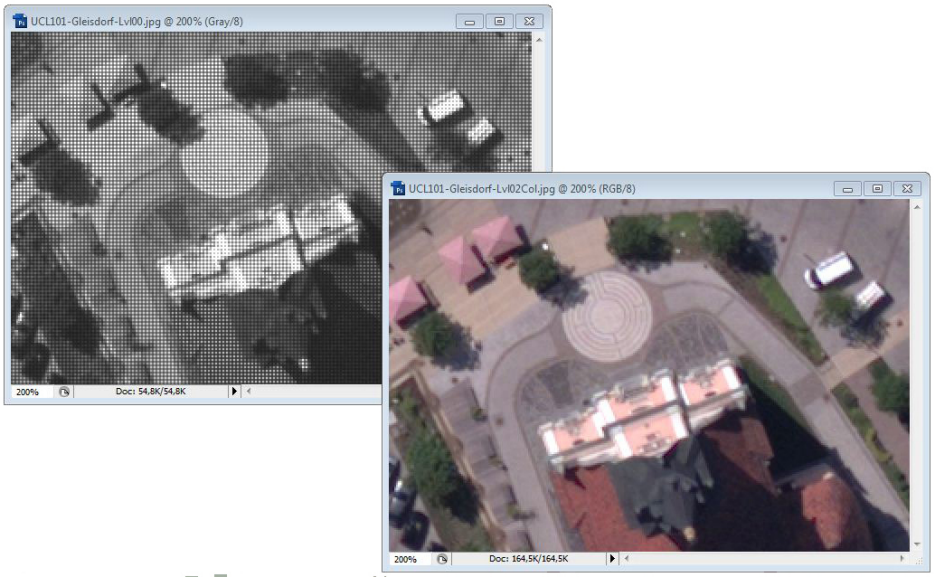

Figure 2.5: Raw Bayerpattern image (back left image) and final demosaicked image (front right image)

Figure 2.6: Direct image sensor by Foveon, collecting red, green and blue color information parallel (source: Foveon (2009))

example DPreview are testing and evaluating the quality of these kinds of sensors.

2.4.4 Filters

Besides the sensor technology, another inevitable influencing factor is how the color filters (band pass filters) have been manufactured. There are several techniques on the market. The filters described above in section 2.4.1 and 2.4.2 are so called *absorption filters* (Braunecker, 2005). These kinds of filters separate the colors according to the wavelength. The disadvantage of these filters is that the wavelengths partially overlap and all three colors contain portions of the neighbouring colors. These kind of filters are typically used for area based digital aerial cameras.

For pushbroom based cameras there is another technology available for collecting color. They use so-called *interference filter* which allow a more accurate color separation (Braunecker, 2005). These kind of filters consist of multiple thin layers with different refraction indices.

Typically with digital aerial cameras it is necessary to use *Ultraviolett/-Infrared (UV/IR)- cut off filter* to cut off unwanted infrared portions of the light. *Antivignetting filters* are sometimes used for a better uniformity throughout the complete image. These filters avoid the decrease of illumination when going away from the center of an image (Lillesand *et al.*, 2004).

2.4.5 Dynamic Range (DR) and Signal to Noise Ratio (SNR)

The *Full Well Capacity (FWC)* is defined as the maximum output signal of the camera system, which is still linear or in other words, the threshold until the signal is still saturated. The *DR* is defined as the ratio of this FWC and the cameras photo responsitivity (Sandau, 2005) and is given in [db].

The *SNR* represents the ratio of the original camera signal to noise (Sandau, 2005; Kraus, 2002). The noise can have different reasons. One important matter for noise is the dark current, which is an thermical effect of photons without incidence of light. This effect can be reduced by cooling the sensor. Further reasons are shot noise, output amplifier noise or reset noise (Sandau, 2005). A correct and well exposed image can reduce the noise to a minimum. How the SNR ratio can be computed and more details for noise can be found in Sandau (2005) and Kraus (2002).

2.5 Radiometric Camera Calibration and Spectral Sensitivity

As digital aerial cameras are measuring instruments of high precision they need to be calibrated radiometrically and geometrically. A detailed explanation about the calibration for the digital aerial camera of the UltraCam series by Vexcel Imaging GmbH can be found in Felber (2007). As this thesis focuses on radiometry and colors of digital aerial cameras it picks out the relevant information necessary for radiometric calibration.

To avoid vignetting and pixel defects on the sensor side, it is necessary to perform a radiometric calibration of a digital aerial camera. The vignetting of an objective can be found out by photographing a white surface which is equally illuminated. Image series are recorded at all aperture and exposure time settings and the resulting images are averaged. The resulting mean

image is usually brighter in the centre of an image than in the corners. The resulting vignetting image is then used to equalize the brightness in the complete image to get an equally balanced image. This is not necessary if an antivignetting filter is used which improves the uniformity of irradianve throughout the image plane (Albertz and Wiggenhagen, 2009).

Furthermore, CCDs and Complementary Metal Oxide Semiconductor (CMOS)s are produced with pixels without the ability to collect information, so called dead or defect pixels, as well as pixel cluster or columns which have not the full capacity. Those pixels need to be detected during calibration procedure. Usually this is being done by photographing a white surface and taking an image in the dark to find misfunctioning pixels. During the calibration processing a software can detect those pixels that do not work (properly). Those pixels are marked and interpolated during postprocessing when the calibration information is being attached to images collected with the specified camera. Depending on the manufacturer, the quality and size of the product, up to thousands of pixels can be affected on a CCD.

The sensitivity of the camera system is defined by the sensor itself, the lens system, the filters and the cover glass from the camera body. The final spectral sensitivity is defined as the integral of the product of the multiplications of the above mentioned influencing factors for a camera (Kim and Kautz, 2008):

$$R = \int L(\lambda)\rho(\lambda)D_r(\lambda)d\lambda \tag{2.1}$$

$$G = \int L(\lambda)\rho(\lambda)D_g(\lambda)d\lambda \tag{2.2}$$

$$B = \int L(\lambda)\rho(\lambda)D_b(\lambda)d\lambda \tag{2.3}$$

where $L(\lambda)$ describes the spectral power distribution of the light source, $\rho(\lambda)$ describes the reflectance of the imaged object and $D_{r/g/b}(\lambda)$ describes the spectral responsitivity of the camera system. Figure 2.7 shows a sample for a spectral sensitivities curve for the three channels Red, Green and Blue for the Canon EOS 300D.

2.6 Summary

This section discusses all relevant theory out of Remote Sensing and Photogrammetry which is relevant for the investigations in this thesis. Basic techniques about radiometric image fusion are mentioned as well as the de-

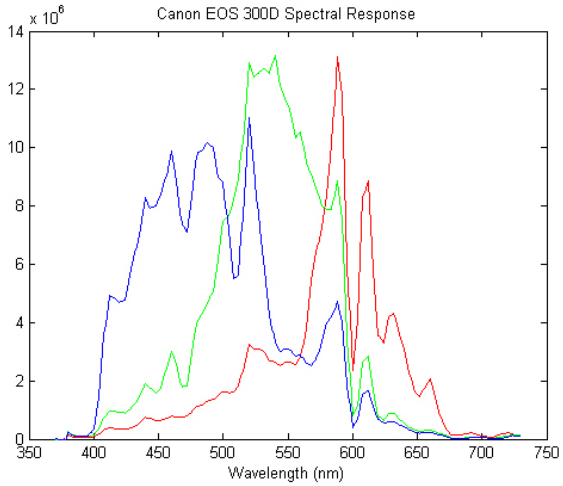

Figure 2.7: Spectral sensitivity diagram of Canon EOS 300D (source: http://scien.stanford.edu/class/psych221/projects/07/camera_characterization, accessed on: 03/12/2009)

sign of digital aerial cameras are being introduced. To get an overview about the market situation the actual digital imaging systems are presented with the most important specifications. A focus is set on issues influencing the recordings of colors for digital cameras and the details concerning the radiometry, which is another further essential part when working with colors, is being discussed.

Chapter 3

Color Theory

The topic of this thesis covers fields of research in remote sensing and color theory. The aim is to use methods developed in color theory on images from optical sensors in the field of remote sensing. Color theory mainly focuses on images from video systems or digital still imaging systems. Standards in color theory try to create a complete color workflow to guarantee that colors that have been recorded, appear in the same color in output medias (as screens, analog media as paper, etc.). This thesis presents investigations which are essential to be able to work with standardized colors and use the advantages they bring up as

- color correction for devices
- color transformation into different, device dependent color spaces

This chapter deals with the main color spaces, the introduction of different kind of methods in color theory for the transformation into different color spaces and the introduction of further possible color adjustment methods. Furthermore, information about the standards developed by the International Color Consortium (ICC) are introduced in the last section of this chapter.

Color is a complex and broad topic. Albertz and Wiggenhagen (2009) define the term *color* as follows:

> *"... is the visual effect generated by electromagnetic radiation incident on the retina of the human eye. But color is also understood as a property of an object and is dependent on the wavelength of the light it reflects."*

According to Johnson and Fairchild (2003) a human observer percept a color depending on the following factors and variables:

- spectral properties of the stimulus

- light source
- size, shape and spatial properties
- relationships of the stimulus
- background and surrounding
- observer experience

All those factors influence the appearance and perception of color for a human observer. As those factors show the perception of color is a very subjective process making it nearly impossible to find a metrics to measure color. For this reason different color spaces have been defined in which color can be described mathematically and independent from observers point of view (Albertz and Wiggenhagen, 2009).

3.1 Color Terminology

In order to discuss the basics of the different color spaces and further concepts, ideas and methods in color theory some definitions are necessary. The following section gives an overview about the most important terms in color research. All definitions have been taken from Johnson and Fairchild (2003) and Reinhard *et al.* (2008).

Color is part of the visual perception of a human observer and depends, as mentioned above, on the spectral distribution of a color stimulus, on the observer's experience and relationships to the stimulus and the shape, structure and size. *Related color* is being perceived to belong to an area of object seen in relation to other colors. On the contrary to this *unrelated color* is being perceived as belonging to an area being in isolation from other colors.

Stimulus describes the color element of interest.

Hue is an attribute of perception. The human observer combines the perceived color with well known colors as for example red, green, blue, yellow etc. *Achromatic color* are colors being perceived as devoid of hue, *chromatic colors* are being perceived as possessing hue.

Brightness is the attribute of visual sensation to which a stimulus appears to be more or less intense. *Lightness*, on the contrary, defines how much a similarly illuminated area is being perceived to be "white". The lightness is also often defined as *relative brightness*. Furthermore it is noteworthy that only related colors can exhibit lightness.

Colorfulness describes how an area appears to be more or less chromatic, it is also known as *chromaticness* in literature.

Chroma defines the proportion of the colorfulness of an area as the proportion of the brightness of a similarly illuminated area (appears nearly white) and can be computed as follows:

$$Chroma = \frac{Colorfulness}{Brightness(White)} \tag{3.1}$$

Saturation describes the degree to which the colorfulness of an area is judged in proportion to its brightness.

$$Saturation = \frac{Chroma}{Lightness} \tag{3.2}$$

Metamerism describes the effect that two colors appear to be equal under a certain illumination and when observing those two colors under different illumination appear to be different (Gierling, 2006).

3.2 Color Spaces

As mentioned in the introduction for this chapter, the perception of color is very subjective. For this reason, a color system was developed which allows to describe color in mathemtical terms. The Commission Internationale de l'Eclairage (CIE) started to standardize and merge knowledge and experiences about color in 1931. The result was mainly a first standardization under which circumstances (illumination) colors can be judged and how they shall be described (Gierling, 2006). This section describes the most important and commonly used color spaces.

3.2.1 CIE XYZ Color Space

The underlying theory of the CIE are three color matching functions Color Matching Function (CMF) which have been defined in 1931 (CIE 1931), based on the so-called standard observer. A number of people matched colors against a mixture of monochrome colors (red, green and blue) resulting in the corresponding color matching functions x(λ), y(λ) and z(λ) (see Figure 3.1). The Formulas 3.3 to 3.5 represent the relative amount or the three

primaries X, Y and Z. The Y primary describes the luminance function of the human eye (*standard luminosity curve*, (Albertz and Wiggenhagen, 2009)).

$$X = \int L(\lambda)\rho(\lambda)x(\lambda)d\lambda \tag{3.3}$$

$$Y = \int L(\lambda)\rho(\lambda)y(\lambda)d\lambda \tag{3.4}$$

$$Z = \int L(\lambda)\rho(\lambda)z(\lambda)d\lambda \tag{3.5}$$

(Kim and Kautz, 2008)

Based on the above mentioned formulas, the computation of the spectral response of digital aerial cameras, as discussed in chapter 2.5, have been developed (Formulas 2.1 to 2.3). The standard observer (averaged observation of the test people) has been defined by an average observer with a field of view of about 2° in the main view direction, which is equivalent to an area of about $9.57cm^2$. To fit better to the human cognition a further standard observer with 10° area was introduced in 1964 (CIE 1964). To be able to reconstruct the exact colors in experiments with color matching the CIE defined the follwoing standard illuminations (Reinhard *et al.*, 2008):

- A - corresponds to a tungsten-filament lightning with 2856K
- B - corresponds to noon sunlight with 4874K
- C - corresponds average daylight at 6774K
- D - describes all standard illuminations corresponding to natural daylight, the exact color temperature is defined further with the two numerals following the character D. The most important daylight standard illuminations are mentioned below:
  - D50 - usually taken in the printing industry, is allocated between artifical light with 2800K and perfect daylight of 6500K
  - D65 - described the color temerature of daylight with 6500K
- E - describes equal energy radiators, it is mainly used as a theoretical reference
- F - corresponds to various types of fluorescent lightnings, similar to the D standard illuminants F is subdivided into F1 to F12 types

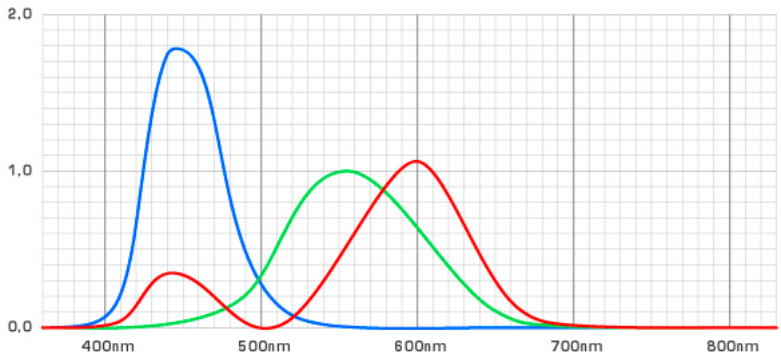

Figure 3.1: Normalized color matching functions x(λ) in red, y(λ) in green and z(λ) in blue (source: http://de.wikipedia.org/wiki/CIE-Normvalenzsystem, accessed on 2009/07/25)

A complete list with detailed description about all standard illuminants and derivations can be found in (Reinhard *et al.*, 2008).

The resulting CIE XYZ color space describes all colors, a human can recognize. It is difficult to represent it graphically in a diagram, as it is three dimensional. For a better representation in a 2D diagram, three variables x, y and z can be computed out of X, Y and Z which describe the chrominance portion of each color. The Y of the CIE XYZ color space remains, as this parameter describes the brightness of luminance of a certain color. This variation of the CIE XYZ color space is also known as the *CIE xyY* color space. The formulas for computing those variables can be found in 3.6 to 3.8.

$$x = \frac{X}{X + Y + Z} \tag{3.6}$$

$$y = \frac{Y}{X + Y + Z} \tag{3.7}$$

$$z = \frac{Z}{X + Y + Z} \tag{3.8}$$

As x + y + z = 1 each coordinate can be reproduced by the two corresponding others, the chrominance of x and y can be represented in a 2D diagram, which is known as *CIE chromaticity diagram* (see Figure 3.2). The achromatic colors are all located in the exact center of the diagram (Gierling, 2006).

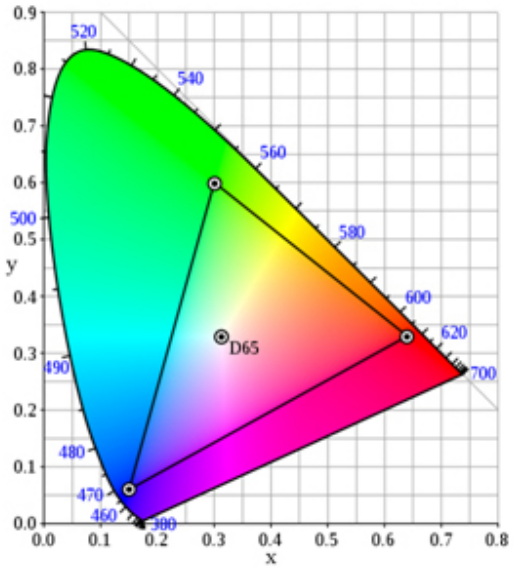

Figure 3.2: Chromaticity diagram of CIE xyY color space, with limitations of sRGB color space and D65 white point (source: http://en.wikipedia.org, accessed on: 2009/04/03)

3.2.2 CIE Lab Color Space

The main disadvantage of the XYZ color space and some other color spaces is that they do not represent any information about the relationship between colors. When looking at the chromaticity diagram, the red and green colors have a huge amount of the area compared to blue and yellow. For this reason the CIE developed further color spaces in the following years. In 1964 the Luv color space was developed which already had more focus on the relationships between colors. As this model is rarely used nowadays, it is mainly mentioned for completeness. Further information on this color space can be found in Reinhard *et al.* (2008).

In 1976 the CIE developed a further color space, which focuses on the relationships between colors. Again, three parameters are used for the description (Albertz and Wiggenhagen, 2009):

- L - luminance channel (the smallest L value describes black)
- a - chromatic component which defines the position of the color between red and green (the smallest a value is green)
- b - chromatic component which defines the position of the color between blue and yellow (the smallest b value is blue)

The Lab values, which have equal distances between colors can be com-

puted by the following formulas:

$$L = 116 * [f(\frac{Y}{Y_n})] - 16 \tag{3.9}$$

$$a = 500 * [f(\frac{X}{X_n}) - f(\frac{Y}{Y_n})] \tag{3.10}$$

$$b = 200 * [f(\frac{Y}{Y_n}) - f(\frac{Z}{Z_n})] \tag{3.11}$$

X_n, Y_n and Z_n represent the values of the reference white values. The following formulas are necessary if X, Y and Z are bigger:

$$f(\frac{X}{X_n}) = \sqrt[3]{\frac{X}{X_n}} \qquad if \frac{X}{X_n} > 0.008856 \tag{3.12}$$

$$f(\frac{Y}{Y_n}) = \sqrt[3]{\frac{Y}{Y_n}} \qquad if \frac{Y}{Y_n} > 0.008856 \tag{3.13}$$

$$f(\frac{Z}{Z_n}) = \sqrt[3]{\frac{Z}{Z_n}} \qquad if \frac{Z}{Z_n} > 0.008856 \tag{3.14}$$

If the values are smaller the following formulas shall be used:

$$f(\frac{X}{X_n}) = 7.7867 * \frac{X}{X_n} + \frac{16}{116} \qquad if \frac{X}{X_n} \leq 0.008856 \tag{3.15}$$

$$f(\frac{Y}{Y_n}) = 7.7867 * \frac{Y}{Y_n} + \frac{16}{116} \qquad if \frac{Y}{Y_n} \leq 0.008856 \tag{3.16}$$

$$f(\frac{Z}{Z_n}) = 7.7867 * \frac{Z}{Z_n} + \frac{16}{116} \qquad if \frac{Z}{Z_n} \leq 0.008856 \tag{3.17}$$

When presenting the above computed values L, a and b graphically this can be done in the form of a sphere with values for a and b between -128 to +127 and for L between 0 and 100. This sphere is shown in Figure 3.3.

3.2.3 LCH Color Space

The LCH color space is a further development of the Lab color space with a focus on the human perception of color. The L channel stays the same as in the Lab color space. The positive a-axis of the Lab channel is the reference and the angle to the color describes the hue(h). The distance from the centre

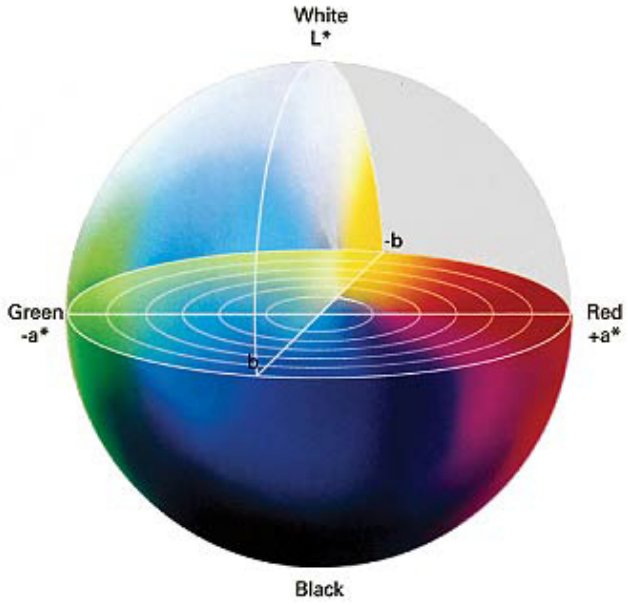

Figure 3.3: Graphical representation of the CIE Lab color space (source: http://www.newsandtech.com/issues/2002/02-02/ifra/images/42Lab.jpg, accessed on 2009/07/25)

of the sphere (achromatic colors) to the color is described as the *Chroma(C)*. The Chroma ranges from 0 (achromatic) to 128 (maximum chroma). Figure 3.4 shows the LCH color space in the graphical representation. The following formulas are necessary to compute out of Lab values the corresponding LCH values:

$$L = L \tag{3.18}$$

$$C = \sqrt{a^2 + b^2} \tag{3.19}$$

$$h = arctan(\frac{b}{a}) \tag{3.20}$$

3.2.4 Color Difference Formulas

The most important properties the Lab and LCH color space have, besides the equal relationships between colors is the possibilty to measure the color difference. This is very important when it comes to measure color qualities and differences in colors. The follwoing formula can be used to compute the color difference ΔE:

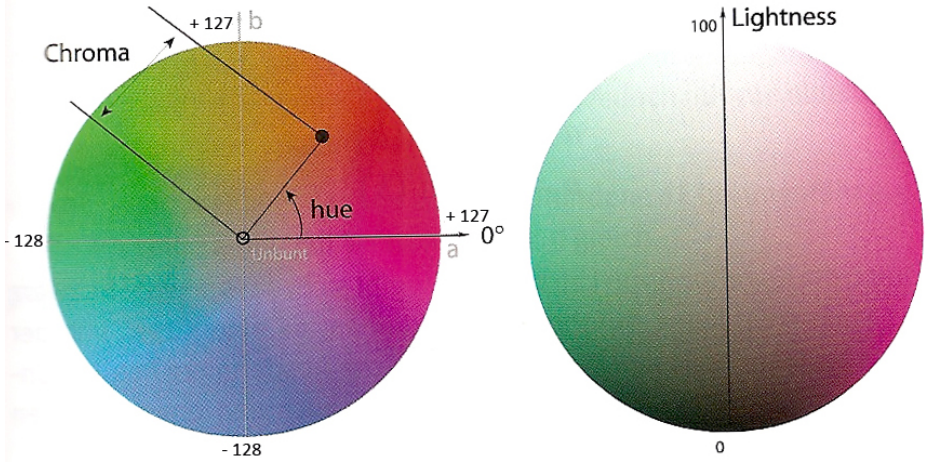

Figure 3.4: LCH color space (source: Gierling (2006)

$$\Delta E = \sqrt{(L_1 - L_2)^2 + (a_1 - a_2)^2 + (b_1 - b_2)^2} \tag{3.21}$$

$$\Delta E = \sqrt{(\Delta L)^2 + (\Delta a)^2 + (\Delta b)^2} \tag{3.22}$$

Parallel to the above mentioned formula, ΔE value can be computed for the LCH color space:

$$\Delta E = \sqrt{(\Delta L)^2 + (\Delta C)^2 + (\Delta h)^2} \tag{3.23}$$

$$\Delta L = L_1 - L_2 \tag{3.24}$$

$$\Delta C = C_1 - C_2 = \sqrt{(a_1^2) + (b_1^2)} - \sqrt{(a_2^2) + (b_2^2)} \tag{3.25}$$

$$\Delta H = \sqrt{(\Delta a)^2 + (\Delta b)^2 - (\Delta C)^2} \tag{3.26}$$

3.2.5 Device Dependent Color Spaces - RGB and CMYK

All above explained color spaces are device independent color spaces. They are used for computation, evaluation and standardization purposes. When it comes to reproducing or recording colors, the device dependent color spaces are necessary. These kinds of color spaces usually cannot represent all colors humans can perceive, due to this, they are called device dependent color spaces. The range of colors they can represent are called the *color gamut*. Each device has its own gamut. When it comes to transforming between

different color spaces, it is possible that the gamuts of two color spaces / devices do not fit together. To find out which color is used to represent colors in the new gamut is a very actual topic in color research. This problem is called *gamut mapping* (Reinhard *et al.*, 2008). The topic gamut mapping is discussed in section 3.4.

The RGB color space is a device dependent color space. This color space consists of three primaries: Red (R), Green (G) and Blue (B). It is usually used for recording devices such as digital cameras and scanners as well as for output devices as for example screens. RGB is an additive color space; which means, when mixing the three primary colors red, green and blue at the same intensities the resulting color would be white (Albertz and Wiggenhagen, 2009). In Figure 3.2 the gamut of the sRGB color space is represented. Figure 3.5 shows the RGB color space as a cube. The complementary colors to the RGB colors are those from the CMYK color space. Red has as its complementary color Cyan, Green has Magenta and Blue has Yellow as complementary color. Black to white can be found in the diagonal.

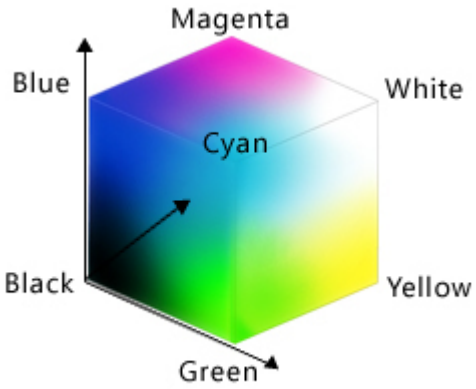

Figure 3.5: RGB cube (source: http://msdn.microsoft.com, accessed on 2009/07/25)

The CMYK color space, on the contrary to the RGB color space is a subtractive color space. In other words this means when summing up Cyan (C), Magenta (M) and Yellow (Y) the resulting color will be Black (K). Usually this color space is used with output devices as printers. They use the advantage of adding all colors until they reach black color. The model was enlarged by the black component, as the printing quality rises when using an additional black ink (Albertz and Wiggenhagen, 2009).

As those two color spaces are complementary, the conversion is easy to handle with the following formulas (Gierling, 2006):

$$C = 1 - R \tag{3.27}$$
$$M = 1 - G \tag{3.28}$$
$$Y = 1 - B \tag{3.29}$$

Going back to the RGB color model, several standardization efforts have been done in the past years:

- Apple RGB
- Adobe RGB
- CIE RGB
- sRGB
- Wide Gamut RGB

A complete list of all known RGB color spaces with transformation matrices for the conversion into device independent color spaces can be found on the website of Bruce Lindbloom (2003).

3.2.6 Hue-Saturation-Lightness Color Spaces

The Hue-Saturation-Lightness spaces are deformations of the RGB color cube. There are several variations of these spaces where the lightness channel is being replaced by intensity (HSI) or value channels (HSV). Another variation is the HCI space where the saturation is being exchanged with the chroma channel. All those channels are linear transformations from the RGB color space and with this share the main disadvantage of being device dependent (Reinhard *et al.*, 2008). The advantage compared to the RGB color space is that they split color information from the intensity/lightness. This fact is used in remote sensing when it comes to pansharpening or image fusion techniques as already mentioned in chapter 2.1. As for those applications the IHS color space is the most important space, this one is represented below and the other color spaces which fall into this category can be found in detail in Reinhard *et al.* (2008).

The following three primaries are used for the IHS color space (Albertz and Wiggenhagen, 2009):

- Intensity (I) - represents the brightness, ranging from black to white

- Hue (H) - represents the dominant color wavelength
- Saturation (S) - represents the purity of the color

The conversion from RGB to IHS can be computed as follows (Gonzalez and Woods, 2002):

$$H = \begin{cases} \theta & if B \leq G \\ 360 - \theta & if > G \end{cases} \tag{3.30}$$

$$I = \frac{R+G+B}{3} \tag{3.31}$$

$$\theta = cos^{-1} + (\frac{\frac{R-G}{2} + (R-B)}{\sqrt{(R-G)^2 + (R-B)(G-B)}}) \tag{3.32}$$

$$S = 1 - \frac{3}{R+G+B}[min(R,G,B)] \tag{3.33}$$

The inverse transformation from IHS back to RGB is defined as follows (Gonzalez and Woods, 2002):

If $0° < H \leq 120°$

$$R = I(1 + [\frac{S\cos H}{\cos(60° - H)}]) \tag{3.34}$$

$$G = 3I - (R+B) \tag{3.35}$$

$$B = I(1-S) \tag{3.36}$$

If $120° < H \leq 240°$

$$H = H - 120° \tag{3.37}$$

$$R = I(1-S) \tag{3.38}$$

$$G = I(1 + [\frac{S\cos H}{\cos(60° - H)}]) \tag{3.39}$$

$$B = 3I - (R+G) \tag{3.40}$$

If $240° < H \leq 360°$

$$H = H - 240° \tag{3.41}$$

$$R = 3I - (G+B) \tag{3.42}$$

$$G = I(1-S) \tag{3.43}$$

$$B = I(1 + [\frac{S\cos H}{\cos(60° - H)}]) \tag{3.44}$$

The graphical representation of the IHS color space is cone-shaped as it can be seen in Figure 3.6.

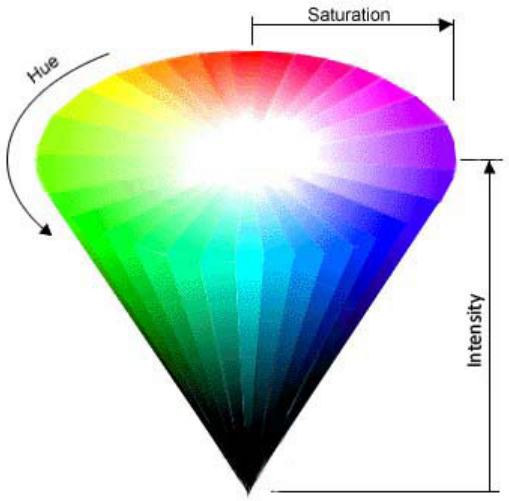

Figure 3.6: IHS cube, where brightness indicates the intensity (source: http://www.ai.rug.nl/vakinformatie/pas/pictures/hsi.jpg, accessed on 2009/07/26)

3.3 Color Space Transformations

In order to tranform colors between different spaces, depending on the color space, different methods are avaliable. Fixed transformations have already been mentioned in the sections above. For standardized color spaces, as the sRGB or Adobe RGB color space, well defined transformation matrices are available. A complete list of those transformation matrices can be found on the webpage of Bruce Lindbloom (Lindbloom, 2003).

Especially when it comes to device dependent color spaces the transformation is challenging, as the gamut of the devices differs. As the device independent color spaces comprehend the complete color spectrum of the human perception, the device dependent colors are usually transformed into the device independent color spaces. Further applications can then transform it into another device dependent color space without any knowledge about the source color space (Vrhel and Trussel, 1999). In order to make an accurate color transformation, several techniques have been developed in color research which are described in the following sections.

3.3.1 Color Characterization for Devices

In the first step, a device needs to be color calibrated and then in a further, second step, the device needs to be characterized. The calibration describes the fixed and known color response. Those color responses usually vary,

depending on the signal processing in a device, from a known reference. Those characteristics of a device can be derived by color measurements and the deriving of color correction functions (Bala, 2003). The characterization process aims to find the relationship between a device-dependent and a device-independent color representation for a calibrated device (Bala, 2003).

To compute this transformation function F_{device}, it is necessary to have color information from the device and the according reference information. If the device is a recording device like a camera or scanner, the function F_{device} is sufficient, if the device is used for reproduction the function F^{-1}_{device} needs to be computed as well (Vrhel and Trussel, 1999). According to Bala (2003) there are two methods for deriving the color characterization relationship:

- based on a model - parameters that describe the physical process by which a device captures or renders colors are derived
- based on empirical results - many samples together with mathematical fitting techniques as splines are used to derive the characterization function

The output of a characterization process are mappings between device-dependent and device-independent color spaces. These are usually implemented as Look Up Table (LUT) or transformation matrices. This information is stored in a so called device profile. The ICC has developed standards how these characterization information needs to be stored in those profiles. Further details are described in section 3.5.

3.3.2 Mathematical Background

The basic mathematics behind color theory is given in the paper of Vrhel and Trussel (1999). The following section summarizes facts out of this paper that are necessary for understanding the experiments in chapter 4 and the results in chapter 5 in this thesis.

For further explanation on color transformation functions, it has been proved in color theory that a vector notation is well suited. For this reason samples of the visible spectrum (from 400 to 700nm) are assumed as N and the illuminant spectrum as $l(\lambda)$, where the vector l contains N elements. The vector r represents the spectral reflectance of an object and contains N elements. Lr represents the reflected radiant spectrum of an object under the illuminant l with the spectral reflectance r. A is a $N\ x\ 3$ matrix containing the color transformation functions into the device independent (eg: CIE XYZ) color space. Therefore the device independent color values for Lr can be computed as follows:

$$t = A^t L r \tag{3.45}$$

A big issue in profiling and creating transformation functions for color space transformations is the illumination. Typically, a transformation function is created for a particular illumination situation. The illumination is important as colors can be different under different illuminations (metamerism effect). The nearest solution would be to create a profile for every illumination situation, which is impossible in most cases. Therefore, mappings can be defined for changes in illumination. Depending on the device there are different methods available. As this thesis focuses on digital aerial cameras, this topic is being discussed. Further information on other color (re)producing devices can be found in Vrhel and Trussel (1999).

Let L_r be the illumination of the recorded image and L_v the illumination when the profile has been created. The newly recorded image under illumination L_r records the following values:

$$c_i = N^T L_r r_i \tag{3.46}$$

and the profile has been created with the following values:

$$d_i = N^T L_v r_i \tag{3.47}$$

If the illumination differs, this is visible in the images when applying the profile recorded with a different illumination than the picture has been taken. Therfore it is necessary to find a mapping B between the two illumination situations which is shown in formula 3.48 The resulting illumination correction needs to be applied to c_i.

$$B_{illum} = arg(\min_{B} E||B(c) - N^T L_v r||^2) \tag{3.48}$$

Linear Least Squares Regression

When the response of a device is known to be linear, the transformation between the device dependent and device independent color space can be

computed by a linear least squares transformation as follows in formula 3.49.

$$m = (P^t P)^{-1} P^t A \tag{3.49}$$

where m describes a 3 x 3 transformation for the device characterization. P is a linear, typically RGB response from a device (in this case the digital camera) and A contains the reference values in the device independent color space. This transformation matrix can now be used to compute the device independent color space values for all values coming from the defined device (Kim and Kautz, 2008).

Robust Least Squares Regression

Wolf (2003) suggests a robust least squares regression technique to alter the accuracy of the transformation matrix. This is an iterative least squares approach with a cost function to reduce the weight of outliers. It starts with the same algorithm as already presented above in the linear least squares regression and introduces in a further step a cost vector which is derived from a normalized error vector and again used for a further least squares fitting, but this time introducing the cost weights. This is done iteratively until the weight is too small to have any influence. The complete description of the algorithm can be found in Wolf (2003).

Polynomic Regression

If the response coming from a device is not linear, the above described two methods are not applicable. In this case it is necessary to obtain the transformation matrix using a multiple polynomial regression technique. Yoon and Cho (1999) suggest several derivations how to obtain the transformation matrix. In this thesis, the 2^{nd} order masking matrix was used to test the polynomic regression method (see section 4.3.3).

3.4 Further Investigations on Color

This section gives an overview about further important algorithms and methods in color theory for a finer and more accurate color adjustment. These methods are explained shortly and due to time limitations not evaluated in

this thesis. This is a major part for future investigations and analysis.

As already mentioned in the previous section, the illumination during characterization is very important. When computing the transformation matrix, the white point of the RGB (device dependent) and CIE XYZ (device independent) color space remains the same. It may be necessary to change the white point for further investigations as some other data was recorded with a different white point or under a different illumination. In the CIE XYZ color space there are well defined transformations that can be used to transform the XYZ values from one standardized illumination to another. Those transformation matrices are known as *chromatic adaption models*. The most widely known and used models used in color theory are the following (according to Johnson and Fairchild (2003)):

- von Kries
- Fairchild
- Bradford
- XYZ Scaling

Lindbloom (2003) lists the transformation matrices, also known as *Chromatic Adaption Transform (CAT)* for the three models and all illumination conditions (A to F). Johnson and Fairchild (2003) describes the definition of the models in more detail. Von Kries was the first that described an chromatic adaption model. Mainly all above mentioned models work on the same principle: the XYZ values shall be transformed into a cone response domain. Gain control coefficients, which can map between the source and the reference white, need to be found and in a further step need to be transformed back to XYZ color space using the inverse transformation. The result of all CAT methods are linear 3 x 3 transformation matrices. The difference between the models are mainly the method how they find the gain control coefficients.

The term *gamut mapping* was already mentioned before when explaining device dependent color spaces. This topic is a very actual one in color theory. Sharma *et al.* (1998) lists the most important methods for gamut mapping and defines the term as

[...] the process of mapping the displayable colors from one media to those of another media.

There are several different approaches how the gamut mapping can be done. The easiest approach is to simply clip colors that do not appear in the gamut of a device or media. Another, already improved approach is to map

colors out of gamut to nearest-in-gamut colors. This brings already better results, but still this method can lead to unwanted hue shifts. For this reason normally restrictions are implemented to map colors as for example to the nearest-in-gamut color but with the same hue. Furthermore compression techniques are used to compress colors which ensures that all colors fit into a gamut of a device but the colorimetric dynamic range decreases. Details about actual developments in the research of gamut mapping algorithms can be found in Morovic (2003).

3.5 ICC Profiling

The ICC has created a standard for all kinds of input and output devices to manage color in the same manner. Figure 1.1 gives an overview of how colors should be managed according to the ICC. Color profiles for devices describe the transformation of colors of a device into a device independent color space, the so-called Profile Connection Space (PCS). Details about the standards defined by the ICC can be found in ICC (2004) and is used as basis for the following section.

The PCS is based on the CIE XYZ or CIE Lab color space and the main challenge is to manage the color gamuts of different devices, that the colors are represented correctly. Four different rendering intents are described in the standard to match color gamuts. The two colorimetric rendering intents operate directly on color values, in relation to a white point and the media which lies beyond. The color values are normalized according to the media white point and then used for transformation. The standard white point in PCS is defined as D50. This method is defined as the *relative colorimetric intent*. This approach inevitably changes the colors in reproduction. When an exact color reproduction is necessary for all colors inside a gamut the *absolute colorimetric intent* can be used.

The *perceptual rendering intent* includes tone scale adjustments and gamut warping techniques if gamut mismatches happen. This rendering intent is usually used for pictorial images. The *saturation rendering intent* is mainly used for images containing for example charts to keep the pureness of hues. Both rendering intents are vendor specific.

Which rendering intent is being used, depends on the purpose for which the images are used. Depending on the rendering intent, different transformations can be specified in the color profiles. Usually the perceptual rendering is used for natural images. A detailed discussion when which rendering intent shall be used can be found in ICC (2004).

The *Color Matching Module (CMM)* is needed for the computation be-

tween the color spaces. The ICC profiles manage the converting of colors from the device color space into the PCS. There are seven classes of ICC profiles, where the three classes for input devices, display devices and output devices are the most widely spread. The general structure of a color profile according to the ICC can be found in Figure 3.7. The *Profile Header* contains information about the device itself. According to Gierling (2006) the following elements are the most relevant in the header of the profile:

- CMM Type - describes which CMM should be privileged, if non is specified the standard CMM is used
- Device Class
- Color Space - the device space
- PCS - which device independent color space should be used, XYZ or Lab
- Device Manufacturer and Device Model
- Rendering Intent
- XYZ-Illuminant - white point of the illumination, standard is D50 and 2°observer

The *Tag Table* is the table of contents for the tags and specifies where which tag is stored and how large this tag is. The *Tags* contain the information about color transformation itself. There are several tags, depending on the device, which are obligatory, optional and others that can be used for further (private) specification. According to Huneke (2002) the tags can be grouped into

- general information tags - such as profile description, copyright, calibration date or device model
- matrix tags - contains a 3x3 transformation matrix and Tone Reproduction Curve (TRC) for all color channels
- LUT tags - contains multidimensional LUTs and input and output curves
- whitepoint tags - such as media white point and chromatic adaption matrix
- postscript tags

The color transformation is stored in the tags in the form of a LUT or a transformation matrix. To assure a linear transformation from a device dependent color space into a device independent color space and vice versa curves can be defined. In the case of the matrix transformation the linearization is computed with the definition of so called TRCs. ICC profiles based on transformation matrices have a small size, just a few kb and can only be used for RGB to XYZ conversions. These kind of profiles are typically used fo for screens. LUT based profiles, on the contrary, are used for output devices, such as printers, and for scanners and digital cameras. As those profiles contain multidimensional LUTs in 8bit or also 16bit space they have large sizes up to 1.5 mb. Depending on the rendering intent and direction of transformation there are different tags defined. A LUT in an ICC profile contains of the following parts:

- 3x3 matrix (usually not used, only for a PCS in XYZ color space)
- Input Curve - 1D input table
- multidimensional LUT - CLUT
- Output Curve - 1D input table

The input and output curve are used for a tonal correction before and after the transformation. The supporting points can vary, depending on the accuracy necessary.

To be able to create a device profile, there are several tools to use. For an input device such as a scanner, special targets are available, which are scanned. A software measures the scanned color values and compares them with the reference color values and calculates a color profile for a scanner from this difference. Special mouses for display devices like Liquid Crystal Display (LCD) screens for example are available which measure the displayed colors. A software can create a profile for the LCD screen out of the measured and reference values. A similar procedure is necessary for profiling printers. In this case printed color targets are measured with a special mouse and compared with the reference values in the software. There are several companies on the market that provide solutions for all three device classes as for example X-Rite (http://www.xrite.com/home.aspx) or Datacolor (http://www.colorite.com/) and many more. More details about available software and hardware can be found in Gierling (2006).

To see the effect when assigning different ICC profiles to images, Figure 3.8 shows a color target with different RGB ICC profiles assigned. The original image was created out of the reference values in sRGB color space as it can be seen in the upper left corner. Photoshop was used to assign

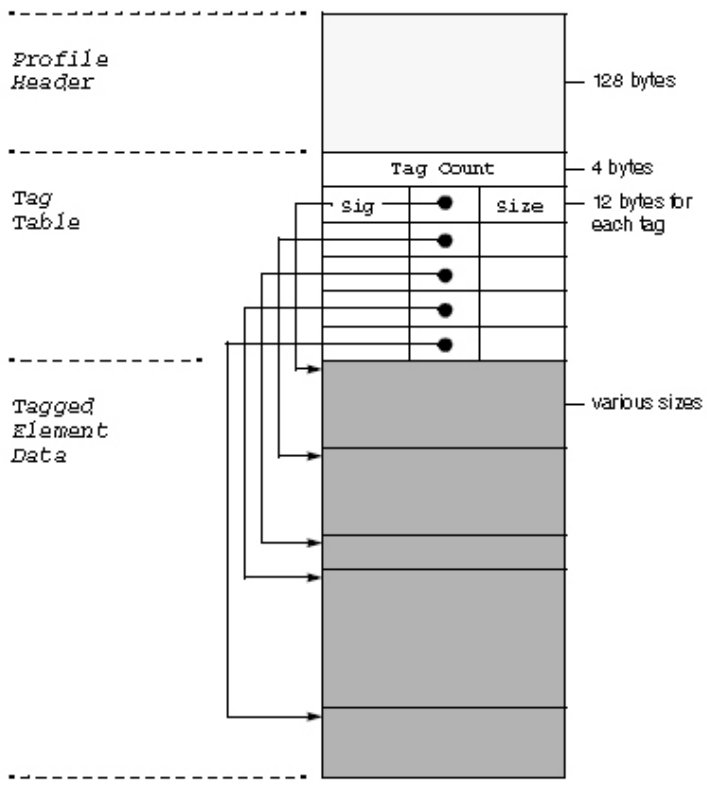

Figure 3.7: ICC profile structure according to the ICC (source: ICC (2004))

different ICC profiles of the RGB color space. Differences to the sRGB color space (in this color space the image has been created) and the CIE RGB and Wide Gamut RGB color space can be seen in the blue colors. The ProPhoto RGB color space has problems with red and magenta color tones as the patches with different chroma cannot be distinguished well. The CMYK color patches from the sRGB color space are most similar with those of the Adobe RGB color target.

3.6 Summary

This section discusses all relevant theories which are necessary for the investigations and analysis for the characterization of digital aerial cameras in conjunction with color theory. The necessary methods and terms of color theory are defined. The main color spaces used in color theory are being introduced and transformation methods are being discussed. More details

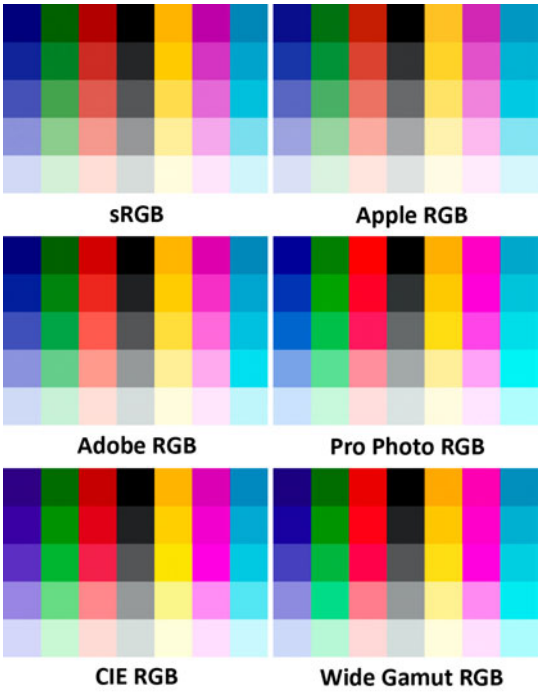

Figure 3.8: Synthetic image of a color target created out of reference values with different ICC profiles assigned

about the ICC and the developed standards and how they are structured and used is described in section 3.5. The combination of the techniques out of remote sensing / photogrammetry and color theory is being immersed in the following chapters.

Chapter 4

Practical Experiments and Investigations

The practical experiments have been performed in a calibration lab of Microsoft Photogrammetry. Further data has been collected with various cameras during production testflights in the area of Graz and Gleisdorf in Styria, Austria. This chapter gives a description of the calibration setup and details about the performed tests and investigations.

To be able to work with a sensor with radiometric quality the stability of reproduction must be given. The cameras used in this thesis have been evaluated and proven. Schneider and Gruber (2008) have made a detailed analysis concerning radiometric stability and bandwidth of the images produced with cameras of the UltraCam series. At that time the Bayerpattern sensor - camera model has not been on the market and not been tested. This has been performed before starting with the work for this thesis. Based on that facts the further work can be done without further concerns to radiometric instability.

4.1 Calibration Setup

The recording of the color targets is the first step in order to make a color device characterization. It is inevitable to produce those images under well known light conditions. The calibration setup used to perform tests with the digital aerial cameras UltraCam Xp (UCXp) and UltraCam L (UCL) is shown in Figure 4.1. The setup is equal for both cameras. The light sources are HEDLER D04 lights which produces even, flickerfree, daylight at a color temperature of 5600K. Two of those lights are used to equally lighten the target. The lights are located beside the camera and lighten the target at an angle of 45°.

The setup, as described above, is the final arrangement after several tests. To avoid influences by variations of the shutters or vignetting, different setups have been tested. The influence of both, shutter and vignetting, can be neglected as the influence amounts less than 2% in a 16bit space. The main problem was to find a light source with equal, flickerfree light

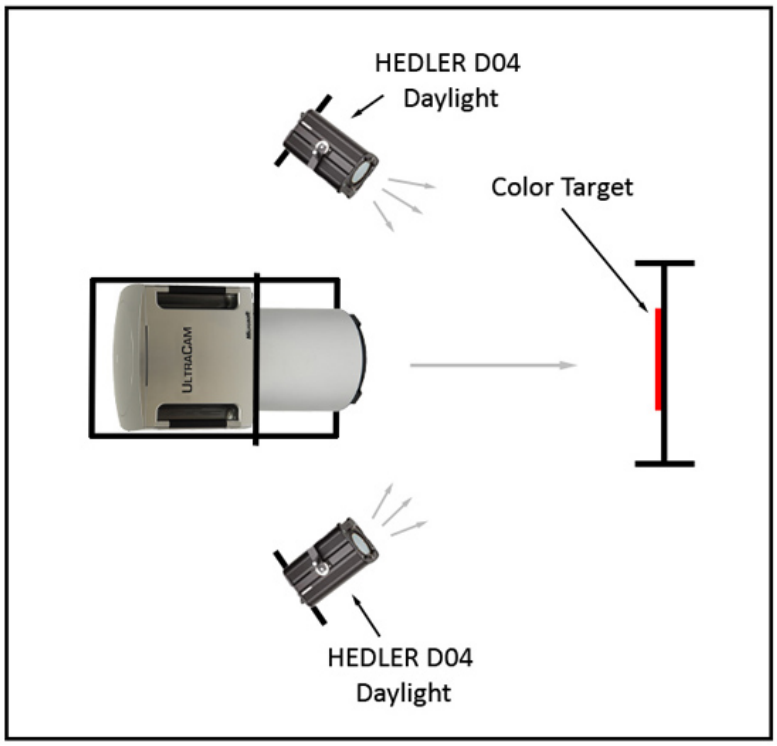

Figure 4.1: Calibration setup for device characterization

distribution. The chosen light source guarantees this and the analysis of the image series shows this as well. The stability of the light source is in every case sufficient for further color analysis. In addition, the light source was cross-checked with flash- and daylight to assure the quality of the light source. These tests showed that the HEDLER lights produce light similar to daylight.

Ryan and Pagnutti (2009) describe another approach how to calibrate a digital aerial camera with the help of an Ulbricht sphere. This setup was not possible as no Ulbricht Sphere was available for the tests in the calibration lab. In addition, such a big Ulbricht Sphere which fits for a complete digital aerial camera is unaffordable. That is the reason why a white board as background and a flickerfree daylight source was used for our calibration tests.

The color target for the calibration lab has been created especially for the purpose of color characterization of the digital aerial cameras. The chosen color patches are a subset of the Kodak IT8 target. The patches are bigger than on usual color targets to cover a bigger area of the produced image, as the CCD is in comparison to a consumer camera bigger. The colors for

the patches have been chosen, as they cover colors of the RGB and CMYK color space. Figure 4.2 shows the target.

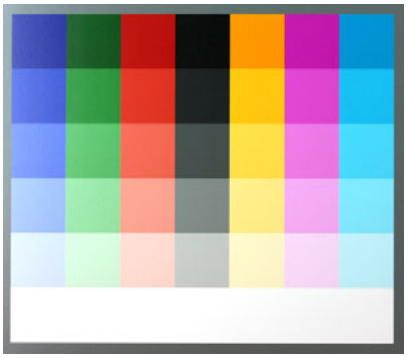

Figure 4.2: Color target used for camera characterization with 42 color patches in three primary colors of RGB and CMYK color space and 6 black to white patches, with neutral gray tones. Each color patch has a size of 10 x 10cm.

To be able to analyze different behaviours of the camera, images with different exposure times and aperture settings have been recorded. Furthermore, image series of 20 images have been taken. The color values over a complete patch and over the 20 images have been averaged to exclude any measurement errrors and influences of noise. Images with all available aperture from F5.6 to F22 have been recorded. During recording of the images, a focus is set on the appropriate exposure for each aperture, as well exposed images are essential for further analysis. Too bright images would bring in non-linear portions of the sensor as well as too dark images would lead to noise in the resulting images.

To check the results of the calibration it is necessary to have defined color information also from the outside under real, production conditions. As with every delivered camera a testflight is performed, outdoor targets are placed in the testflight area. Those color targets have a size of 50x100cm and are recorded at a GSD of about 10cm. In Figure 4.3 the outdoor targets are shown. The testflight is planned so that the targets appear in different parts of the images (center and corner areas of the images).

The material of the outdoor targets are a challenging topic. There have been several tests and evaluations performed by Honkavaara and Markelin (2007), Schönermark *et al.* (2009) and Weber (2009) with targets out of tarps, gravel (for different gray densities), different roof colors and plastics. All materials have pros and cons. The main problem is that nearly all materials are anisotrop, or in other words, the colors change slightly depending on the illumination. Being aware of the anisotropic property of the targets, coloured plastic boards have been bought and used.

The spectral sensitivity curves for both cameras are well known and

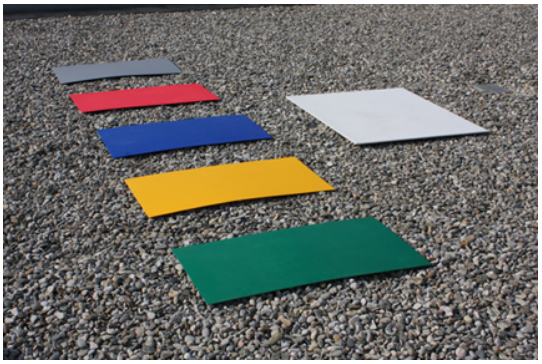

Figure 4.3: Outdoor targets on the roof of the office building of Microsoft Photogrammetry

coming from the corresponding calibration report, which is delivered with each camera. Figure 4.4 and Figure 4.5 show the corresponding spectral sensitivities for the UCL and UCXp cameras which are used for further experiments in this thesis. These figures show also the Near Infrared (NIR) channel, which is collected in parallel with panchromatic and RGB color information during recording. It is mentioned here for completeness, but not used for the investigation, as this thesis is focused on RGB colors.

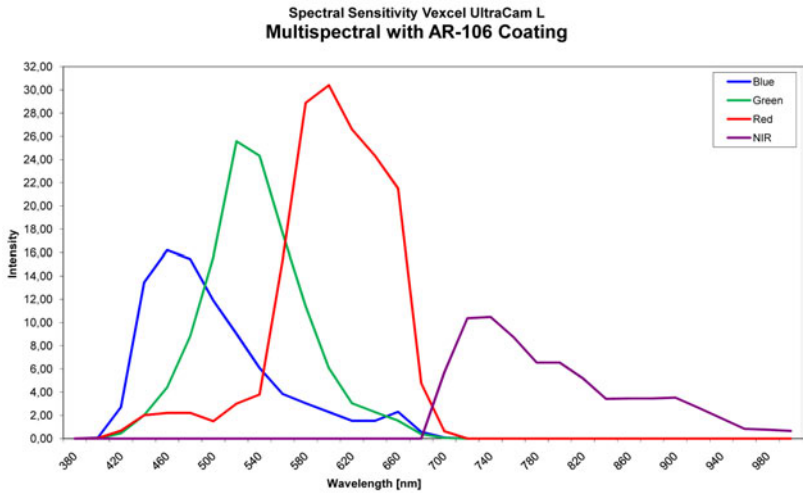

Figure 4.4: Spectral sensitivity diagram of the UCL camera series

4.2 Reference Information

To create a color characterization of a digital camera it is necessary to have reference information about the used targets. As mentioned before, the color target is created out of patches from the Kodak IT8 target. This brings the

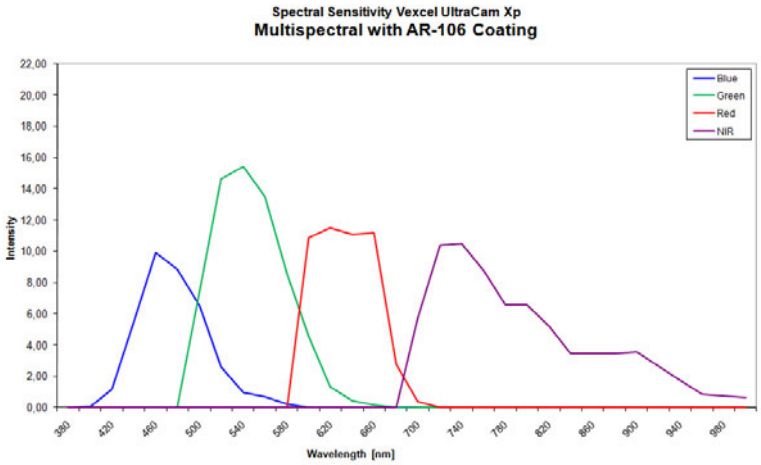

Figure 4.5: Spectral sensitivity diagram of the UCXp camera series

advantage that the color patches have already defined color values which can be used as reference information for the investigations.

For the verification of the reference material a spectrometer was used to measure the colors of the color target in the calibration lab and outdoor during a testflight. The Avantes AvaSpec-2048 (http://www.avantes.com) has been used to verify the available reference information. Figure 4.6 shows the available reference information and confronts the collected reference information with the spectrometer (top) and the original reference data from the Kodak IT8 target (bottom).

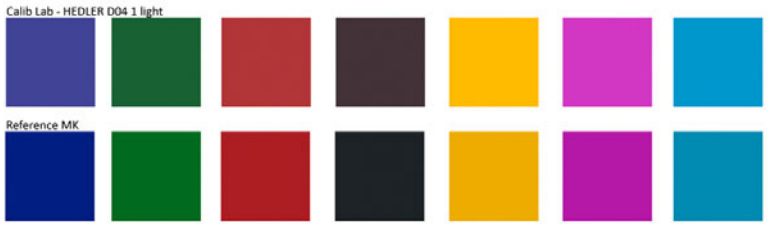

Figure 4.6: Available reference information (top: verification with spectrometer, bottom: original reference data from Kodak IT8 target)

The outputs of the spectrometer are color values for all measured patches in device independent color space coordinates as XYZ, Lab or Lhc. These coordinates can, in a further step, be used for the conversion of the recorded color target values with the cameras (RGB color space) into a device independent color space.

The targets have been measured under different illuminations. Besides the measurement under lab conditions (with the daylight lights HEDLER

D04) measurements have been performed under real daylight conditions. In addition, the outdoor targets have also been measured to have specific color values for all further investigations.

4.3 Color Transformation

For the device characterization it is necessary to apply a color correction and transformation (into another color space). Different kind of techniques for this transformation and color correction are described in chapter 4.7. An important issue which should not be neglected is the correct white- and black-balancing before device characterization. In this case, as the images are averaged and it is exactly known which colors appear in the reference image, the darkest, lowest value in each channel is assumed to be responding to black color and the brightest, highest value is assumed to represent white. The following methods have been tested and evaluated to find the best suiting for the available UCL and UCXp camera series:

- Spline interpolation in white to black color patches (for red, green and blue channel)
- Linear Least-squares regression method
- Robust Least-squares regression method
- Polynomial regression method

A first approach was to use the black to white color patches in a 2D diagram and interpolate a spline in the corresponding values. But already the first results showed that the spline interpolation methods are not sufficient for the needs of an digital aerial camera device characterization. The spline interpolation does correct intensities but not the colors themselves. As a result the intensity of the image is being adjusted but the colors are not changed as it can be seen in Figure 4.7.

The next three methods produced better results as they are proven methods in color theory. The theoretical background of these methods have been shown in chapter 3.3.2 and is being discussed in detail in the following sections. All methods below work basically on the same principle. A color transformation matrix (m) is being computed and in a further step this matrix is multiplied with the original RGB image data values. Depending on which color space the reference information is used for the calculation of the transformation matrix the color correction and transformation can be performed. For example, when the reference information contains reference values in the RGB color space, the transformation matrix includes

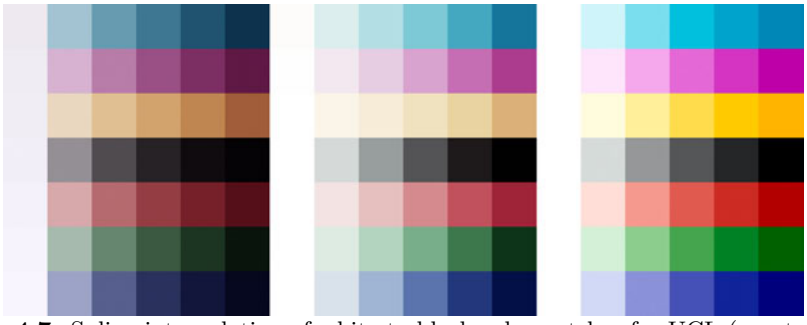

Figure 4.7: Spline interpolation of white to black color patches for UCL (aperture F8). The left image shows the original image coming from the camera, the center image shows the result after applying the spline correction and the right color target shows the referenced used for creating the spline

information for color correction. In another case, when the reference information contains XYZ or Lab values, the calculated transformation matrix can be used to perform the color correction as well as the transformation into another color space. This principle is being used for the analysis and evaluation. Below each method is evaluated visually in the RGB color space, and in comparison to the other methods with the help of the chromaticity diagram in xy color space and with the resulting ΔE values in Lab color space. All figures below show the results of the Bayerpattern sensor (UCL). The corresponding images for the band separated camera can be found in Appendix A.

4.3.1 Linear Least Square Regression Method

The linear least square regression method computes a 3x3 transformation matrix with the following formula:

$$m = (RGB^t * RGB)^{-1} * RGB^t * RefRGB \tag{4.1}$$

where *RGB* stands for the recorded RGB values with the camera, and *RefRGB* represents the reference values from the color target, in this case in RGB values.

The result applied to the color target image can be seen in Figure 4.8. The correction is already very promising but still there are some visible differences especially in the ”full color” patches on the left side of the target. The main advantage of this method is that the image is changed only linearily which is especially for further processing steps important, as the sensor response is not changed in an unexpected matter, and remains linear.

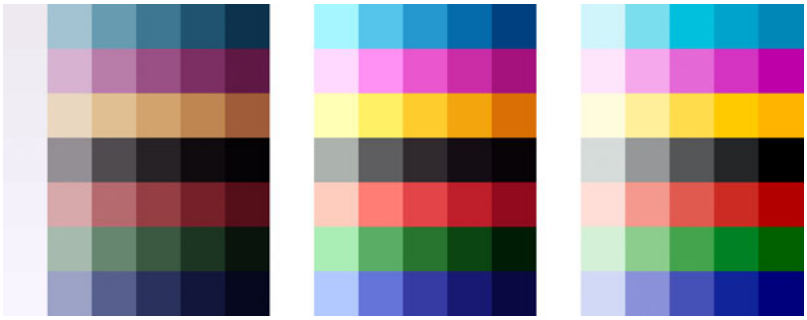

Figure 4.8: From left to right: UCL image, linear least square fitted image and reference image

4.3.2 Robust Least Squares Regression Method

Wolf (2003) suggests to optimize the linear least squares regression in the following manner: A normalized cost vector is introduced to minimize errors. The result is a 4x3 transformation matrix. The following formula is used iteratively until the error is as small as possible:

$$m = (RGB^t * cost * RGB)^{-1} * RGB^t * cost * RefRGB \tag{4.2}$$

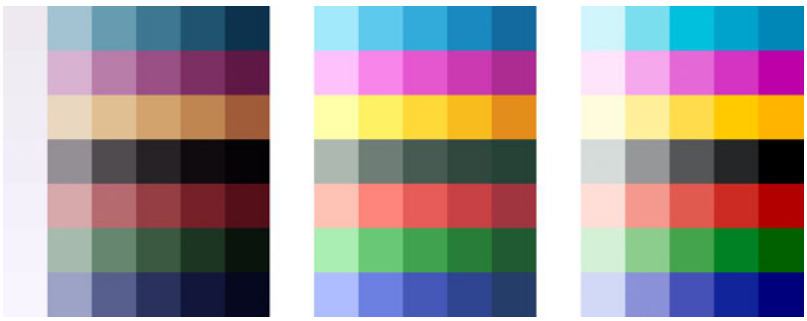

Figure 4.9: From left to right: UltraCam L image, robust least square fitted image and reference image

The results are very promising as it can be seen in Figure 4.9. There is one main problem that the white-to-black color patch line has a tendency to green. But nevertheless, the colors on the right side of the target fit better to the reference than the linear least square method result.

4.3.3 Polynomial Regression Method

The polynomial regression method is a special form of the least squares method. The RGB input is polynomial weighted. It is possible to introduce different degrees of the polynom, in this case a second order polynom was used as this produced the best visual results. The following input is used:

$$RGB_{new} = [R, G, B, (R * G), (G * B), (B * R), R^2, G^2, B^2] \tag{4.3}$$

As a conclusion the result of this method is a 9x3 transformation matrix. The follwing formula is used to compute the matrix m:

$$m = (RGB_{new}^t * RGB_{new})^{-1} * RGB_{new}^t * RefRGB) \tag{4.4}$$

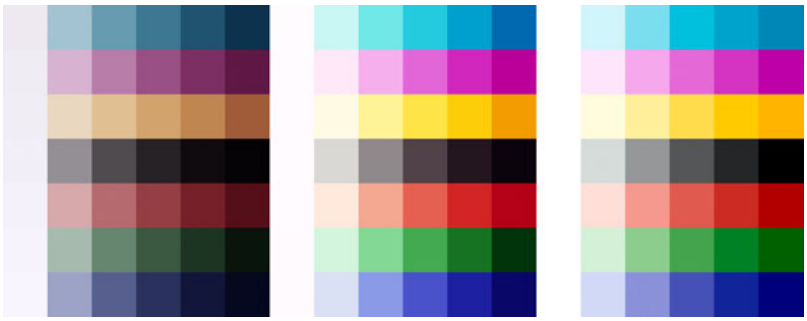

Figure 4.10: From left to right: UltraCam L image, fitted image via polynomial regression and reference image

Figure 4.10 shows the results of the polynomial regression method. Comparing to the other two results, this transformation seems to work best as besides the colors also unlinear portions of intensities are corrected. The main difference is, that the darkest green patch is too dark and all other patches seem to fit well in a visual quality check.

4.4 Software

The postprocessing of the raw image data is done in OPC, the office processing software (Vexcel Imaging GmbH, 2009) by Vexcel Imaging GmbH. Here the radiometric and geometric calibration information is added to the images. The color images are registered to the panchromatic image and the result are the complete 16bit image information stored as TIFF images. This data is used for all analysis and evaluation presented in this thesis.

To analyse the collected, postprocessed data and compute the color transformation matrices the mathematical software package MathWorks Matlab R2006b (The MathWorks Inc., 2009) is being used. Several scripts have been written to average and extract the necessary information for further evaluation and calcualtions. The computation of the color transformation matrices and numerical analysis and quality evaluation is also performed in Matlab. The visual quality checks and analysis are performed in Adobe Photoshop CS3 (Adobe Systems Inc., 2009). Furthermore a cluster analysis is performed in Clark Labs IDRISI Taiga (Clark Labs, 2009) and in Matlab to evaluate the performance of color corrected images in regard to for further GIS and Remote Sensing applications.

4.5 Summary

In this chapter the practical experiments are explained. The setup of the calibration and the outdoor and indoor targets are presented. The verification of available reference data with a spectrometer is shown and the three methods chosen for evaluation of color transformation and correction are discussed. The main formulas and first results with the color targets give already a first impression. In the last section of this chapter the software used for the complete analysis in this thesis is named.

Chapter 5

Detailed Comparison, Anaylsis and Results

The color target figures in chapter 4 give a first impression about the quality for color correction of each method. All three methods bring already an improvement when it comes to reproduce accurate color information. But as visual checks are subjective, further analysis are necessary for an accurate and objective quality measurement. In the first part of this chapter, the sensors (band separated and Bayerpattern) are evaluated according to the reference target. In the following section the results of the two different sensors are confronted to give a first insight whether the approach using color theory for sensor fusion works or not. The chromaticity diagram in xyZ color space and the ΔE in Lab and LCH color space are used to evaluate the accuracy of color reproduction. All shown results are based on the images made with an aperture of F8. Those images have been used for this investigation, as this the aperture is recommended as preferred setting from the manufacturer (as images recorded with this aperture produce the most accurate and sharp images).

In the table in Figure 5.1 the computed Color Correction Matrix (CCM) for the three methods mentioned in chapter 4 are listed. These matrices are used for the computation of the new color corrected image in RGB color space. In all three colors (red, green and blue), the main proportion comes from the color itself. This can be observed in all three methods. Nevertheless, each color is influenced by the other two colors. This is important especially with the band separated camera, as this contains only pure color information. It is different with the Bayerpattern sensor, as the demosaicking already mixes red, green and blue for constructing the complete full resolution color image. The polynomic method has a more complex distribution of the proportions of colors as the Linear Least Squares (LLS) and Robust Least Squares (RLS) adjustment. The factors for the other aperture settings (F5.6, F11, F16 and F22) can be found in Appendix B. Summarized it can be said that the factors have no severe variation depending on aperture, the highest difference amounts up to 2 positions after decimal point.

The CCM have been calculated in the same manner as described above for the XYZ and Lab color space, in order to be able to evaluate the accuracy of color reproduction in other color spaces using well known accuracy

measures out of color theory.

UCXp				UCL		
LLS				LLS		
1,3	-0,06	0,21	R	1,74	-0,11	-0,13
-0,22	1,21	-0,6	G	-0,86	1,41	-1,12
0,05	0,04	1,58	B	0,24	-0,11	2,44
RLS				RLS		
0,14	0,24	0,21		0,15	0,26	0,21
1,14	-0,21	0,07	R	1,56	-0,27	-0,26
-0,19	1,21	-0,57	G	-0,7	1,54	-1,02
-0,04	-0,17	1,36	B	0,04	-0,48	2,13
Poly				Poly		
2,54	-0,31	0,25	R	3,15	-0,48	-0,5
-0,36	2,43	-0,9	G	-1,23	3	-1,72
0	-0,04	2,84	B	0,21	-0,41	4,37
1,98	0,23	0,29	RG	4,02	0,13	0,22
0,24	0,64	1,55	GB	1,11	2,08	3,91
-0,01	-0,18	-0,14	BR	-0,54	-0,23	1,3
-2,22	0,15	-0,22	R^2	-3,25	0,35	-0,43
-1,02	-1,73	-0,35	G^2	-2,02	-2,73	-1,05
-0,16	-0,21	-2,34	B^2	-0,46	-0,72	-5,11

Figure 5.1: Comparison of color correction factors for aperture F8 for LLS, RLS and Polynomic color correction method for both sensors

To visualize how colors are being changed, the corresponding values for a LUT curve has been computed. Figure 5.2 shows the LUT curve for the three adjustment methods for 16 bit images in RGB color space. The diagram visualizes only the pure red, green and blue values, no mixture of the three color channels. Apparently it can be seen that the first two methods, the LLS and RLS adjustment are linear methods, while the polynomic adjustment is represented as a fitted curve.

The RLS adjustment is still a linear method but the error minimization process leads to a great shift in the dark values. There is no fix black point anymore. The polynomic method fits a curve and no straight line. Here, the differences in intensity are better fitted than with the other two methods.

5.1 Accuracy for Single Sensors

In this section the band separated and the Bayerpattern sensor is evaluated separately, to check the accuracy in correspondence to the reference target. Firstly, the evaluation is performed in the xyZ color space with a visualization of the color patch values in the chromaticity diagram, and in a further section the ΔE values for each color patch of the target are listed

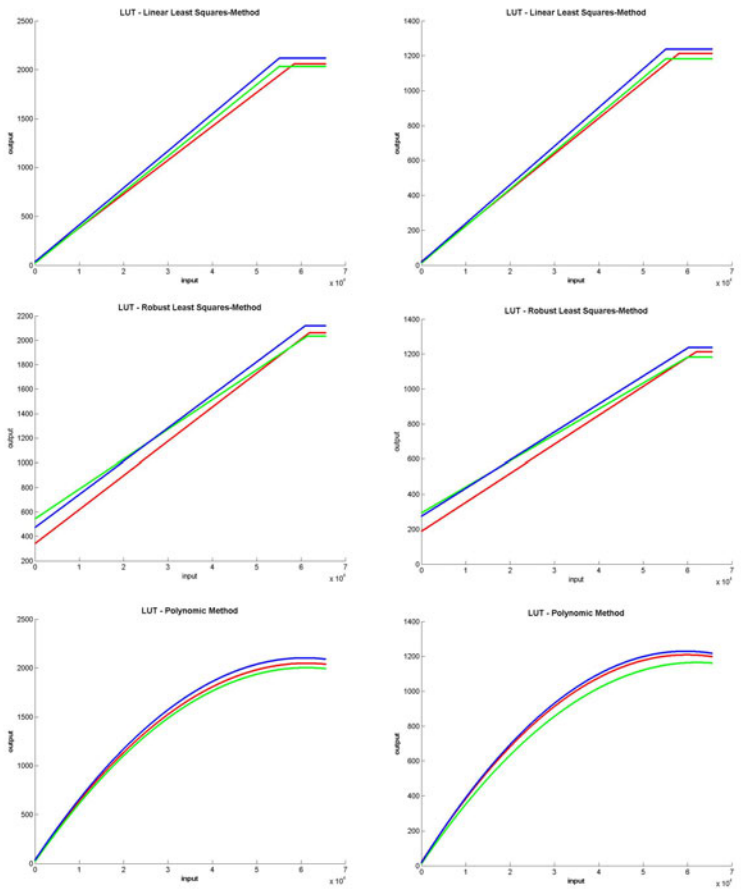

Figure 5.2: Comparison of Look Up Table (LUT) curve for LLS, RLS and polynomic adjustment for UltraCam L (UCL) (left side) and UltraCam Xp (UCXp) (right side) in Digital Number (DN)

and displayed in a chart.

To get a first insight about the degree of linearity of the data the reference values are confronted with the the original and furthermore with the color transformed image values of the band separated and Bayerpattern sensor. In an ideal situation all color values are located on a line going through the origin in a diagonal axis. All three methods show an improvement. Both sensors work best with the polynomic transformation matrix and show a better linearity than the other two linear methods. All values in Figure 5.3 and 5.4 are shown in RGB color space. Figure 5.3 presents the resulting charts for the red color channel of the Bayerpattern sensor. Figure 5.4 shows the results of the red channel of the band separated sensor image. The results for the green and blue color channels for both sensors can be found in Appendix B.

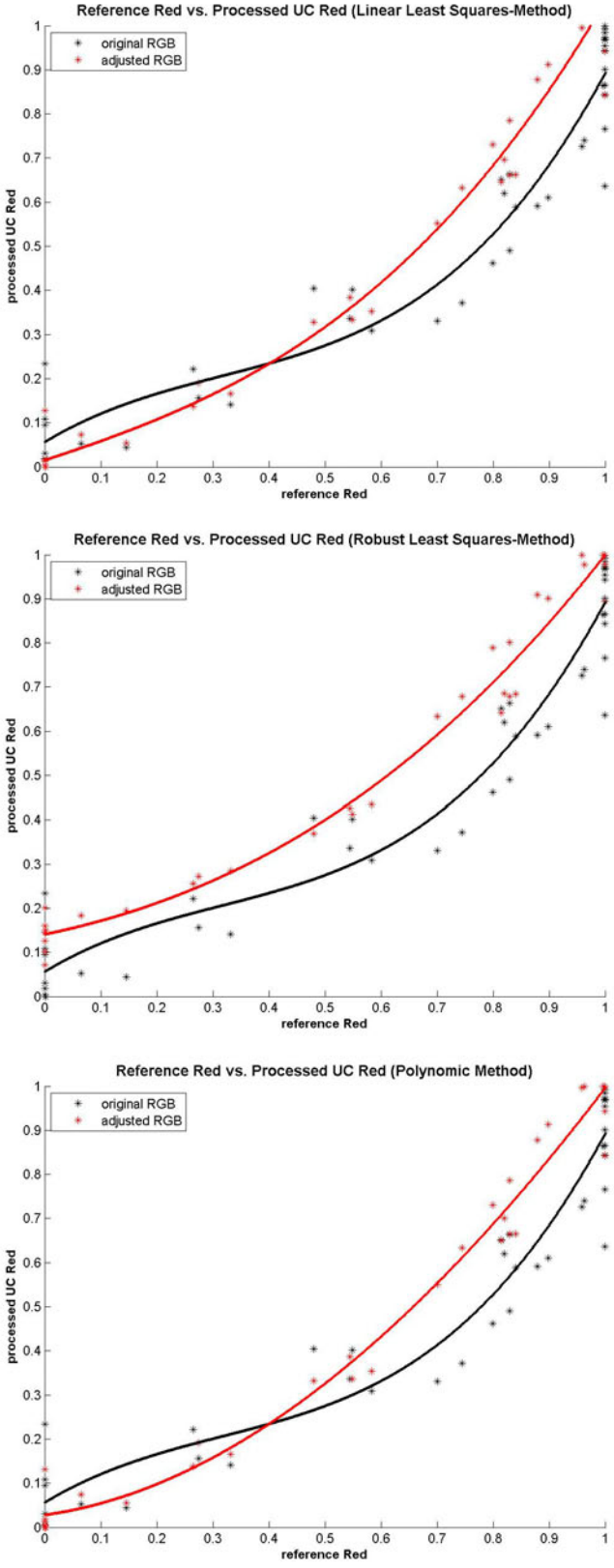

Figure 5.3: Linearity chart of the three color transformation methods for UCL and red color channel (aperture F8) in normalized DN

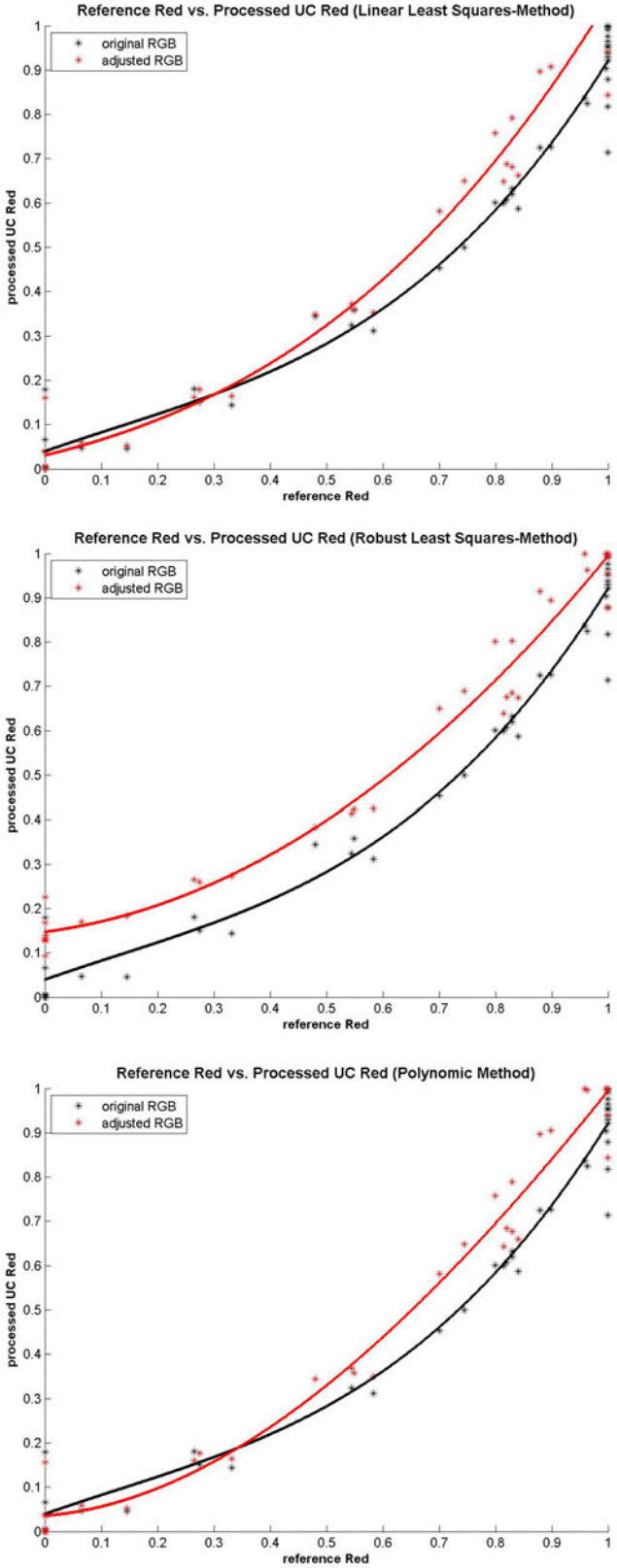

Figure 5.4: Linearity chart of the three color transformation methods for UCXp and red color channel (aperture F8) in normalized DN

Chromaticity Diagram Evaluation

When calculating x- and y-values out of the XYZ values, those coordinates can be displayed on a chromaticity diagram to get an idea which colors are being represented. Figure 5.6 shows the chromaticity diagram with the reference target values and the xy values resulting from the camera characterization for the band separated sensor. Figure 5.5 shows the same content with the Bayerpattern sensor results.

When displaying the convex hull about the xy values from the cameras the gamut of the camera can be defined. In this case the RLS method has one very prominent outlier, where the other two methods produce a better result. The tendency that the brighter colors fit better than the colors with the most chroma which was already visible in the color patches in RGB can here be confirmed. Especially in red this is very obvious for all 3 CCM.

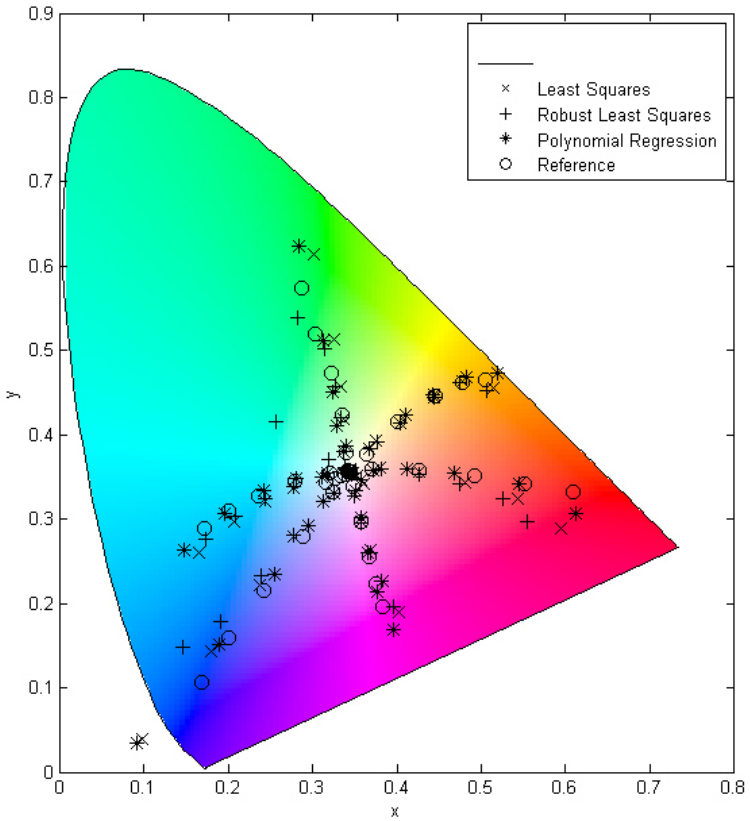

Figure 5.5: Chromaticity diagram with the xy values of the reference data and the xy results of the UCL image data (aperture F8)

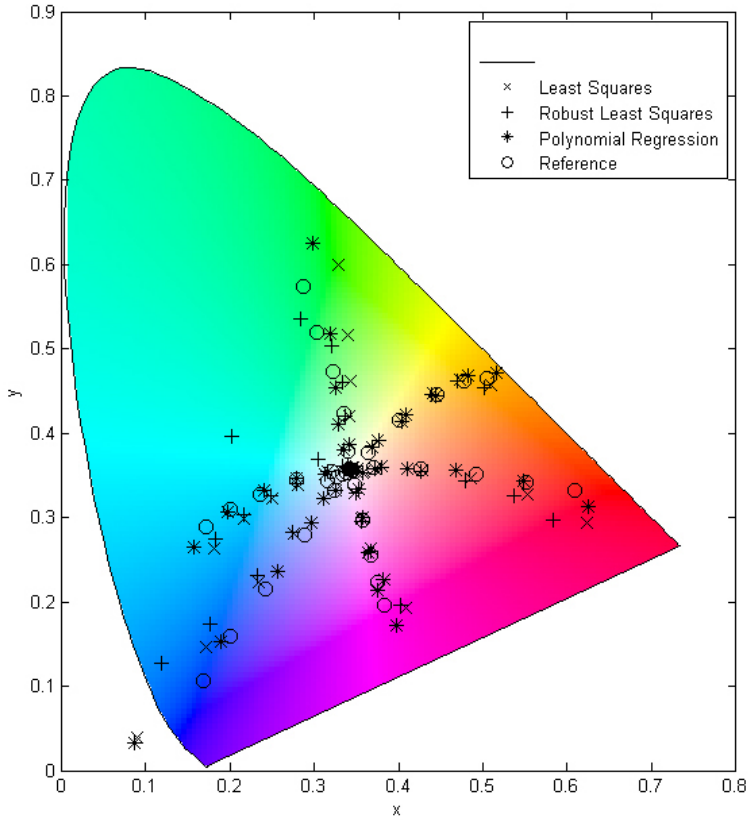

Figure 5.6: Chromaticity diagram with the xy values of the reference data and the xy results of the UCXp image data (aperture F8)

Δ *Lab and* Δ *LCH Differences*

The above discussed evaluation methods give an impression about the linearity and the accuracy in the xyZ color space. The ΔE values are being used in color theory and graphic industry to measure the accuracy of color representation. This value can be computed in the Lab or in the LCH color space. Both show the distance between two colors (in this case between the reference colors and the original colors, and between the reference colors and the results of the three transformation methods). The separate color patches are enumerated for a better and faster analysis, the numeration of the complete color target can be found in Figure 5.7.

For a better comparison, the original image data values of the color patches have been transformed into Lab and LCH color space with the standard transformation for sRGB color values offered by International Color Consortium (ICC), assuring that no device-specific color correction is applied. The Lab and LCH values of the color target are available and used

Figure 5.7: Numeration of the color patches of the color target for further investigations of the ΔE values

as reference to compute the ΔE values.

According to Gierling (2006) a ΔE value below ten indicates tolerable color differences. As the original differences are much higher, this value is plotted in the charts as optimum and the defined aim to achieve. Figure 5.8 represents the ΔE color differences in the LCH color space in a line chart for the Bayerpattern sensor. A table with the exact color difference values and the results of the Lab color space, which differ slightly, can be found in Appendix B. Figure 5.8 shows that not all three methods are an improvement in color for the Bayerpattern sensor, as the mean difference (of the original image data is 23.36) over all color patches is being reduced only with the Robust Least Squares Transformation Matrix (RTM) (mean value of 14.85) and the Polynomic Transformation Matrix (PTM) (mean value of 8.43). By far the best results when computing the difference between the reference image and the resulting, color transferred image, brings the PTM. All values are below the original image data and only 9 values out of 42 are above the optimum of 10. The RTM has only 19 color patches that are below a value of 10 and the Linear Least Squares Transformation Matrix (LTM) has only two color patches that are below 10. As the original values have been much higher than 10 (12 values are below the optimum) the results have improved a lot. In some cases the LTM produces better results than the original image data.

The band separated camera produces similar results. When comparing the mean values with the band separated camera, they are slightly smaller, and with this better, than those of the Bayerpattern sensor camera. The mean value for the color difference between original image data and reference data in the LCH color space amounts 20.18, while the LTM produces a mean of 21.9 and the RTM method a mean value of 14.3 and the PTM a mean value of 8.15. Again, the Polynomic method produces the most accurate color reproduction.

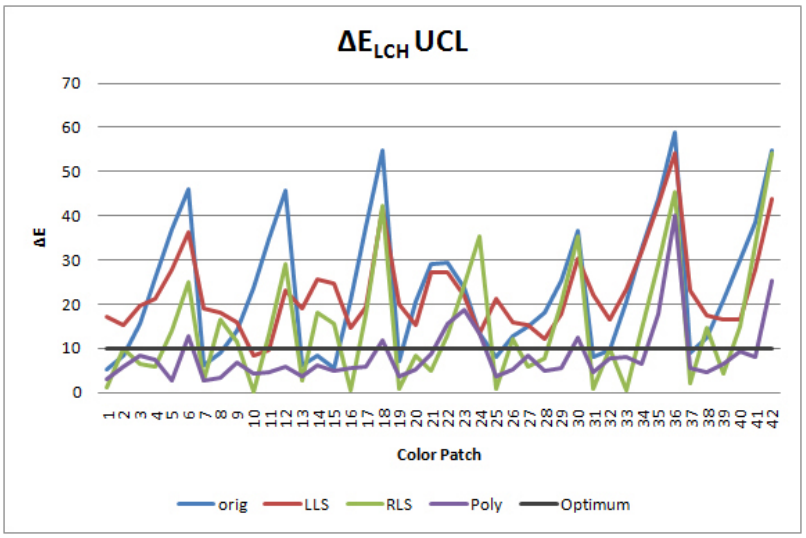

Figure 5.8: Chart representing the ΔE values (LCH color space) of the color differences of the original UCL image data (aperture F8) and the results of the color transformations to the reference image data

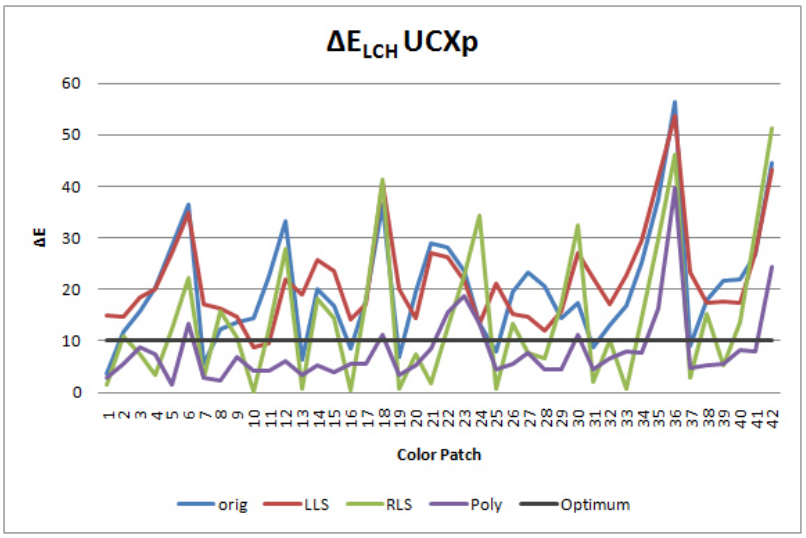

Figure 5.9: Chart representing the ΔE values (LCH color space) of the color differences of the original UCXp image data (aperture F8) and the results of the color transformations to the reference image data

A complete list of all ΔE values for the LCH color space and the Lab color space as well as the missing charts for the Lab color space can be found in the Appendix B. Summarized it can be said that the values vary from patch to patch, but the tendency is the same in all charts - the PTM produces by far the most accurate color correction. This analysis was repeated with three more cameras of the band separated camera and two of the Bay-

erpattern sensor camera. The ΔE values differ about less than 10DN, which can be traced back to slightly different illumination situations (as the illumination setup was changed to find an optimal setup during the recordings with the different cameras). The cameras presented here had the exact same setup during calibration.

5.2 Accuracy for Multiple Sensors

The main aim of this thesis is to show that a color characterization of digital aerial cameras makes sense for radiometric sensor fusion. For this reason, it is necessary to confront the results of the color-corrected color targets from the two camera models, to see if it makes sense to perform further tests with "real" images. To be consistent in the analysis, the same methods, as presented in the previous section, are being used for evaluation. First, the chromaticity diagram shows if the colors fit better in the xyZ color space. The ΔE values are again used for a numerical comparison. For the same reasons as mentioned in the previous section, the images taken with an aperture of F8 are used in this confrontation.

Figure 5.10 gives an overview of the original image data from the camera sensors and the resulting color target images. The histogram of the original camera image was linearily stretched, without adding any gamma, white balancing or channel-separate treatment). The resulting targets are also direct results when computing the CCM. The results of the CCM (which are always the two color target images that are on top of each other) are very similar compared to the original image data and their color differences. Visually checked, it can be said that all three methods are an inprovement for sensor fusion.

Chromaticity Diagram Evaluation

Figure 5.11 shows the chromaticity diagram with four different contents. The original image data of the band separated and the Bayerpattern sensor are confronted in the upper left chart. It is obvious that the differences in color are very big. Even the white point is slightly different (as no white balancing was applied). The upper right diagram shows the results of the LLS adjustment. An improvement compared to the original data is already visible. The lower two charts show the results of the RLS(left side) and the Polynomic color correction (right side). In this case it is not clearly visible which method is producing the better results, as all three methods produce an improvement. The RTM produces a few stronger outliers compared to

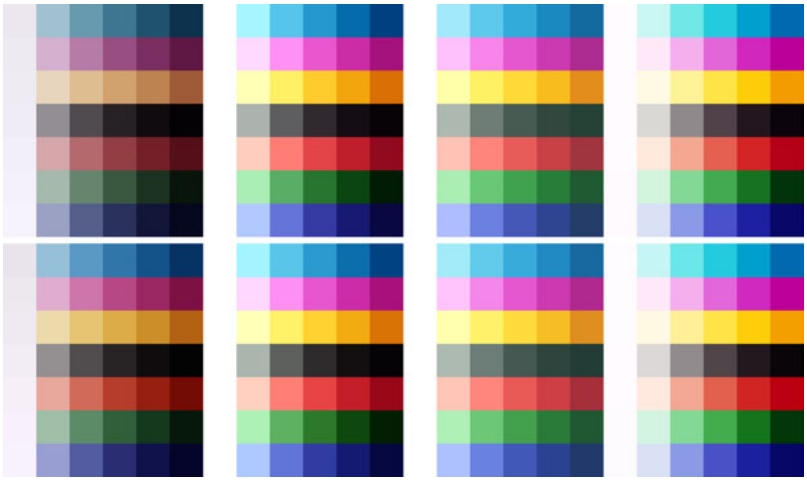

Figure 5.10: Comparison of color targets from UCL (upper row) and UCXp (lower row), from left to right in the following sequence: LLS, RLS, poly and original image data

the other two methods, and when checking the distances between the values the PTM produces the most accurate results.

Δ *Lab and* Δ *LCH Differences*

The ΔE values in the Lab and LCH color space are computed using the UCXp as reference data and the Bayerpattern images from UCL. Figure 5.12 shows the results in the LCH color space. The orginal image data, transformed into Lab- and LCH color space show big differences with the growing chroma of each color. The white color patches (no. 1, 7, 13, 19, 25, 31 and 37) are accurate, as well as the white-to-black color patches (no. 19-24). The improvement and reduction of the color difference is working with all three adjustment methods. The color differences for the white-to-black color patches are slightly bigger for the RLS-CCM than for the LLS and the Polynomic color transformation. The mean ΔE values can be reduced from 9.81 to 1.27 in the LLS, to 1.47 in the RLS and to 0.83 by the polynomic adjustment method.

5.3 Evaluation and Summary of Color Adjustment

All evaluations above show different accuracy measures, besides the visual check which was already performed in chapter 4. No matter which method was used for evaluation, all brought the same result; the polynomic color transformation and correction method produces the most accurate results

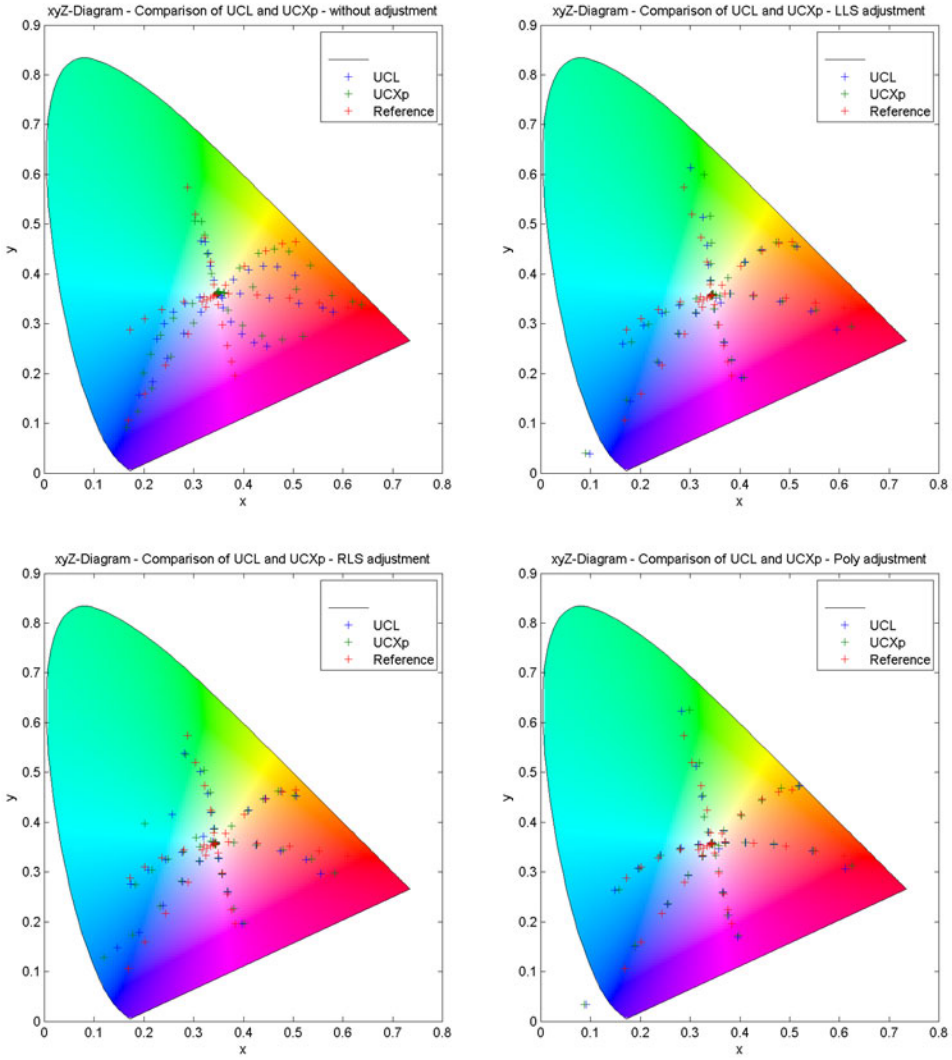

Figure 5.11: Chromaticity diagrams showing the original (in red) and color corrected image data of the UCL (in blue) and of UCXp (in green)

for both sensors. Also, when checking the accuracy between the two sensors, not focusing on the reference image data, this method is the most accurate. The RLS adjustment and the LLS method produce already promising results for a linear fitting method. A few color patches have been corrected more accurately by the Polynomic correction. Depending on the analysis method, the RTM produces better accuracy than the LTM and vice versa. Visually checked, it seems that the LTM is more accurate, as the RTM has a severe color shift in the white-to-black color patches, which is not acceptable without any histogram adjustments. Summarized, after the analytical accuracy evaluation, it can be said that the color representation is more accurate after

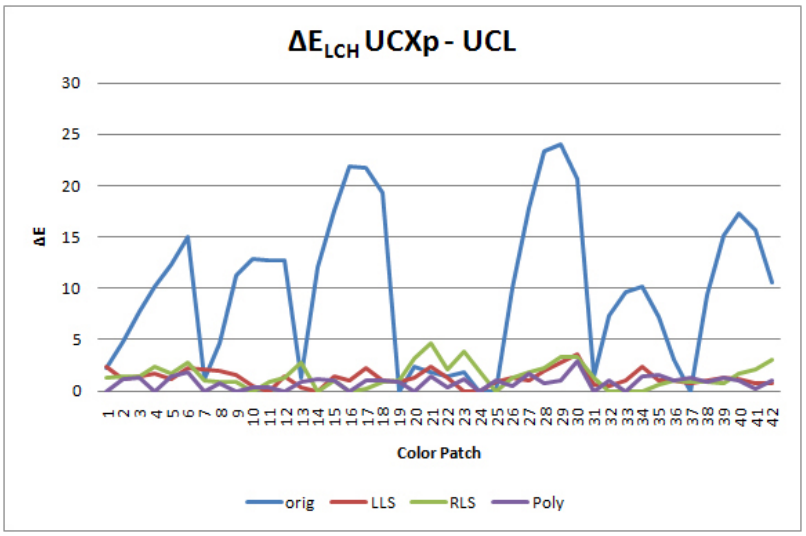

Figure 5.12: Chart representing the ΔE values (LCH color space) of the color differences of the UCXp image data (aperture F8) and the UCL images of the three color transformation methods

camera characterization, than before.

After performing a detailed analysis with color targets, recorded under a well specified illumination situation in the calibration lab, the next chapter focuses on aerial images. As there are several influencing factors for colors in the images, the CCM computed for the two sensors, are applied to the aerial images and compared, to show if one of the three methods are applicable for aerial photography.

Chapter 6

Color Correction on Aerial Images

In the previous chapters the practical setup for the calibration has been introduced and detailed accuracy discussions have been done in different color spaces, to verify that the transformation works not only with one color space. In this chapter, the Color Correction Matrix (CCM) are applied on "real" aerial images to get an impression if the presented methods work with aerial photography. For this reason testflights have taken place with both camera models. The investigation area is located in Graz, Austria. The testflight area covers the center of Graz. Here it was possible to lay out color targets on an office building to verify the suggested methods and to be able to compare the resulting images. Figure 6.1 shows the location of the test area.

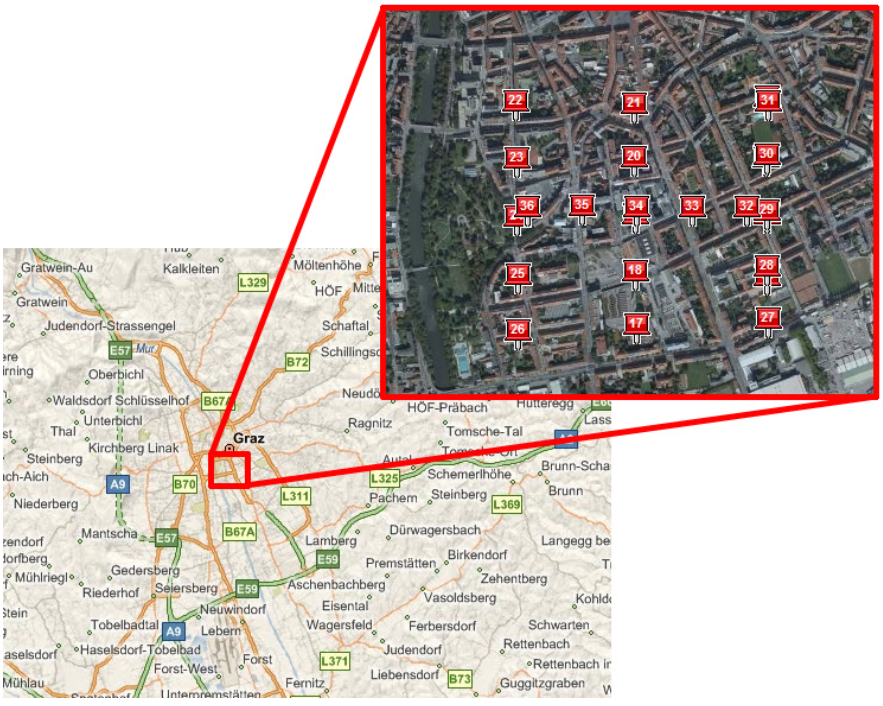

Figure 6.1: Testflight area Graz-Anzengrubergasse in Styria, Austria

First, this chapter shows a comparison of the three color transformation methods with images from the Bayerpattern sensor. The corresponding analysis for the band separated sensor follows. Next, the images from the two sensors are compared to check if the color correction improves the fitting of the colors from the two different sensors. Different scenes have been checked, to verify if the correction works in different surroundings. One good example is presented which best represents the analysis of further investigations with different scenes in this thesis. In the last part of this chapter a cluster analysis is being performed to get an impression of what effects the CCM has on further applications in remote sensing and GIS.

6.1 Color Correction on Aerial Images

The analysis in the previous chapter have shown that the color correction works, theoretically. This chapter gives an idea, if the suggested method produce an usable and feasable result on real images, where the recording conditions are not as well defined as in a calibration lab. Furthermore, these methods should help to adjust colors from different sensors. The first section shows the result for the Bayerpattern sensor and the next section gives the results for the band separated camera. Results from all three CCM are presented.

Color Correction for UltraCam L (UCL) Images

The original and resulting, color-corrected images contain up to 13bit of information (depending on the exposure of the images during recording) stored in a 16bit image, therefore, a histogram adaption for all three results are necessary to get equal comparable colors. When checking the images visually in detail in an image analysis software as for example Adobe Photoshop it can be found out that the histograms are changed differently depending on the color correction method (see Figure 6.2) used. The polynomic method brightens the image as the histogram of the transferred images get broader. The Robust Least Squares (RLS) adjustment changes the blackpoint for each channel separately. The blackpoints from red, green and blue do not fit together well, which makes a channel separate histogram adjustment necessary. Only the Linear Least Squares (LLS) modified image produces a comparable result as the original image. The histogram of the image has nearly the same range, with the advantage that the resulting image appears more colorful.

Figure 6.3 shows an UCL aerial image, processed with the color correc-

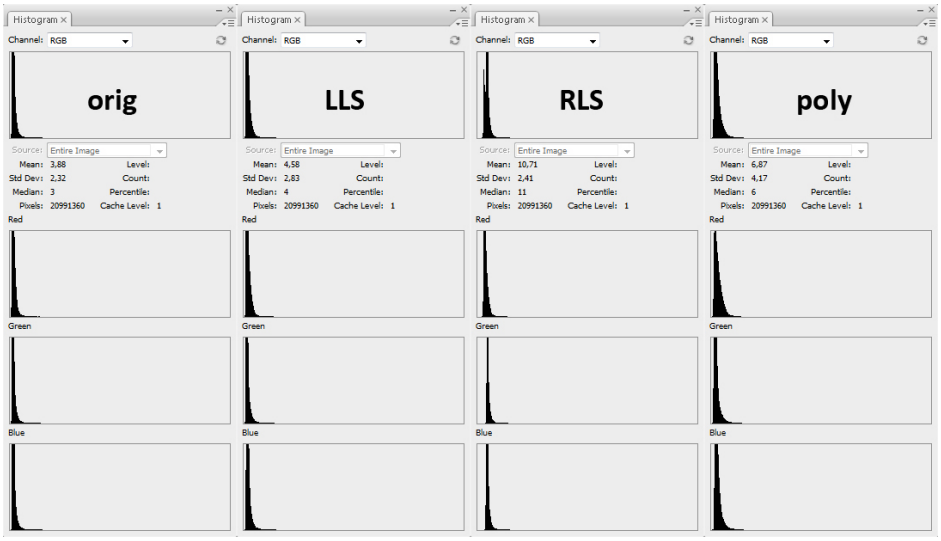

Figure 6.2: Comparison of resulting histograms (of original 16bit images), the histograms are ordered in the following sequence: original UCL image, LLS corrected image, RLS corrected image and polynomic adjusted image

tion matrices derived in chapter 4 and presented in chapter 5. The differences to the original (upper left image) are obvious, as the colors are more saturated and colorful. The upper right corner shows the resulting image of the LLS adjustment, the lower left corner represents the result of the RLS adjustment and the lower right image shows the result of the polynomic color correction. The LLS adjustment seems to produce the results closest to the original image data. The polynomic adjusted image is the most colorful one, but the LLS image appears to fit better to nature. The RLS image has, also after the histogram adaption, a strong, unnatural green tint in the image.

During the investigation for this thesis, many images, also from other cameras of the same model, have been analysed and all brought similar results. No matter which scene was taken, if rural or urban, the colors are much brighter with all three adjustment methods resulting in a more realistic image representation.

Color Correction for UltraCam Xp (UCXp) Images

As with the UCL the histograms of the images change by applying the CCM in a similar manner. The histogram comparison figure can be found in Appendix C. The band separated camera, the UCXp, produces similar results as the Bayerpattern sensor. Figure 6.4 shows the results of an UCXp image. The original UCXp image has a slight greyish tint. The color correction

Figure 6.3: Comparison of aerial images (from UCL) in an urban area in Graz, Austria, treated with the three different color correction methods in the following order: upper left: original UCL image, upper right: LLS corrected image, lower left: RLS corrected image and lower right: polynomic adjusted image

methods correct the color channel ratio and produce nice looking outputs. Differences are visible between the three adjustment approaches, but not as obvious as with the Bayerpattern sensor camera. Again, as with the UCL, before stretching the histogram, the result of the RLS adjustment is green tinted. After adjusting the separate color channels with the RLS method and stretching the histogram for all other images (original, LLS and Polynomic adjusted image) they can be compared. The resulting image of the LLS method appears to be less colorful in comparison to the other two results. The polynomic image is similar to the LLS result, but still more colorful, especially in green areas as vegetation. The RLS method is the most colorful, with an already artificial green tone of the vegetation. As a result the LLS image appears to be most realistic and best fitted.

6.2 Comparison of Color Corrected UCL and UCXp Images

When comparing color targets on the roof of an office building in Graz in Figure 6.5, it can easily be seen that the colors coming from the two sensors are very different. The application of the CCM helps to let the images appear more similar. As the two testflights have taken place on

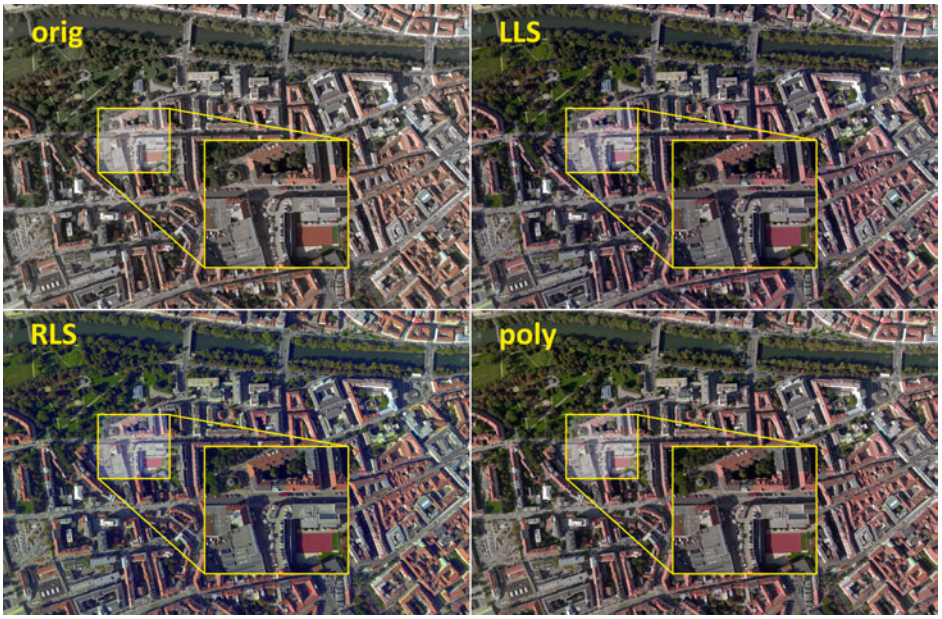

Figure 6.4: Comparison of aerial images (from UCXp) in an urban area in Graz, Austria, treated with the three different color correction methods in the following order: upper left: original UCXp image, upper right: LLS corrected image, lower left: RLS corrected image and lower right: polynomic adjusted image

two different days (about 3 weeks between the testflights), the athmospheric influence and weather situations are completely different. The UCL testflight took place on October 29^{th}, 2009 in the early afternoon on a cloudy, but for aerial phtography, still okay, day. The testflight of the UCXp took place on October 6^{th}, 2009 on a bright and sunny day. For this reason the images of the band separated camera UCXp are in general more colorful, with more contrast and long shadows, as the sun angle in October is already quite flat in Graz (see Figure 6.4). The images from the Bayerpattern sensor camera are, on the contrary, appearing more greyish with less contrast (see Figure 6.3).

The Digital Number (DN) of the color targets have been measured and evaluated for a better comparison. This has been done based on the images seen in Figure 6.5 as the different illuminations and white points have been treated in Photoshop to get a comparable basis. In both cases, only linear histogram stretches have been used, no curves have been applied. The images have been stored in 8bit and a 6x6 pixel large window have been averaged for the comparison. The table with the complete DN values and the selected targets can be found in Appendix C. The table on the left side in Figure 6.6 gives an overview of the differences between the two sensors. The green highlighted cells indicate that there has been an improvement, in other words, a decrease in the difference. All three methods produce equal

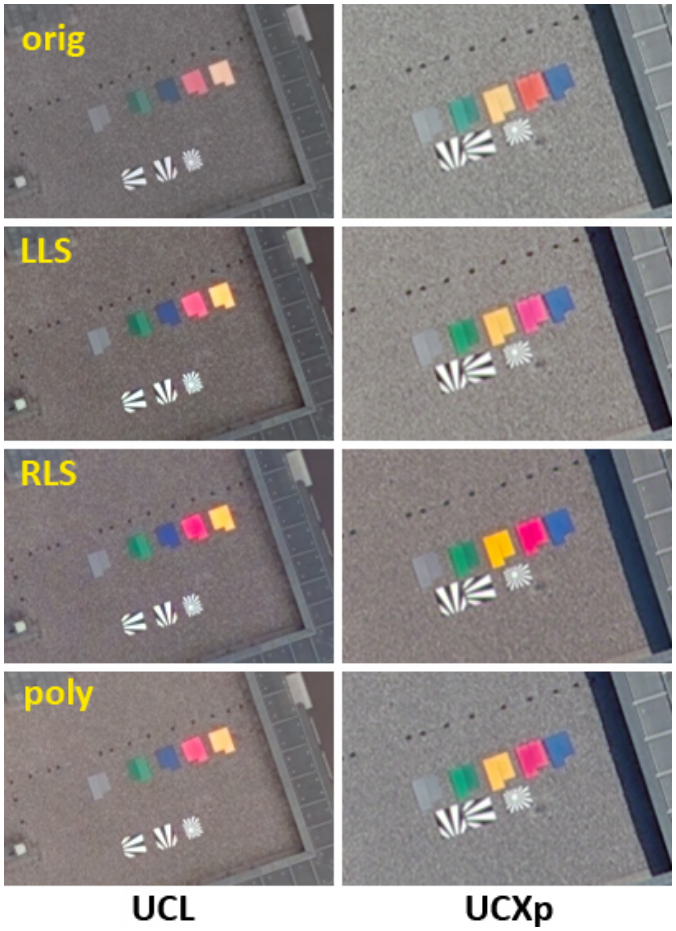

Figure 6.5: Comparison of outdoor color target images from UCXp and UCL treated with the three different color correction methods in the following order: original UltraCam (UC) image, LLS corrected image, RLS corrected image and polynomic adjusted image

improvements, with at least 9 highlighted cells. The table in Figure 6.6 on the right side shows the differences to the original difference. The smaller the value, the better the improvement. Green highlighted cells indicate the best improvement of each method, the red highlighted cells show the least improvement. It can easily be seen that the differences in general are smaller with the LLS method than with the two other methods. The RLS method has the highest difference with 60DN. The best improvement are with all three methods similar, about 30 to 32DN. The LLS method has in general the smallest deviation to the original. The RLS and polynomic method have greater improvements and also greater deterioration in some cases. Summing up both methods have greater improvement than worsening.

UCL - UCXp		
R	G	B
ORIG		
11,27	12,84	40,25
14,05	32,19	26,06
0,34	26,08	48,44
5,22	10,33	32,47
24,72	32,3	27,64
LLS		
10,19	21,61	9,47
6,77	24,16	6,78
4,03	32,25	31,31
5,25	20,8	27,47
20,69	20,17	16,42
RLS		
4,11	35,69	14,09
8,89	1,03	9,83
11,31	17,25	15,47
1,53	26,75	93,31
4,31	3,2	1,33
POLY		
16,03	44	11,77
47,22	0,53	3,97
25,77	9,36	16,64
3,5	17,33	52,95
10,75	0,84	1,97

Difference to ORIG		
R	G	B
LLS		
-1,08	8,77	-30,78
-7,28	-8,03	-19,28
3,69	6,17	-17,13
0,03	10,47	-5
-4,03	-12,13	-11,22
RLS		
-7,16	22,85	-26,16
-5,16	-31,16	-16,23
10,97	-8,83	-32,97
-3,69	16,42	60,84
-20,41	-29,1	-26,31
POLY		
4,76	31,16	-28,48
33,17	-31,66	-22,09
25,43	-16,72	-31,8
-1,72	7	20,48
-13,97	-31,46	-25,67

Figure 6.6: Difference between averaged DN values of UCL and UCXp for original, LLS, RLS and polynomic of the corrected outdoor color targets on the left side. Green indicates improvements. The table on the right side shows the differences to the original difference (from the right table). Green indicates the minimum, red the maximum of each method.

6.3 Cluster Analysis

As images are typically used as a basis for further analysis, it is important to find out whether the color correction affects the images in a way that the quality of further analysis suffers. Image classifications, in other words assigning pixels of the images to classes with similar spectral signatures, is an important analysis topic in Geographic Information System (GIS) and Remote Sensing when working with aerial images.

For the work in this thesis the technique of cluster analysis have been chosen for evaluation purposes. The analysis is performed in IDRISI and Matlab. The unsupervised approach of a cluster analysis is used to be independent of collecting any training samples and to avoid any subjective influence in the analysis. A cluster analysis tries to find groupings in multidimensonal (image) data. A typical approach for such a cluster analysis is the *k-means* algorithm. The user specifies the number of output classes and the algorithm seeds the specified number of centers (clusters) and tries to optimize the distances of pixels to the corresponding centers over various iterations (Lillesand *et al.*, 2004).

The scene taken for this analysis can be seen in Figure 6.7. The resulting images of all three CCM for UCL are shown in Figure 6.10 and for UCXp can be found in Appendix C. For all tests described in this section the original 16 bit image data was used.

Figure 6.7: Scenes taken for further cluster analysis, left side shows the UCL image and right side shows the UCXp image

At a first glance, the DNs of a certain scene are confronted in a 2D-diagram. Always two color channels are confronted to check how the relation between the color channels change through the color correction step. Figure 6.8 shows that all three color correction methods broaden the relation in comparison to the original image data. Best, and closest to the original image data is again the LLS method (in blue). The polynomic adjustment method (in red) broadens the relation most and the RLS method (in green) has a complete different origin which is more obvious with the UCXp. Another fact, which is noteworthy, is that the band separated camera has a more compact representation than the Bayerpattern camera image. This property stays the same in all three correction methods and over all channel confrontations.

When performing a cluster analysis based on the k-means technique in Matlab (see The MathWorks Inc. (2009)), the clusters are formed depending on the channel confrontation differently, especially in comparison to the original image data. The result for all channel confrontations and all color correction methods as well as the original image data for the UCL is shown in Figure 6.9. The analog figure for the UCXp can be found in Appendix C. Especially in the case of Red:Blue confrontations, with the RLS and the polynomic method, the shape of the clusters changes drastically. The borders of the clusters change, but the seeds or centers of each cluster stay nearly the same, excluding the RLS method, as the blackpoint has been changed completely. With the UCXp the same phenomenon can be observed. The drastic change of one cluster class cannot be found.

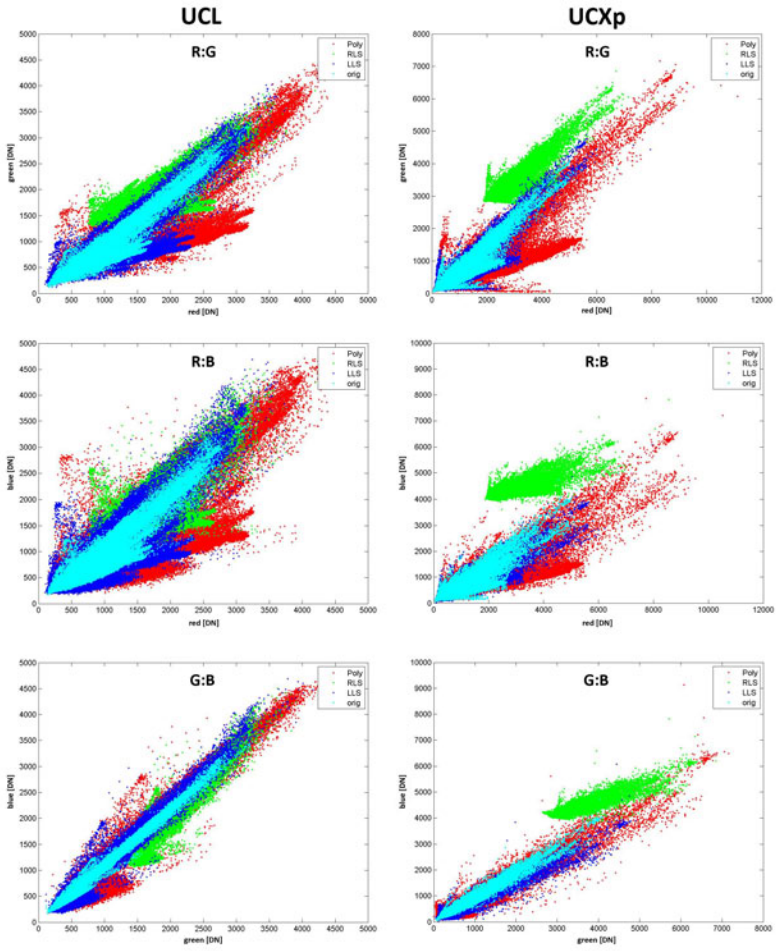

Figure 6.8: Confrontation of the color channels, left side UCL and right side UCXp, first row represents Red:Green, second row represents Red:Blue and last row represents Green:Blue

When performing a cluster analysis using a GIS software, as IDRISI, the results are displayed directly on the images, also known as classification of an image. Both samples represented above have been used to perform such an analysis in IDRISI and the results can be found in Figure 6.10. In this case, another clustering method was used were the number of clusters were fixed to eight. The clustering method in this case is based on the image histogram. The algorithm searches for peaks in histograms, also in correlation with other bands and evaluates which part belongs to one cluster. In this case not only two color channels are compared, but all three color channels are taken into account to decide which pixels form a cluster. A detailed description about the implemented algorithm can be found in Clark Labs (2009).

In Figure 6.10 the UCL images are displayed on the left side and on

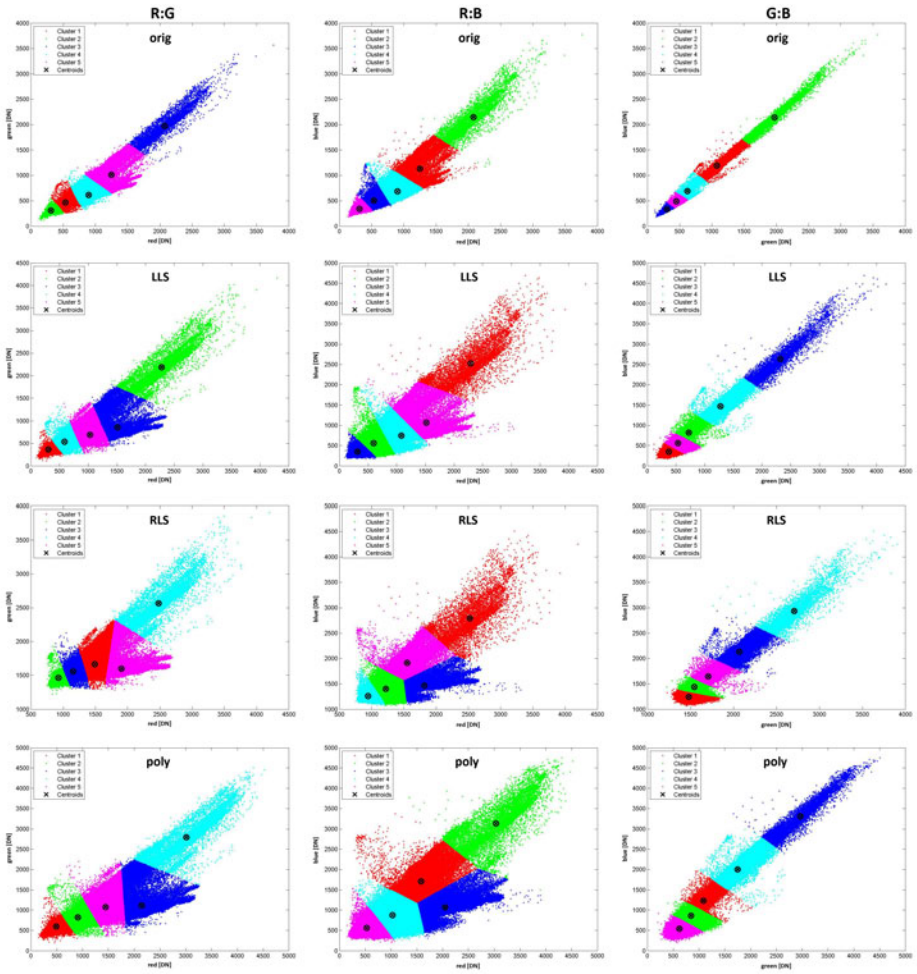

Figure 6.9: Cluster analysis of UCL imagery for the different CCM: first row represents original image data, second row represents LLS adjustment results, the third row represents results from the RLS adjustment and the last row represents the results from the polynomic adjustment. The different columns represent the different confrontation of the color channels: left columns represents Red:Green, middle column represents Red:Blue and the right column represents Green:Blue

the right side the results of the IDRISI clustering. The limit was set to eight clusters. The original image classification did a good job with the houses. The trees have not been recognized well, as they have the same class as the street. The grass and gardens have been classified well again. The LLS corrected image has been classified differently. In this case the grass and streets have the same class, whereas the trees have been clustered into another class. Trees and houses have been clustered together. The RLS image has well classified houses. Some trees have been recognized as separate class and streets and grass have been, similar to the LLS method, clustered together. The polynomic adjusted image has classified trees in

the same class as some streets. The houses have not been recognized as a separate class as with the RLS method. Altogether the clustering results differ a lot. There is no clear statement possible, which of the computed classifications produce the best results, as all four images find single classes better than others.

The classification with the UCXp produces again different results. The overall result, that there is no definit best classification result, is the same as with the UCL. The LLS result is most similar to the original image clustering. The polynomic and RLS method produce in the vegetation a different, more accurate result, as the trees are better recognized. The corresponding cluster results for the UCXp can be found in the Appendix C. The classification used in this investigation is a first test. To be able to get good and usable classification results it is necessary to perform the classification with more sophisticated methods as for example supervised classification methods.

6.4 Summary

In general it can be said, that applying CCM to aerial images, has an advantage in every case. A first important fact is that with all three methods the colors have been freshed up. A first visual quality check showed that the histogram of the images are modified. The nearest, most similar histogram has the LLS method. The RLS method produces a very strange histogram where a histogram adjustment is always necessary, as the histograms for red, green and blue are completely different. The polynomic method broadens the histogram most. After applying a linear histogram stretch, the images can be compared visually. The main impression is that the LLS method produces the most naturally looking image with refreshed colors compared to the original image. The RLS adjustment produces very colorful images with very unnaturally looking images. The polynomic method produces very colorful images, which still appear naturally, but with less grayish character and in some cases too much chroma.

Furthermore, images from both sensors have been compared to check if the CCM helps in adjusting the colors of different sensors. It was proved with an anaylsis of DN values of the outdoor targets that all three methods bring an improvement for the accuracy of color reproduction and with this more accurate color values. Due to the fact that the CCM does not take into account any surrounding information, no weather and athmospheric conditions can be corrected. The fact that the color accuracy is better than before the adjustment of colors, is being alleviated.

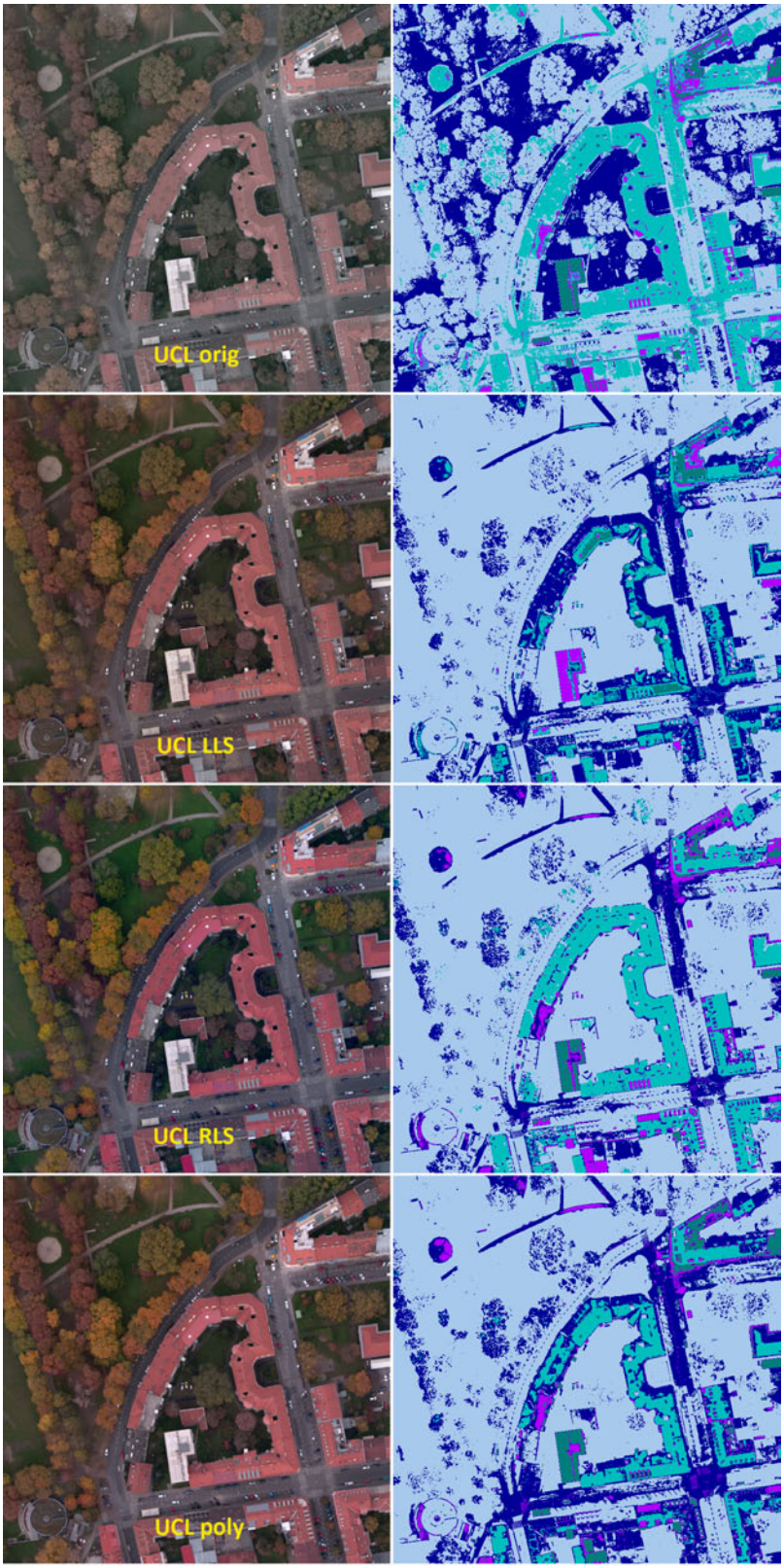

Figure 6.10: Cluster analysis of UCL imagery for the different CCM: right side image data and left side the corresponding cluster analysis result

The clustering analysis gave no clear result, whether color correction improves the performed analysis or not. In every case, the clustering produces different results with the color corrected images. The clustering in Matlab showed the different relations between the color channels. In IDRISI another clustering method was used. It is no clear statement possible, which image produced the best classification result, as all four images classified single classes better than the others.

Chapter 7

Discussion and Future Outlook

The aim of this thesis is to evaluate, if methods out of color theory can be used to enhance the color quality and accurate representation of aerial images to benefit, especially when fusing images from different sensors. As the field of color theory is very broad, this thesis focuses on the characterization of digital cameras, which implicates a correction of the three color channels. Three methods are being evaluated in detail. The methods are:

- Linear Least Squares Method (LLS)
- Robust Least Squares Method (RLS)
- Polynomic Method

The result of all three methods are Color Correction Matrix (CCM), which are multiplied with the original image data of a sensor type. The results have been evaluated in detail and the effects on the images discussed, in conjunction to further Geographic Information System (GIS) applications, as image classifications or image mosaicking. The complete workflow which was used throughout this thesis is shown in Figure 7.1, which is a more detailed view from Figure 1.2 in chapter 1. The colors indicate which chapter describes which parts of the workflow from calibration on to extracting the CCM and to the application and evaluation on real aerial images.

For a reasonable application in sensor fusion, images of two different sensors have been color characterized. The first one is a sensor, where the color comes from three different, monochrome sensors with red, green and blue color filters in front of the lens system. The second sensor has a Bayer-pattern filter installed directly on the sensor. The color image is a result of a demosaicking postprocessing step, where the missing color information is being computed out of the recorded data. The colors that are recorded by the two sensors are different.

The analytical evaluation on the recorded color targets (which have also been used for the computation of the CCM) has shown that the Polynomic method produces the most accurate results. Overall, it can be said that

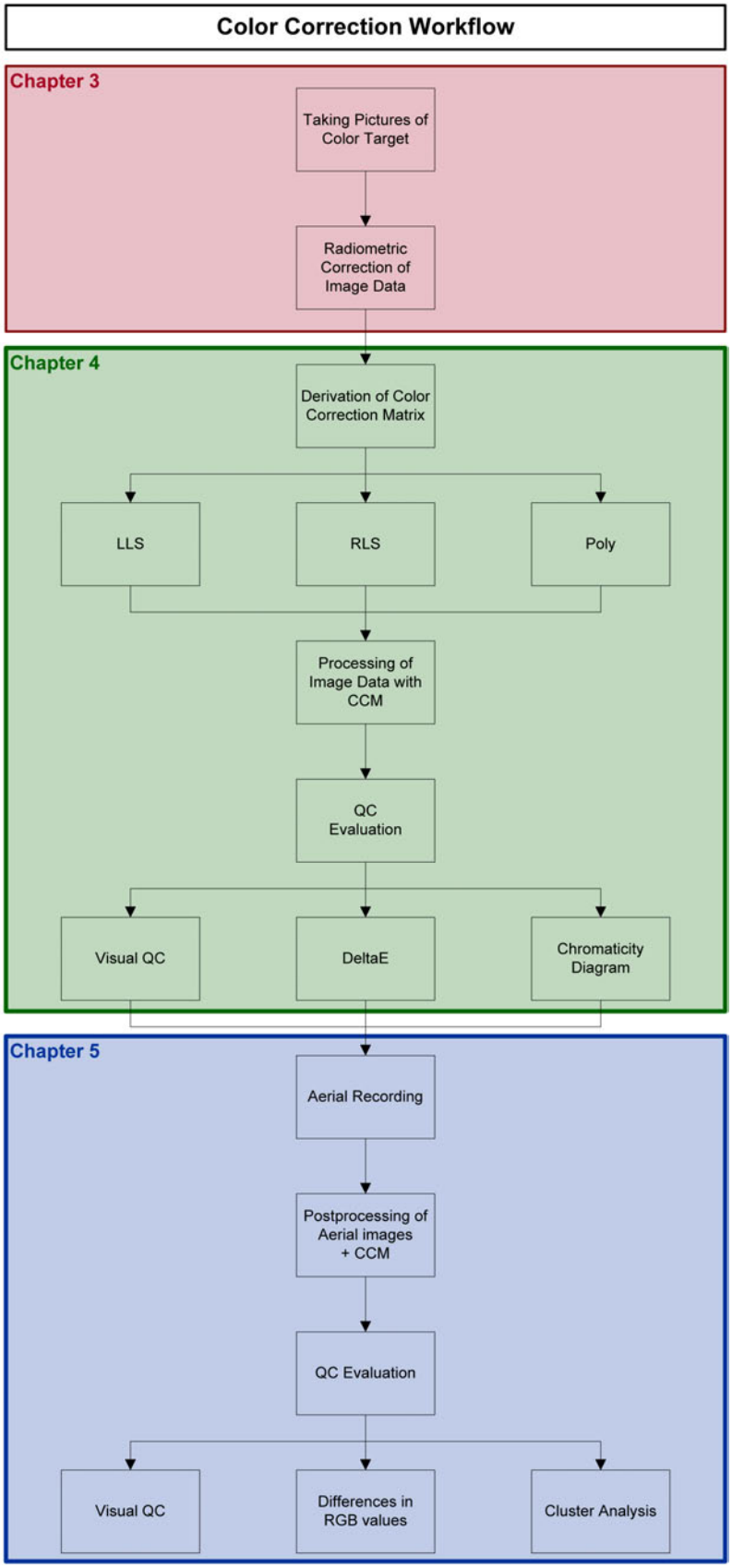

Figure 7.1: Color correction workflow, and color indexed structure of the master thesis, enhanced workflow compared to the workflow-figure presented in the introduction

all three methods bring an improvement for the colors. The Robust Least Squares (RLS) method showed problems in the white-to-black color patches with a green tint. The Linear Least Squares (LLS) method produced already an improvement, but the color targets with the most chroma (left located color patches on the color target) appear too dark, which can also be seen in the chromaticity diagram. The ΔE values showed even a partly worse result of the Linear Least Squares Transformation Matrix (LTM) than the original image data. On the contrary to this, the chromaticity diagram and linearity chart show an improvement to the original image data. Also the visual check gave this impression. The comparison among the color corrected images of both sensors showed a definite improvement in all accuracy measurements. Again, the Polynomic Transformation Matrix (PTM) showed the best results.

The application of the color correction matrices on real aerial images was a success. There have been problems with green color casts in the RLS images. The LLS images appeared to be less colorful than the other two results. The Polynomic adjustment brought very colorful results. The most natural and realistic representation of color, closest to the original image data, has been produced by LLS adjustment.

When applying the corresponding color correction matrices for the sensors and color correcting the aerial images, the differences in colors have been reduced. The verification has been performed with outdoor color targets which have been placed on the roof of a building in the city of Graz, Austria. With both cameras a testflight has taken place and the resulting images of the color targets have been compared. The colors does not fit perfectly, but the differences have been reduced clearly with all three color correction methods. The remaining differences can be traced back to different athomspheric and weather conditions during aerial missions. Radiometric sensor fusion algorithms implemented in image mosaicking software packages can treat those smaller differences in color better, than those with bigger color differences before color correction.

As CCM mix color information from different channels it was interesting to find out whether further GIS analysis, as a cluster analysis, affects the quality. With the Bayerpattern sensor the mixing of color information from different color channels should not result in loss of quality of image content, as the colors are already mixed before adding the color correction matrix during image demosaicking. This is different with the band separated camera. As the original image from the sensor contains the pure color information, the CCM mixes the color information (for example for the correction of the red channel also a small amount of green and blue channel are added or subtracted).

The results for the cluster analysis for the color corrected images have been mixed. Two different approaches have been evaluated. The cluster analysis was performed in Matlab to check the changing of relations between colors. Using the GIS software IDRISI a cluster analysis was computed based on histogram peaks. The results have been directly displayed on the images, as classifications results. The first approach showed that the relations between colors got broader as with the original image. The seeds of the single clusters stayed the same, excepting the RLS adjusted images, as there the blackpoint is completely different. The clusters itself changed depending on the used method more or less. The LLS adjusted image clusteriung produced the most similar results to the original image clustering. The clustering in IDRISI produced different results, depending on the images used for input. Even the original image classification produced not an appropriate classification result. Each classification result contained classes which have been classified better than the others. As this test was a first try to check the accuracy of color corrected images for a GIS analysis, there is a lot more evaluation and testing work to do. There are better classification methods, as for example supervised or segment-based classification methods, which would lead to results with better accuracy.

With all the results described above and in more detail in the previous chapters the first assumption from chapter 1

A camera characterization for digital aerial mapping cameras results in a more accurate color representations of post processed aerial images.

can be verified. The above discussed accuracy evaluations show on the whole that the color representation are more accurate in comparison to the reference. Also the visual impression is better, as the images appear to be more colorful and saturated. When taking into account all the information collected throughout this investigation, the polynomic adjustment method produces the best results. Secondly, the LLS method produces good results as well. In a few cases the RLS method is better than the LLS method, or even better than the polynomic method, but really suffers in the visual representation. This is the reason why this method is not recommended to be used for the characterization of an aerial camera. The LLS method has the advantage that the represenation of color sticks nearest to the original image data, with a linear improvement, with the disadvantage that the accuracy is not the best possible. The polynomic method produces the best in every case, and most accurate, color representation, but with the disadvantage that the colors are changed no more linearily.

The second assumption of this thesis

Camera characterization is a method for improving the quality for radiometric fusion of images of different aerial sensors.

can also be verified. The investigations in this thesis showed improvements for a radiometric fusion of sensors in all cases. Again, as with the single sensor evaluation, the polynomic adjustment method produced the best results. It can be clearly stated that images, coming from different sensors have smaller differences in colors than without a camera characterization. The camera characterization improves the base colors of each sensor / camera model, but the influences of the surroundings such as weather, sun angle, athmosphere etc. cannot be removed completely as they are not taken into account. For this task, color theory offers several more possibilities in device independent color spaces to try. The main advantage of a camera characterization, besides the color correction, is that the transformation into a device independent color space is being defined.

7.1 Further Approaches in Color Theory

The methods chosen for the transformation into another color space are most widely spread. There are several others available which can be tested and evaluated in near future to check if they produce even better results. Bala (2003) mentions techniques using distance-weighted, lattice-based interpolation techniques or neural networks. Distance weighted techniques are based on parametric functions. The main advantage of these techniques is that both allow extrapolation. Lattice-based interpolation methods assume that the training samples lie on a regular lattice. Cubes or tetrahedras are used as basic lattice. The neural networks are based on neurons, which are simple processing units. The connections between the neurons, the so-called inter-neuron connection strengths, contain the processing ability. Neural networks are trained and afterwards can be used to derive forward and inverse characterisation functions (Bala, 2003).

As mentioned in the theoretical part of this thesis, there are more methods in color theory, besides a camera characterization, which can be applied to correct and adjust colors. Once a valid transformation into a device independent color space is defined, several methods can be applied. Very important algorithms, when it comes to white balancing images are the Chromatic Adaption Transform (CAT). They can be applied to compute a different white point for given colors. Furthermore, when it comes to working with different color spaces, it is necessary to think about gamuts and the corresponding and correct mappings. Reinhard *et al.* (2008) suggests another method to transfer colors from one image to another. This can be of interest when it comes to fusing images from two different camera sensors. A main part of the future work after this thesis will be invested in the testing and evaluation of further methods for improving the color quality of

aerial images.

7.2 ICC Profiling

The International Color Consortium (ICC) has specified device profiles, which describe the color transformation of a device dependent into a device independent color space and vice versa. With the work done for this thesis, the basis for the introduction of ICC profiles for digital aerial cameras has been built - a device calibration and characterization.

The collected information is stored in the tags of the corresponding tags for color space transformation of the ICC profile as presented in detail in chapter 3.5. The rendering intent is defined as perceptual and the transformaton direction is from the device dependent color space RGB into a device independent color space LAB or XYZ.

The resulting transformation information with additional information about the device itself and white point (D50) can be feeded into the information and whitepoint tags of the ICC profile. The transformation information can be stored as a matrix or Look Up Table (LUT). The LLS adjustment results can be stored directly as the transformation matrices in the profile, as the IÇC has specified a 3x3 size for transformation matrices. In the case of the RLS and polynomic adjustment methods, a LUT needs to be extracted out of the computed parameters for all available RGB values (in the case of the UltraCam (UC) in 16bit) and stored as a LUT in the ICC profile.

7.3 Concluding Remarks

There is great potential in performing a professional color management based on the ICC in the GIS and Potogrammetry industry. Aerial and satellite images are becoming more and more important for the GIS sector as the computing power do not limit working with huge amount of data. Thus, it is inevitable to focus on an accurate color representation.

The results of this thesis showed that it makes sense to characterize aerial sensors - as a first step for a professional color management. The output, besides a color correction based on reference materials, is a well defined transformation into a device independent color space as XYZ or Lab. This opens up many possibilities for further color adjustment and professional output on different medias, as Liquid Crystal Display (LCD) screens or printers.

Bibliography

Adobe Systems Inc., "Adobe.com", URL: http://www.adobe.com/products/-photoshop/ 2009. [51]

Albertz, J. and Wiggenhagen, M., 2009, *Guide for Photogrammetry and Remote Sensing* (Upper Saddle River, New Jersey 07458: Herbert Wichmann Verlag). [3, 7, 9, 18, 20, 21, 23, 25, 29, 30]

Bala, R., 2003, Device characterization. In *Digital Color Imaging Handbook*, G. Sharma (Ed.) (CRC Press LLC), pp. 269–384. [33, 82]

Braunecker, B., 2005, Filters. In *Digital Airborne Camera - Introduction and Technology*, R. Sandau (Ed.) (Springer), pp. 180–183. [16, 17]

Chandelier, L. and Martinoty, G., 2009, A Radiometric Aerial Triangulation for the Equalization of Digital Aerial Images and Orthoimages. *Photogrammetric Engineering and Remote Sensing*, **75**, 193–200. [8]

Clark Labs, "Clarklabs.org", URL: http://www.clarklabs.org/ 2009. [51, 73]

Ehlers, M., 2005, Urban Remote Sensing: New Developments and Trends. . [10, 11]

Felber, G., "Kalibrierung digitaler Luftbildkameras der UltraCam-Serie", Master's thesis, Campus 02 Graz 2007. [17]

Foveon, "Foveon.com", URL: http://www.foveon.com/ 2009. [viii, 15, 16]

Gierling, R., 2006, *Farbmanagement* (Heidelberg: Redline GmbH). [viii, 22, 24, 28, 29, 38, 39, 59]

Gonzalez, R. and Woods, R., 2002, *Digital Image Processing* (Upper Saddle River, New Jersey 07458: Prentice Hall International). [3, 31]

Gruber, M., 2005, UltraCam, Digital Large Format Aerial Frame Camera System. In *Digital Airborne Camera - Introduction and Technology*, R. Sandau (Ed.) (Springer), pp. 313–329. [13]

Hirakawa, K. and Parks, T.., 2005, Adaptive Homogeneity-Directed Demosaicing Algorithm. *IEEE Transactions on Image Processing*, **14**, 360–369. [15]

Honkavaara, E. and Markelin, L., 2007, Radiometric Performance of Digital Image Data Collection - A Comparison of ADS40/DMC/UltraCam and EmergeDSS. In *Proceedings of the 50th PHOWO Proceedings 2007*, D. Fritsch (Ed.), Stuttgart, pp. 117–129. [44]

Huneke, T., "Internetseite zur Visualisierung von ICC-Profilen mit Hilfe von 3D-Farbraummodellen http://www.iccview.de", URL: http://www.iccview.de/images/stories/iccview/ICCView-Colormanagement.pdf 2002. [38]

ICC, "International Color Consortium Specification", URL: http://www.color.org 2004. [ix, 37, 40]

Johnson, G.M. and Fairchild, M.D., 2003, Visual psychophysics and color appearance. In *Digital Color Imaging Handbook*, G. Sharma (Ed.) (CRC Press LLC), pp. 115–171. [20, 21, 36]

Kim, M. and Kautz, J., 2008, Characterization for High Dynamic Range Imaging. *EUROGRAPHICS 2008*, **27**. [18, 23, 35]

Kraus, K., 2002, *Photogrammetrie - Band 1, Geometrische Informationen aus Photographien und Laserscanneraufnahmen* (10785 Berlin: Walter de Gruyter GmbH & Co. KG). [3, 13, 17]

Lillesand, T., Kiefer, R. and Chipman, J., 2004, *Remote Sensing and Image Interpretation* (605 Third Avenue, New York, NY: John Wiley & Sons, Inc.). [3, 17, 71]

Lindbloom, B., "BruceLindbloom.com", URL: http://www.brucelindbloom.com/ 2003. [30, 32, 36]

Malvar, H.S., He, L. and Cutler, R., 2004, High-Quality linear Interpolation for Demosaicing of Bayer-patterned Color Images. In *Proceedings of the Acoustics, Speech, and Signal Processing*, pp. 485–488. [15]

Morovic, J., 2003, Gamut Mapping. In *Digital Color Imaging Handbook*, G. Sharma (Ed.) (CRC Press LLC), pp. 639–686. [37]

Perko, R., 2004, Computer Vision for Large Format Digital Aerial Cameras. PhD thesis, Graz University of Technology. [11, 13]

Pohl, C., 1999, Tools and Methods for Fusion of Images of different spatial Resolution. *International Archives of Photogrammetry and Remote Sensing*, **32**. [9, 10]

Reinhard, E., Khan, E., Akyüz, A. and Johnson, G., 2008, *Color Imaging: Fundamentals and Applications* (Wellesley, MA: A.K. Peters Ltd.). [3, 21, 23, 24, 25, 29, 30, 82]

Ryan, R.E. and Pagnutti, M., 2009, Enhanced Absolute and Relative Radiometric Calibration for Digital Aerial Cameras. In *Proceedings of the 52nd PHOWO Proceedings 2009*, D. Fritsch (Ed.), Stuttgart, pp. 81–90. [43]

Sandau, R. (Ed.) , 2005, *Digital Airborne Camera - Introduction and Technology* (Berlin, Germany: Springer). [3, 11, 17]

Schneider, S. and Gruber, M., 2008, Radiometric Quality of UltraCam-X Images. In *Proceedings of the ISPRS Beijing Proceedings 2008*. [42]

Schönermark, M., KirchgäSSner, U., Schwarzbach, M., Putze, U. and Zhou, D., 2009, Überblick über die Arbeiten der Radiometriegruppe zur DGPF - Jahrestagung. In *Proceedings of the DGPF Tagungsband 18 / 2009*, Stuttgart, p. 12. [44]

Scholz, S. and Gruber, M., 2009, Radiometric and Geometric Quality Aspects of the Large Format Aerial Camera UltraCam Xp. In *Proceedings of the High-Resolution Earth Imaging for Geospatial Information*, H. C. (Ed.), Hannover, pp. 143–147. [13]

Sharma, G. (Ed.) , 2003, *Digital Color Imaging Handbook (Electrical Engineering & Applied Signal Processing)* (2000 N.W. Corporate Blvd., Boca Raton, Florida 33431: Crc Press LLC). [3, 4]

Sharma, G., Vrhel, M. and Trussel, H., 1998, Color Imaging for Multimedia. *Proceedings of the IEEE*, **86**, 1088–1108. [36]

The MathWorks Inc., "MathWorks.com", URL: http://www.mathworks.com/ 2009. [51, 72]

Vexcel Imaging GmbH, 2009, UltraMap Manual. Technical report, Microsoft Photogrammetry, Graz, Austria. [50]

Vrhel, M. and Trussel, H., 1999, Color Device Calibration: A Mathematical Formulation. *IEEE Transactions on Image Processing*, **8**, 1796–1806. [4, 32, 33, 34]

Weber, J., 2009, Radiometrische Testtafeln zur Qualitätsuntersuchung digitaler Kamerasysteme. In *Proceedings of the DGPF Projektsitzung Herbst 2009*, Stuttgart. [44]

Weidner, U. and Centeno, J., 2009, Pansharpening - Simple Approaches and their Evaluation. *PFG - Photogrammetrie, Fernerkundung, Geoinformation*, **4/2009**, 317–327. [10]

Wolf, S., 2003, Color Correction Matrix for Digital Still and Video Imaging Systems. *NTIA Technical Memorandum*, pp. 1796–1806. [4, 35, 49]

Yoon, C. and Cho, M., 1999, Colorimetric Characterization for Digital Camera by using Multiple Regression. *IEEE Tencon*, pp. 585–588. [4, 35]

Appendix A

Appendix - Chapter 3

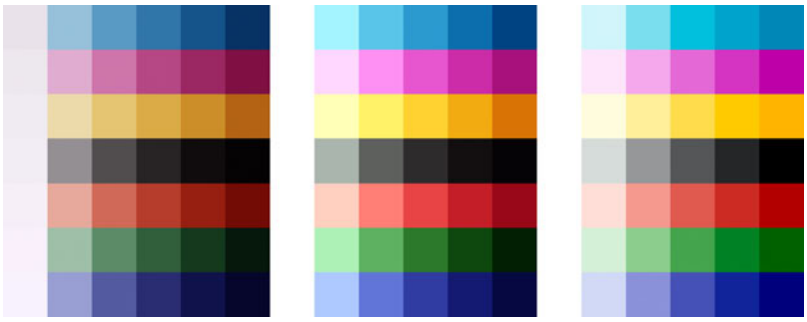

Figure A.1: UltraCam Xp (UCXp) image, LLS fitted image and reference image

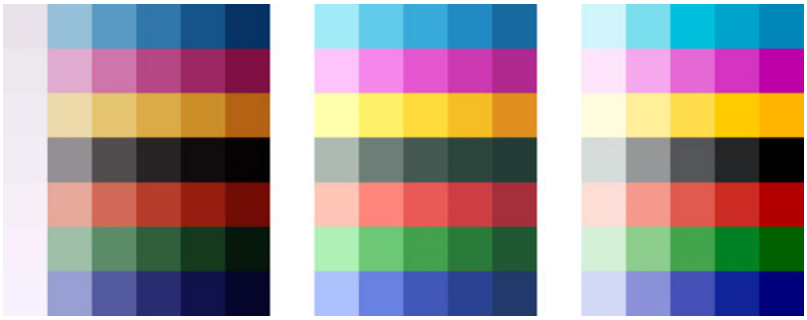

Figure A.2: UCXp image, RLS fitted image and reference image

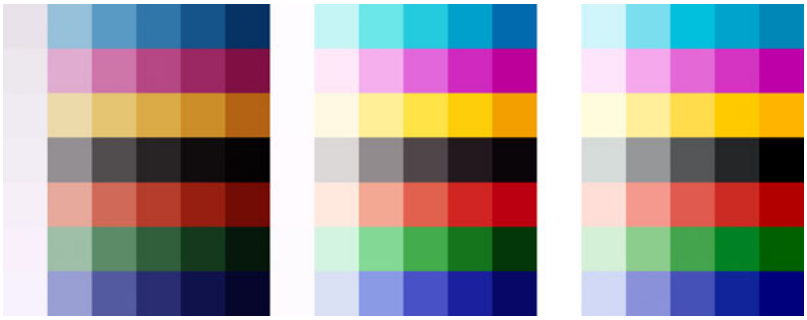

Figure A.3: UCXp image, polynomic fitted image and reference image

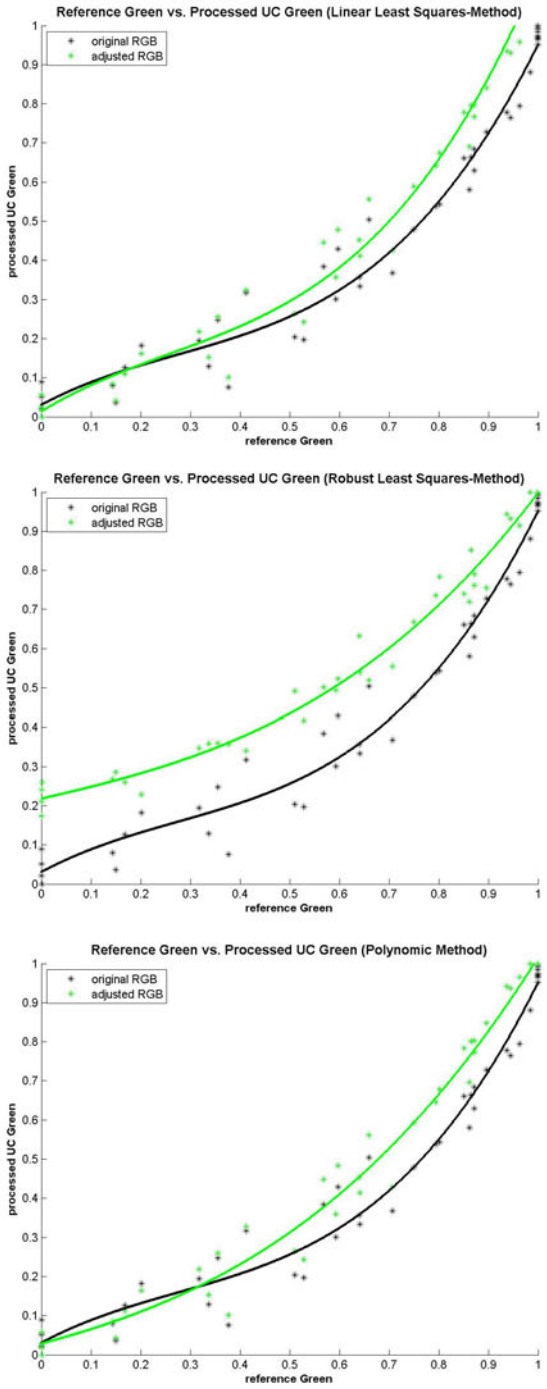

Figure A.4: Linearity chart of green channel of UltraCam L (UCL) in normalized Digital Number (DN)

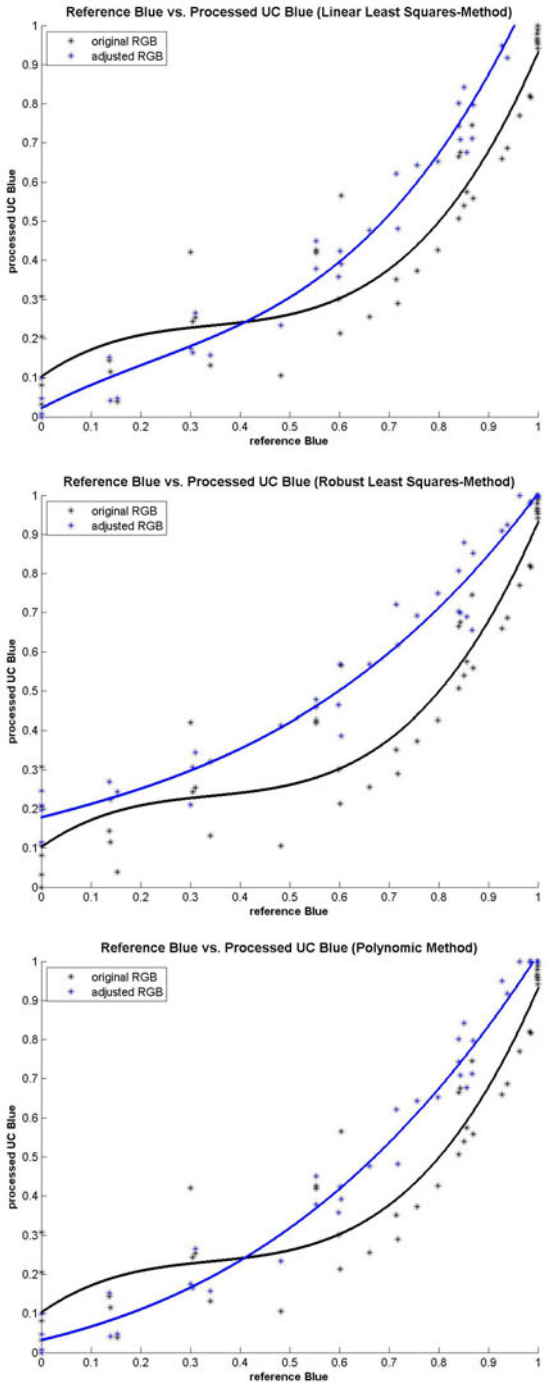

Figure A.5: Linearity chart of blue channel of UCL in normalized DN

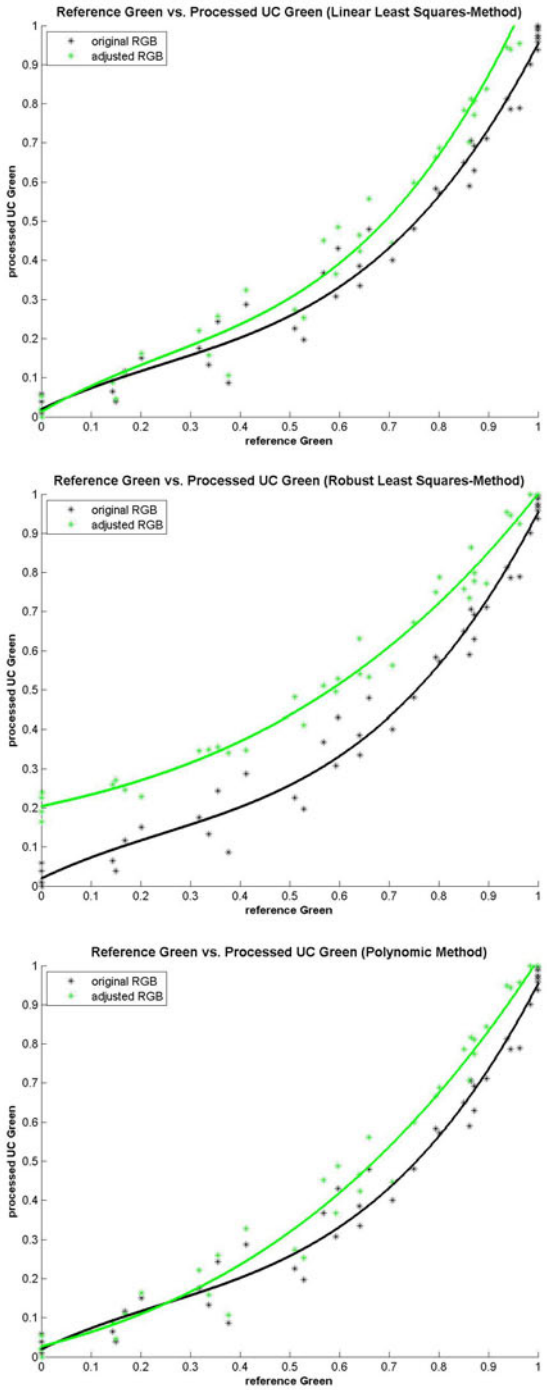

Figure A.6: Linearity chart of green channel of UCXp in normalized DN

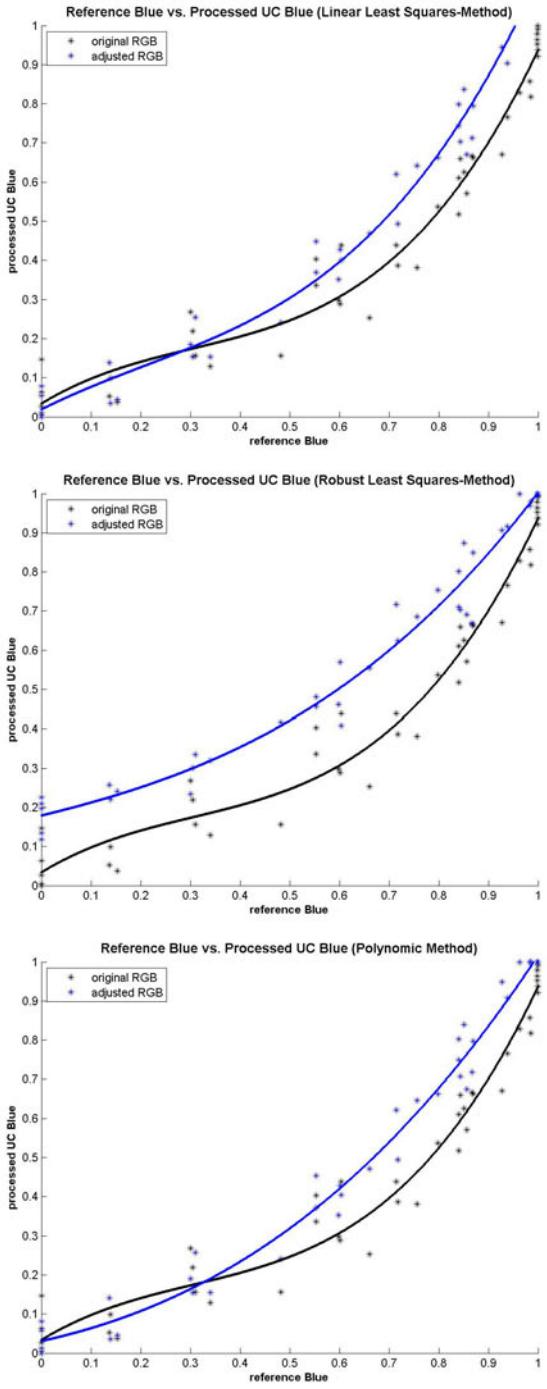

Figure A.7: Linearity chart of blue channel of UCXp in normalized DN

Appendix B

Appendix - Chapter 4

UCXp				UCL		
LLS				LLS		
1,3	-0,06	0,21	R	1,7	-0,11	-0,13
-0,22	1,2	-0,6	G	-0,83	1,4	-1,08
0,05	0,05	1,58	B	0,25	-0,1	2,4
RLS				RLS		
0,14	0,24	0,21		0,15	0,25	0,21
1,14	-0,21	0,08	R	1,53	-0,27	-0,26
-0,19	1,2	-0,57	G	-0,69	1,52	-0,99
-0,05	-0,17	1,37	B	0,05	-0,46	2,11
Poly				Poly		
2,54	-0,3	0,24	R	3,11	-0,46	-0,49
-0,36	2,4	-0,89	G	-1,21	2,94	-1,69
0	-0,03	2,82	B	0,21	-0,39	4,3
1,97	0,26	0,3	RG	3,97	0,22	0,28
0,22	0,64	1,47	GB	1,13	2,11	3,87
-0,01	-0,18	-0,12	BR	-0,53	-0,21	1,26
-2,22	0,14	-0,22	R^2	-3,19	0,27	-0,46
-1,01	-1,72	-0,32	G^2	-2,03	-2,74	-1,09
-0,15	-0,21	-2,29	B^2	-0,47	-0,77	-5

Figure B.1: Comparison of color correction factors for aperture F5.6 for LLS, RLS and polynomic color correction method for both sensors

UCXp				UCL		
LLS				LLS		
1,3	-0,05	0,22	R	1,74	-0,11	-0,13
-0,22	1,2	-0,61	G	-0,86	1,41	-1,13
0,05	0,05	1,58	B	0,24	-0,11	2,46
RLS				RLS		
0,14	0,24	0,21		0,15	0,26	0,21
1,14	-0,21	0,07	R	1,56	-0,27	-0,26
-0,19	1,21	-0,58	G	-0,7	1,54	-1,03
-0,04	-0,17	1,37	B	0,04	-0,48	2,15
Poly				Poly		
2,55	-0,31	0,26	R	3,16	-0,48	-0,52
-0,37	2,42	-0,92	G	-1,23	2,99	-1,74
0	-0,03	2,83	B	0,21	-0,4	4,4
1,99	0,23	0,33	RG	4,03	0,13	0,2
0,24	0,65	1,55	GB	1,1	2,12	3,95
-0,02	-0,19	-0,13	BR	-0,53	-0,25	1,34
-2,23	0,16	-0,24	R^2	-3,26	0,36	-0,43
-1,03	-1,73	-0,36	G^2	-2,02	-2,75	-1,04
-0,16	-0,22	-2,33	B^2	-0,46	-0,74	-5,17

Figure B.2: Comparison of color correction factors for aperture F11 for LLS, RLS and polynomic color correction method for both sensors

UCXp				UCL		
LLS				LLS		
1,3	-0,06	0,22	R	1,74	-0,11	-0,13
-0,22	1,21	-0,61	G	-0,86	1,42	-1,13
0,04	0,04	1,58	B	0,24	-0,11	2,46
RLS				RLS		
0,14	0,24	0,21		0,15	0,26	0,21
1,14	-0,22	0,08	R	1,56	-0,27	-0,26
-0,19	1,21	-0,58	G	-0,7	1,55	-1,04
-0,04	-0,17	1,36	B	0,04	-0,48	2,15
Poly				Poly		
2,54	-0,31	0,27	R	3,16	-0,49	-0,51
-0,37	2,42	-0,92	G	-1,24	3	-1,76
0	-0,04	2,83	B	0,2	-0,4	4,42
1,98	0,22	0,33	RG	4,04	0,12	0,23
0,24	0,64	1,53	GB	1,11	2,14	4
-0,02	-0,18	-0,14	BR	-0,53	-0,25	1,34
-2,22	0,16	-0,25	R^2	-3,26	0,36	-0,45
-1,02	-1,72	-0,35	G^2	-2,03	-2,76	-1,07
-0,15	-0,21	-2,31	B^2	-0,46	-0,75	-5,22

Figure B.3: Comparison of color correction factors for aperture F16 for LLS, RLS and polynomic color correction method for both sensors

UCXp				UCL		
LLS				LLS		
1,31	-0,06	0,22	R	1,74	-0,11	-0,13
-0,23	1,21	-0,62	G	-0,85	1,43	-1,14
0,05	0,05	1,58	B	0,24	-0,12	2,46
RLS				RLS		
0,14	0,24	0,21		0,15	0,25	0,22
1,15	-0,22	0,08	R	1,56	-0,27	-0,26
-0,19	1,21	-0,59	G	-0,7	1,55	-1,05
-0,04	-0,17	1,37	B	0,03	-0,48	2,16
Poly				Poly		
2,55	-0,32	0,27	R	3,16	-0,49	-0,53
-0,37	2,43	-0,94	G	-1,23	3,01	-1,76
0	-0,04	2,85	B	0,2	-0,41	4,44
1,99	0,22	0,36	RG	4,03	0,13	0,16
0,24	0,66	1,56	GB	1,09	2,14	3,97
-0,01	-0,19	-0,14	BR	-0,53	-0,26	1,36
-2,23	0,17	-0,26	R^2	-3,26	0,36	-0,41
-1,02	-1,74	-0,37	G^2	-2,02	-2,78	-1,02
-0,15	-0,22	-2,34	B^2	-0,45	-0,73	-5,23

Figure B.4: Comparison of color correction factors for aperture F22 for LLS, RLS and polynomic color correction method for both sensors

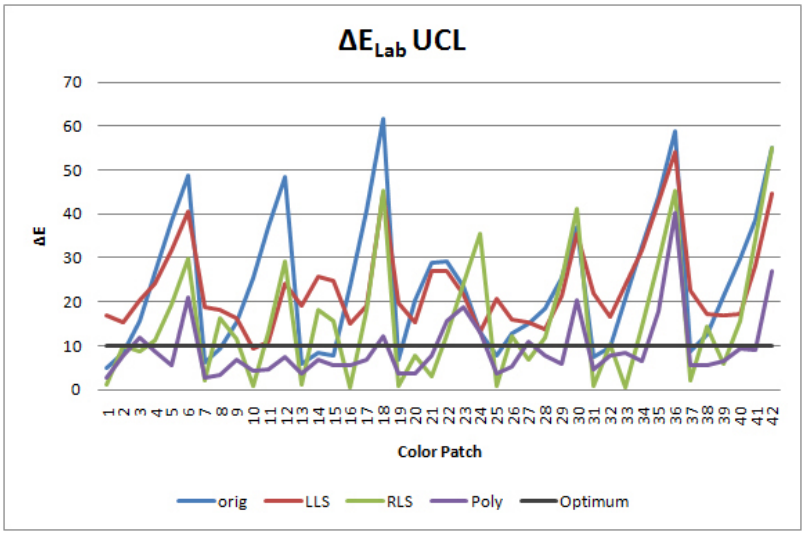

Figure B.5: Chart representing the ΔE values (Lab color space) of the color differences of the original UCL image data (aperture F8) and the results of the color transformations to the reference image data

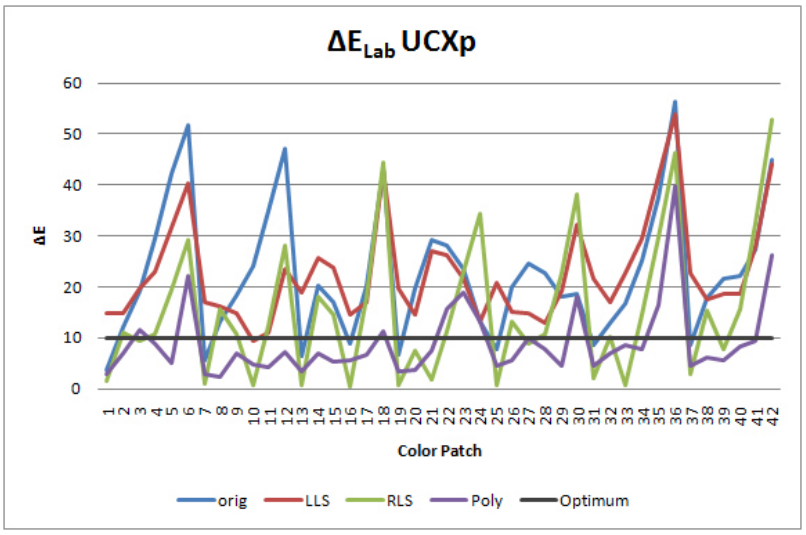

Figure B.6: Chart representing the ΔE values (Lab color space) of the color differences of the original UCXp image data (aperture F8) and the results of the color transformations to the reference image data

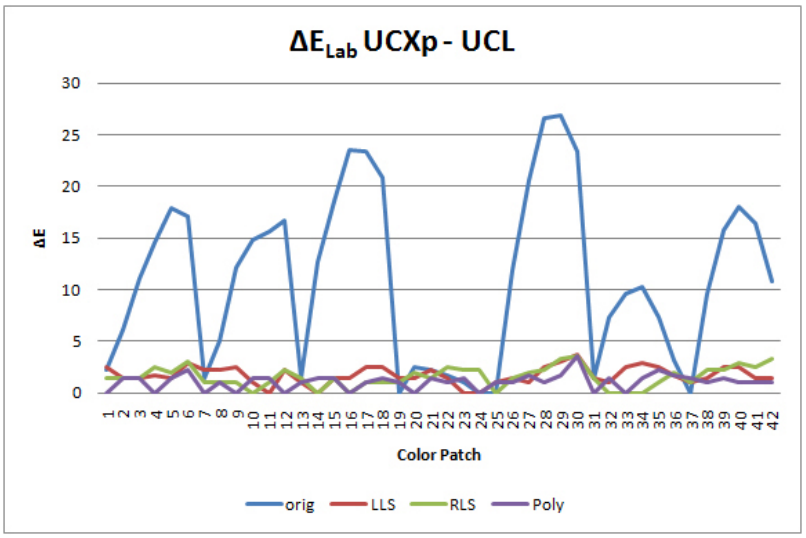

Figure B.7: Chart representing the ΔE values (Lab color space) of the color differences of the UCXp image data (aperture F8) and the UCL images of the three color transformation methods

UCL - ΔE_{LCH}				
	orig	LLS	RLS	Poly
1	5,1455	17,049	1,1136	2,8506
2	8,3547	15,209	9,7889	5,7348
3	15,546	19,49	6,3877	8,483
4	25,843	21,305	5,6968	7,342
5	36,936	27,839	13,995	2,6146
6	45,922	36,237	24,849	12,855
7	6,1467	19,006	2,6181	2,8105
8	8,8833	18,191	16,402	3,161
9	14,1	15,931	11,49	6,8433
10	23,842	8,2286	0,28362	4,2802
11	34,61	9,5748	13,061	4,5944
12	45,791	23,13	29,079	5,9438
13	6,0931	19,051	2,7465	3,6945
14	8,1943	25,626	18,103	6,174
15	5,4983	24,594	15,487	4,7947
16	20,912	14,722	0,53303	5,449
17	37,387	19,192	17,762	5,6712
18	54,663	41,692	42,348	11,7
19	6,9989	20,064	0,72334	3,7261
20	20,429	15,364	8,3035	5,1447
21	29,217	27,245	4,755	8,5447
22	29,23	27,309	13,014	15,602
23	23,685	21,733	24,233	18,733
24	13,379	13,379	35,492	13,379
25	7,9221	21,1	0,7355	3,53
26	12,632	15,801	11,981	5,3279
27	14,998	15,22	5,7775	8,4194
28	18,219	12,1	7,8334	4,8936
29	25,202	17,625	20,373	5,5168
30	36,534	30,289	35,408	12,466
31	7,973	22,065	0,71637	4,5291
32	9,7274	16,488	9,975	7,6782
33	20,627	23,562	0,62838	8,0712
34	32,536	31,765	14,379	6,4568
35	43,889	42,701	29,13	17,668
36	58,943	54,207	45,3	40,169
37	8,9001	23,092	2,0066	5,536
38	12,333	17,336	14,469	4,6234
39	20,886	16,366	4,3945	6,4779
40	29,875	16,611	14,882	9,2185
41	38,522	27,678	33,438	8,064
42	54,745	43,926	54,299	25,276
MAX	**58,943**	**54,207**	**54,299**	**40,169**
MEAN	**23,363581**	**22,5974619**	**14,8569367**	**8,4297119**

Figure B.8: Table representing the ΔE values (LCH color space) of the color differences of the UCL image data (aperture F8) and the results of the color transformations to the reference image data

UCXp - ΔE_{LCH}				
	orig	LLS	RLS	Poly
1	3,7065	15,083	1,6164	2,8506
2	11,787	14,725	10,971	5,4187
3	15,762	18,583	7,4398	8,7344
4	20,434	20,139	3,3078	7,342
5	28,309	26,986	12,319	1,5073
6	36,363	34,949	22,152	13,413
7	5,5621	17,121	2,7941	2,8105
8	12,216	16,247	15,635	2,4119
9	13,644	14,65	10,704	6,8433
10	14,433	8,6354	0,28362	4,2946
11	22,373	9,5748	12,238	4,2259
12	33,126	21,884	27,841	5,9438
13	6,4302	19,1	0,67872	3,4958
14	20,16	25,626	18,103	5,3966
15	16,864	23,558	14,498	3,8113
16	8,4068	14,063	0,53303	5,449
17	17,989	17,018	17,939	5,6038
18	36,481	40,9	41,439	11,079
19	6,9989	20,098	0,76369	3,5133
20	19,442	14,345	7,3565	5,1447
21	28,985	26,943	1,776	8,4102
22	28,158	26,179	12,62	15,508
23	23,585	21,733	22,886	18,715
24	13,379	13,379	34,409	13,379
25	7,9221	21,051	0,7355	4,5212
26	19,591	15,118	13,275	5,5797
27	23,389	14,814	7,6311	7,6526
28	20,581	11,89	6,4903	4,394
29	14,525	15,663	17,166	4,4813
30	17,389	26,968	32,424	11,26
31	8,8713	22,131	1,9907	4,5291
32	12,966	16,982	9,975	6,7268
33	16,771	22,669	0,62838	8,0712
34	25,217	29,53	14,379	7,6618
35	37,555	41,726	29,687	16,401
36	56,431	53,804	46,287	39,747
37	8,9001	23,212	2,7244	4,6085
38	17,884	17,485	15,244	5,1309
39	21,637	17,618	5,1649	5,5066
40	21,927	17,367	13,698	8,3023
41	26,777	27,033	31,37	8,076
42	44,633	43,174	51,367	24,376
MAX	**56,431**	**53,804**	**51,367**	**39,747**
MEAN	**20,18002381**	**21,89890952**	**14,29859381**	**8,150659524**

Figure B.9: Table representing the ΔE values (LCH color space) of the color differences of the UCXp image data (aperture F8) and the results of the color transformations to the reference image data

UCL - ΔE_{Lab}				
	orig	LLS	RLS	Poly
1	4,8357	16,935	1,0508	2,8538
2	8,3698	15,265	9,9446	7,6808
3	15,653	20,468	8,5555	11,755
4	26,655	24,038	11,087	8,7723
5	38,367	31,869	19,443	5,5104
6	48,895	40,603	29,918	20,97
7	6,1946	18,912	1,963	2,8131
8	9,3418	18,239	16,412	3,3271
9	15,415	16,256	11,505	6,9162
10	25,474	9,4298	0,66408	4,3222
11	37,04	11,052	13,067	4,6876
12	48,394	24,133	29,091	7,3091
13	5,8439	18,959	1,0543	3,6975
14	8,4406	25,71	18,103	6,9271
15	7,8422	24,773	15,5	5,4295
16	23,448	14,95	0,53935	5,5813
17	40,971	19,209	18,137	6,8206
18	61,551	44,695	45,309	12,182
19	6,7727	19,858	0,7278	3,7296
20	20,435	15,44	7,7008	3,7179
21	28,994	27,005	3,0989	7,8028
22	29,188	27,114	12,599	15,545
23	23,527	21,56	24,088	18,875
24	13,134	13,134	35,524	13,134
25	7,7271	20,813	0,74068	3,5311
26	12,641	15,855	12,015	5,328
27	15,067	15,264	6,7604	10,809
28	18,48	13,814	11,785	7,6627
29	25,353	21,24	24,975	5,8539
30	37,16	35,47	41,184	20,22
31	7,558	21,789	0,72374	4,5303
32	9,7656	16,494	10,189	7,7063
33	20,648	23,692	0,62873	8,4437
34	32,537	31,795	14,414	6,6394
35	43,892	42,727	29,179	17,686
36	58,943	54,246	45,3	40,308
37	8,5378	22,667	2,0134	5,5366
38	12,349	17,354	14,47	5,6334
39	21,166	16,786	5,7723	6,5269
40	29,949	17,119	15,702	9,2507
41	38,562	28,253	34,139	8,8552
42	55,205	44,556	55,079	26,828
MAX	**61,551**	**54,246**	**55,079**	**40,308**
MEAN	**24,05530476**	**23,3224**	**15,71791381**	**9,3264**

Figure B.10: Table representing the ΔE values (Lab color space) of the color differences of the UCL image data (aperture F8) and the results of the color transformations to the reference image data

UCXp - ΔE_{Lab}				
	orig	LLS	RLS	Poly
1	3,7476	14,708	1,6199	2,8538
2	12,121	14,746	11,126	7,0636
3	19,198	19,578	9,4264	11,655
4	29,554	22,999	10,824	8,7723
5	42,276	31,528	19,463	4,9804
6	51,752	40,404	29,214	22,036
7	5,5185	16,884	1,1015	2,8131
8	13,102	16,258	15,636	2,4391
9	18,283	14,744	10,705	6,9162
10	23,998	9,4287	0,66408	4,7287
11	34,801	11,052	12,274	4,2442
12	47,044	23,636	28,01	7,3091
13	6,3868	18,891	0,68673	3,4974
14	20,167	25,71	18,103	7,0245
15	16,893	23,747	14,5	5,2191
16	8,8403	14,495	0,53935	5,5813
17	20,223	17,022	18,119	6,7646
18	42,974	43,036	44,32	11,33
19	6,7727	19,694	0,76792	3,5142
20	19,735	14,472	7,3826	3,7179
21	29,187	27,06	1,812	7,5022
22	28,222	26,247	11,191	15,691
23	23,435	21,56	22,917	18,792
24	13,134	13,134	34,411	13,134
25	7,7271	20,667	0,74068	4,522
26	20,045	15,208	13,289	5,6787
27	24,659	14,859	8,7489	10,053
28	22,752	13,044	10,847	7,7831
29	17,987	19,04	22,609	4,5242
30	18,605	32,269	38,101	18,035
31	8,6985	21,683	1,9959	4,5303
32	13,009	17,012	10,189	6,9085
33	16,829	22,674	0,62873	8,4437
34	25,223	29,533	14,414	7,7719
35	37,63	41,756	29,69	16,427
36	56,476	53,809	46,415	39,769
37	8,5378	22,745	2,7557	4,5928
38	17,909	17,545	15,3	6,2093
39	21,64	18,49	7,7253	5,5082
40	22,276	18,523	15,703	8,3183
41	27,211	27,983	32,589	9,3034
42	45,018	44,224	52,834	26,125
MAX	**56,476**	**53,809**	**52,834**	**39,769**
MEAN	**22,60945952**	**22,66899286**	**15,4616355**	**9,097216667**

Figure B.11: Table representing the ΔE values (Lab color space) of the color differences of the UCXp image data (aperture F8) and the results of the color transformations to the reference image data

UCXp-UCL - ΔE_{LCH}				
	orig	LLS	RLS	Poly
1	2,2361	2,3355	1,3373	0
2	4,7941	1,1857	1,4133	1,1459
3	7,7303	1,414	1,4139	1,2718
4	10,1	1,7248	2,4015	0
5	12,383	1,1348	1,6807	1,4137
6	15,011	2,165	2,7292	1,8845
7	1,1273	2,0322	1	0
8	4,6726	1,969	0,83226	0,78317
9	11,193	1,6096	0,84868	0
10	12,884	0,45378	0	0,3097
11	12,663	0	0,87043	0,36909
12	12,676	1,4617	1,3102	0
13	1,3202	0,36036	2,748	0,88259
14	12,002	0	0	1,1065
15	17,597	1,4133	0,9898	1,0064
16	21,88	1,0008	0	0
17	21,761	2,1753	0,17891	1
18	19,315	1,0191	0,91549	1,0216
19	0	0,89362	1	0,88259
20	2,4039	1,3338	3,1416	0
21	1,8621	2,3923	4,7124	1,3751
22	1,4	1,3373	2,1136	0,36036
23	1,8621	0	3,8561	1,206
24	0	0	1,9374	0
25	0	0,93702	0	1
26	9,9711	1,2934	1,346	0,46087
27	17,872	1	1,857	1,7291
28	23,397	1,9611	2,2124	0,80363
29	24,048	2,7344	3,3084	1,0677
30	20,631	3,549	3,2909	2,9178
31	1,4142	0,57134	1,3338	0
32	7,2801	0,53414	0	1,084
33	9,6409	1,0351	0	0
34	10,197	2,3002	0	1,386
35	7,2651	1,0409	0,58017	1,4939
36	3,0856	1,0463	1,0367	1,0584
37	0	0,8018	0,93702	1,3373
38	9,3409	1,0018	0,84958	0,92224
39	15,141	1,253	0,77796	1,2246
40	17,329	1,1955	1,7144	0,96288
41	15,719	0,79815	2,0904	0,25548
42	10,638	0,78588	3,0261	0,97086
MAX	**24,048**	**3,549**	**4,7124**	**2,9178**
MEAN	**9,8058**	**1,267880714**	**1,471228571**	**0,8260419**

Figure B.12: Table representing the ΔE values (LCH color space) of the Color differences of the UCXp image data (aperture F8) and the UCL images of the three color transformation methods

UCXp-UCL - ΔE_{Lab}				
	orig	LLS	RLS	Poly
1	2,2361	2,4495	1,4142	0
2	6,1644	1,4142	1,4142	1,4142
3	11,091	1,4142	1,4142	1,4142
4	14,56	1,7321	2,4495	0
5	17,916	1,4142	2	1,4142
6	17,029	2,8284	3	2,2361
7	1,4142	2,2361	1	0
8	5	2,2361	1	1
9	12,083	2,4495	1	0
10	14,866	1	0	1,4142
11	15,588	0	1	1,4142
12	16,733	2,2361	2,2361	0
13	1,4142	1	1,4142	1
14	12,689	0	0	1,4142
15	18,547	1,4142	1,4142	1,4142
16	23,537	1,4142	0	0
17	23,367	2,4495	1	1
18	20,833	2,4495	1	1,4142
19	0	1,4142	1	1
20	2,4495	1,4142	2	0
21	2,2361	2,2361	1,4142	1,4142
22	1,7321	1,4142	2,4495	1
23	1	0	2,2361	1,4142
24	0	0	2,2361	0
25	0	1	0	1
26	11,874	1,4142	1,4142	1
27	20,518	1	2	1,7321
28	26,627	2,4495	2,2361	1
29	26,87	3	3,3166	1,7321
30	23,431	3,7417	3,6056	3,6056
31	1,4142	1,4142	1,4142	0
32	7,2801	1	0	1,4142
33	9,6437	2,4495	0	0
34	10,198	2,8284	0	1,4142
35	7,3485	2,4495	1	2,2361
36	3,1623	1,7321	2	1,7321
37	0	1	1	1,4142
38	9,5394	1,4142	2,2361	1
39	15,684	2,4495	2,2361	1,4142
40	18,028	2,4495	2,8284	1
41	16,401	1,4142	2,4495	1
42	10,77	1,4142	3,3166	1
MAX	**26,87**	**3,7417**	**3,6056**	**3,6056**
MEAN	**10,98273333**	**1,69612381**	**1,551092857**	**1,073164286**

Figure B.13: Table representing the ΔE values (Lab color space) of the color differences of the UCXp image data (aperture F8) and the UCL images of the three color transformation methods

Appendix C

Appendix - Chapter 5

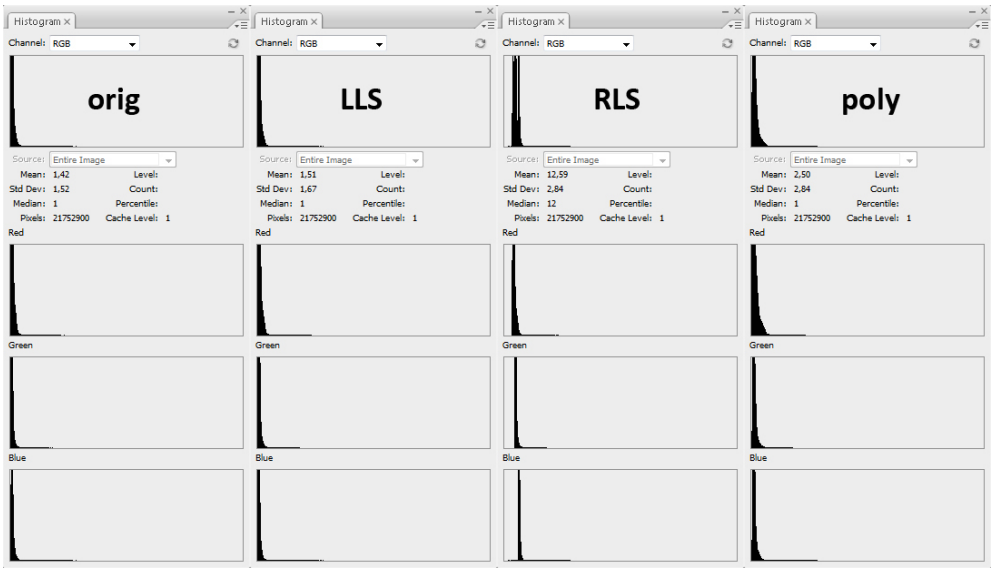

Figure C.1: Comparison of resulting histograms (of original 16bit images), the histograms are ordered in the following sequence: original UCXp image, LLS corrected image, RLS corrected image and polynomic adjusted image

UltraCam L				UltraCam Xp		
R	G	B		R	G	B
			ORIG			
221,67	119,03	137,47	**red**	232,94	106,19	97,22
81,83	118,28	112,19	**green**	67,78	150,47	138,25
78,08	95,03	120,42	**blue**	78,42	121,11	168,86
239,11	195,17	171,75	**yellow**	244,33	205,5	139,28
132,5	132,78	139,72	**gray**	157,22	165,08	167,36
			LLS			
255	99,42	141,92	**red**	244,81	77,81	151,39
40,94	123,78	100,61	**green**	34,17	147,94	107,39
65,69	88	144,5	**blue**	69,72	120,25	175,81
255	219,69	123,97	**yellow**	249,75	198,89	96,5
133,5	138,5	146,22	**gray**	154,19	158,67	162,64
			RLS			
255	35,86	129,28	**red**	250,89	0,17	115,19
35,5	141,92	116	**green**	26,61	140,89	106,17
65	88,19	162,03	**blue**	53,69	105,44	177,5
255	214,72	93,31	**yellow**	253,47	187,97	0
138,83	140,47	154,19	**gray**	143,14	143,67	152,86
			POLY			
255	94,69	137,83	**red**	238,97	50,69	126,06
73,36	147,97	125,11	**green**	26,14	147,44	121,14
90,19	109,78	157,5	**blue**	64,42	119,14	174,14
255	213,61	138,31	**yellow**	251,5	196,28	85,36
156,72	153,58	159,53	**gray**	145,97	154,42	161,5

Figure C.2: Comparison of averaged DN values for outdoor color targets for UCL and UCXp with the selected patches out of the images

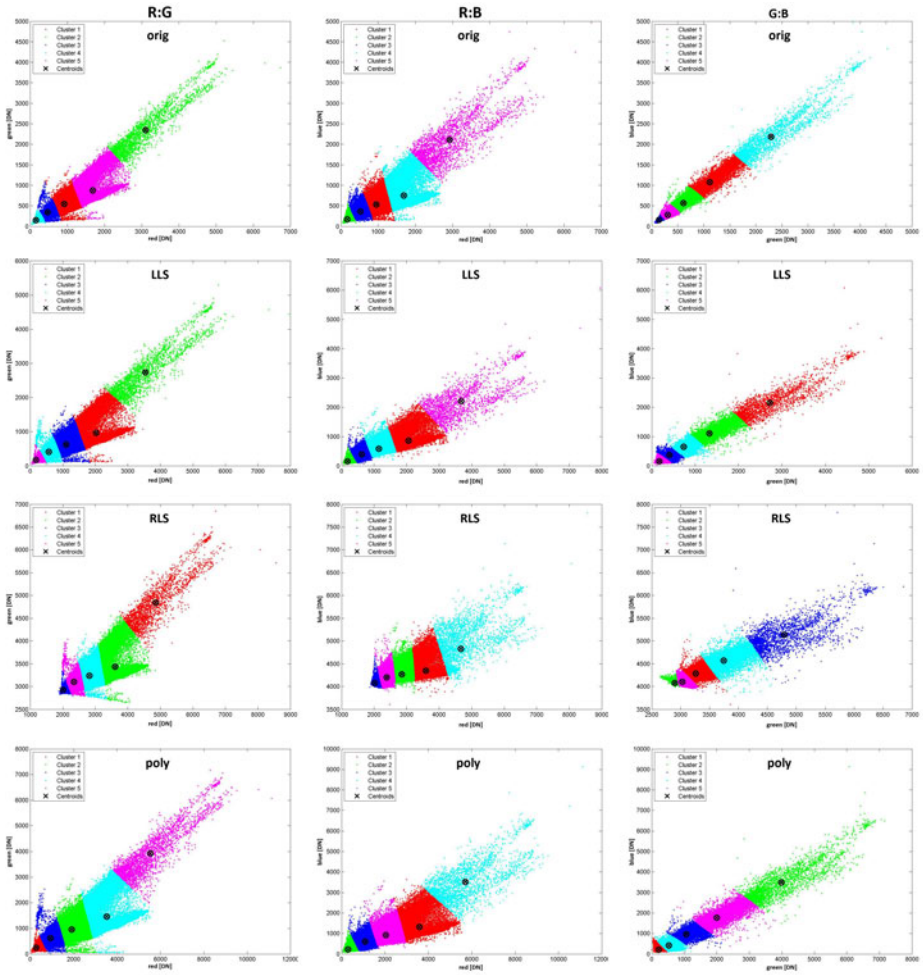

Figure C.3: Cluster analysis of UCXp imagery for the different CCM: first row represents original image data, second row represents LLS adjustment results, the third row represents results from the RLS adjustment and the last row represents the results from the polynomic adjustment. The different columns represent the different confrontation of the color channels: left columns represents R:B, middle column represents R:B and the right column represents G:B

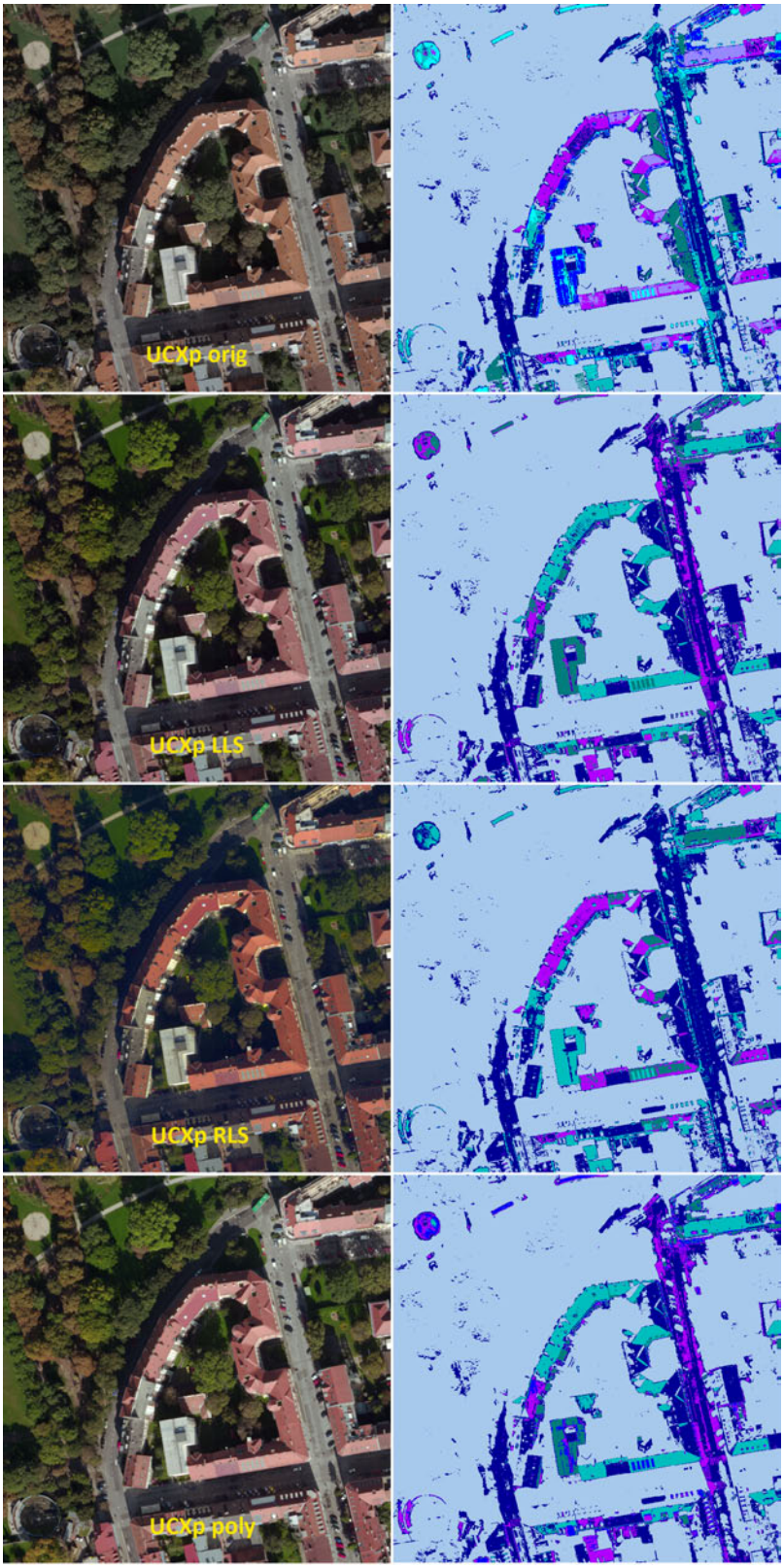

Figure C.4: Cluster analysis of UCXp imagery for the different CCM: upper left image represents original image data, upper right image represents LLS adjustment results, lower left image represents results from the RLS adjustment and the lower right image represents the results from the polynomic adjustment.